WEIDLINGER ASSOCIATES, CONSULTING ENGINEERS

110 EAST 59TH STREET

NEW YORK, NEW YORK 10022

and

SUITE 245, BUILDING 4

3000 SAND HILL ROAD

MENLO PARK, CALIFORNIA 94025

EFFECT OF LOCAL INHOMOGENEITY ON THE DYNAMIC RESPONSE OF PIPELINES

By

Ivan Nelson, Paul Weidlinger and Melvin L. Baron

Grant Report No. 14

Prepared for

National Science Foundation (ASRA Directorate)

1800 G Street

Washington, D.C. 20550

Grant No. PFR 78-15049

October 1979

50272-101

REPORT DOCUMENTATION PAGE	1. REPORT NO. NSF/RA-790528	2.	3. Recipient's Accession No. PB81 122533

4. Title and Subtitle
Effect of Local Inhomogeneity on the Dynamic Response of Pipelines, Grant Report No. 14

5. Report Date
October 1979

6.

7. Author(s)
I. Nelson, P. Weidlinger

8. Performing Organization Rept. No.
No. 14

9. Performing Organization Name and Address
Weidlinger Associates
Consulting Engineers
110 East 59th St.
New York, NY 10022

Weidlinger Associates
Consulting Engineers
Suite 245, Building 4
3000 Sand Hill Road
Menlo Park, CA 94025

10. Project/Task/Work Unit No.

11. Contract(C) or Grant(G) No.
(C)
(G) PFR7815049

12. Sponsoring Organization Name and Address
Engineering and Applied Science (EAS)
National Science Foundation
1800 G Street, N.W.
Washington, D.C. 20550

13. Type of Report & Period Covered

14.

15. Supplementary Notes

16. Abstract (Limit: 200 words)

The dynamic axial response of long segmented pipelines induced by incoherent seismic ground motion in inhomogeneous soil conditions is reported. Seismic response of pipeline "lifelines" is important because of the potential grave consequences of an earthquake disruption of vital services. Results indicate that, in general, a local inhomogeneity may contribute to a change in pipe response in three different ways: (1) a local variation in delay time in the case of wave propagation; (2) a variation in the free field waveform at adjacent segments caused by inhomogeneity; and (3) a variation in soil stiffness from soft to firm material. All three effects generally occur simultaneously. Changes in the phase delay are not significant. Large amplifications in pipe response, relative to the homogeneous case, can occur when the incoherent component of the input ground motion is large. For a two degree of freedom system,a local change in soil stiffness can cause a large increase in pipe response, even for a coherent ground input. A two degree of freedom system appears to be a reasonable model for the behavior of a multisegment system.

17. Document Analysis a. Descriptors

Earthquakes
Dynamic response
Soil dynamics
Seismic response
Pipe joints
Axial stress
Pipelines

b. Identifiers/Open-Ended Terms
Ground motion
Inhomogeneous soils

Earthquake Hazards Mitigation

c. COSATI Field/Group

18. Availability Statement	19. Security Class (This Report)	21. No. of Pages
NTIS	20. Security Class (This Page)	22. Price

(See ANSI-Z39.18) See *Instructions on Reverse*

OPTIONAL FORM 272 (4-77)
(Formerly NTIS-35)
Department of Commerce

TABLE OF CONTENTS

ABSTRACT

Transition zones between soil types are locations in which disproportionate pipe damage occurs due to seismic shaking. The authors previously considered the dynamic axial response of long segmented pipelines induced by the incoherent seismic ground motion. Homogeneous soil conditions were assumed. The present paper extends the authors' previous work to include local inhomogeneity. The results are expressed in terms of the appropriate spectra.

In general, a local inhomogeneity may contribute to a change in pipe response in three different ways. In the case of wave propagation, there will be a local variation in delay time. Inhomogeneity will cause a variation in the free field waveform at adjacent segments. Finally, the soil stiffness will vary from soft to firm material. In general, all three effects will occur simultaneously. However, to help understand the phenomena, each effect is considered separately.

Changes in the phase delay are not very significant. Large amplifications in pipe response, relative to the homogeneous case, can occur when the incoherent component of the input ground motion is large. Finally, for a two degree of freedom system, a local change in soil stiffness can cause a large increase in pipe response, even for a coherent ground input. Moreover, a two degree of freedom system appears to be a reasonable model for the behavior of a multisegment system.

LIST OF SYMBOLS

c_T = transmission coefficient

c = wavespeed in soil

D_{max} = peak ground displacement

D_m^k = influence coefficient for center joint displacement in mode k, for unit ground relative displacement across joint m, see Eq. (3)

f = frequency, function

$G = G(\bar{\omega}, \bar{\xi}, \bar{z})$ = maximum value of the integral in Eq. (65)

h = depth of soil layer

i, j = joint or segment number

k_G, k_{G1}, k_{G2} = soil stiffness

k_p = pipe/joint stiffness

ℓ = length of pipe segment

$\bar{\ell}$ = length of transition region

m = mass of pipe segment and attached soil; joint or segment number

N = number of pipe segments

P_1, P_2 = modal participation factors for coherent ground motion

Q_1, Q_2 = modal participation factors for incoherent ground motion

R_v^k, R_z^k = response in the k^{th} mode due to input $v(t) = \dot{z}(t)$ and $z(t)$, respectively

$R_{\Delta z_m}^k$ = response in the k^{th} mode due to input $\Delta z_m(t)$ across the m^{th} joint

r_δ = response of single degree of freedom system to a Dirac delta

S_D^A, S_V^A = absolute displacement and absolute velocity spectra

S_D^R = (standard) relative displacement spectrum

S_I = interference response spectrum

s = Laplace transform variable

t = time

V_{max} = maximum ground velocity

$v = \dot{z}(t)$ = ground velocity

x_i = absolute displacement of the i^{th} pipe segment

$\bar{x}$ = coherent motion of system

Y = normalized difference in response, see Eq. (74)

y = horizontal coordinate

$y_{\bar{z}}$ = response, relative to the ground, of a single degree of freedom system subjected to ground motion $\bar{z}(t)$

z_i = free field ground displacement at the i^{th} segment

$\bar{Z}(s)$ = Laplace transform of $\bar{z}(t)$

$\bar{z}$ = coherent free field ground motion

$\Delta X(s)$ = Laplace transform of $\Delta x(t)$

Δx = center joint displacement

Δz = incoherent free field ground motion; i.e., difference in free field ground displacement between successive segments

$\delta(t)$ = Dirac delta function

θ = phase angle, radians

κ = difference in soil stiffness relative to the pipe stiffness, see Eq. (37)

λ = wavelength

μ = average soil stiffness relative to the pipe stiffness, see Eq. (45)

ξ_k = fraction of critical damping in the k^{th} mode

ρ = mass density of the soil

τ = phase delay

ϕ_j^k = j^{th} element of k^{th} modal vector

$\bar{\phi}$, $\Delta\phi$ = elements of modal vector corresponding to coherent and incoherent motion

$\psi = 1 - \Omega/\bar{\omega}$

Ω = circular frequency on the input motion

ω_k = circular natural frequency of k^{th} mode of undamped system

Subscripts

A, B = soil A, soil B

G, g = ground

I, R, T = incident, reflected, transmitted

i, j, m = segment or joint number

k = mode number

p = pipe/joint

Superscripts

k = mode number

T = transpose of matrix

I. INTRODUCTION

Lifelines include pipelines, highways, transit, communications and power distribution systems. Pipelines carry fluids - water, sewage, gas, liquid fuels - which are of vital importance to modern civilization. Their disruption by an earthquake can add greatly to the destruction and injuries caused by the seismic shaking itself. Moreover, the disruption of highways, telephone and power lines will hinder enormously recovery from the emergency. Consequently, there is a growing interest in the seismic response of lifelines.

Weidlinger and Nelson, Refs. [1] and [2], showed that the seismic analysis of lifelines differs fundamentally from that of conventional structures. Whereas the foundation of a conventional building extends over a limited area, and consequently the ground motion may be assumed to be the same - i.e., coherent - over the entire foundation, this is not true for lifelines, where the structure extends essentially parallel to the ground surface for a distance long in comparison with its other dimensions. While the coherent motion may contribute to the stresses in the lifeline structure, in other cases it corresponds to a stress-free rigid body motion. In all cases, however, a key component of the seismic input is the incoherent motion, i.e., the difference in ground motion along the lifeline. By analogy with the standard response spectrum, Weidlinger and Nelson, Refs. [1] to [3], defined the interference response (IR) spectrum, the maximum difference in absolute displacement of two adjacent points on the structure, caused by the corresponding incoherent ground input.

Nelson and Weidlinger, Refs. [4] and [5], considered the dynamic response of long segmented lifelines due to a variety of seismic inputs. Their analysis was restricted to the axial direction and to incoherent

ground motion caused by a phase delay. Moreover, they assumed homogeneous soil conditions along the lifeline. They showed that when the joint stiffness is much smaller than the soil stiffness ($k_p/k_G << 1$), the peak joint displacement is given directly in terms of the interference response spectrum. For the case of a bridge which lacks intermediate support, modal decomposition can be used, and the response in each mode is merely the appropriate IR spectrum multiplied by a modal participation factor. The problem of combining the various modal contributions is analogous to that of a conventional multi-degree of freedom structure with widely spaced natural frequencies.

For the case of a long continuously supported pipe of non-negligible joint stiffness, the authors found that the center joint displacement was predominantly a local phenomenon, which essentially was not influenced by conditions more than a few pipe segments away from the joint. Moreover, they showed that the IR spectrum, evaluated at the lowest (antisymmetric) frequency, was an excellent tool for estimating the maximum joint response over a broad range of parameters.

The current paper is an extension of the previous work to cases in which the soil is no longer locally homogeneous. As such, it is again restricted to axial motion. Kubo et al, Ref. [6], point out that the relative pipe damage from the 1923 Kanto earthquake in Japan was greatest in the transition zone between soil types. Shinozuka and Kawakami in a probabilistic study, Refs. [7] and [8], show that free field strain increases as the "correlation distance" decreases. Moreover, in that study and in an extension to it, Ref. [9], they show correlation between the RMS value of strain and the damage statistics from the Kanto earthquake.

Studies of buried pipes by other authors show transition regions between two materials to be a critical area for pipe response. Wang and

Cheng, Refs. [10] and [11], considered a constant phase delay between adjacent segments in their quasistatic analysis. They showed a large increase in peak joint displacement when there was a large sudden change in soil stiffness. Hindy and Novak, Ref. [12], studied the pipe response (maximum stress) for the reflection refraction of a plane P-wave by a vertical plane interface. The appropriate soil stiffness was used in each media. The input ground motion record from the San Fernando 1971 earthquake was assumed to represent either the incident or the transmitted wave in the softer soil. They showed a significant increase in pipe stress near the interface for waves traveling from the softer to the stiffer material. When the wave traveled in the opposite direction, even larger increases in stress appeared near the interface.

The present paper is an attempt to extend the authors' previous work to include local inhomogenuity, and to corroborate the results of other researchers. Again, the results are expressed in terms of the appropriate spectra.

In general, a local inhomogenuity may contribute to a change in pipe response in three difference ways. In the case of wave propagation, there will be a local variation in delay time. The inhomogenuity will cause a variation in the free field wave form at adjacent segments. Finally, the soil stiffness will vary from soft to firm material. In general, all three effects will occur simultaneously. However, to help understand the phenomena, each effect will be considered separately.

II. EFFECT OF VARIATION IN PHASE DELAY

The simplest case to consider is that in which the ground motion z(t) (except for phase delay) is the same across the entire pipeline, but where the phase delay T varies from across one link to the next. In Refs. [4] and [5], the center joint displacement in (antisymmetric) mode k, for an incoherent free field motion $\Delta z_m(t)$ across the m^{th} joint of a long continuously supported pipe is given as

$$\Delta x_m^{(k)} = D_m^k \, R_{\Delta z_m}^k (t) \tag{1}$$

where $R_{\Delta z_m}^k$ is the solution to

$$\ddot{R}_{\Delta z_m}^k + 2\omega_k \xi_k \dot{R}_{\Delta z_m}^k + \omega_k^2 R_{\Delta z_m}^k = \omega_k^2 \Delta z_m(t) + 2\omega_k \xi_k \Delta \dot{z}_m(t) \tag{2}$$

where "$\cdot$" means differentiation with respect to time, and where

$$D_m^k = 2\phi_{\frac{N}{2}}^k \frac{\omega_g^2}{\omega_k^2} \sum_{j=1}^{m} \phi_j^k \qquad \text{, k antisymmetric} \tag{3}$$

is the influence coefficient for center joint displacement, in mode k, for a unit ground relative displacement across joint m. It should be noted that the D_m^k depend only on the geometry and mechanical properties of the system, via the eigenvalues ω_k and eigenvectors ϕ_j^k, and are independent of the input ground motion. The quantity ξ_k is the fraction of critical damping in the k^{th} mode, and ω_g is the natural frequency of each pipe segment if the joint stiffness k_p were zero. For convenience, the number of links N has been taken as even so that there is a joint exactly at the center of the pipe. The contribution of the symmetric modes is then zero.

As was mentioned in the introduction, the phase delay from segment to segment will be varied independently of the corresponding soil stiffness k_G. This assumption may be justified when the same backfill is used irrespective of the native soil. The discrete soil/pipe stiffness k_G represents the integrated force/displacement relation for the buried pipe segment. The

major contribution will depend on the shear modulus of the soil immediately adjacent to the pipe, i.e., the backfill.

The assumed input ground motion across the m^{th} joint is

$$\Delta z_m(t) = z_m(t) - z_{m+1}(t) = z\left(t - \sum_{i=1}^{m-1} \tau_i\right) - z\left(t - \sum_{i=1}^{m} \tau_i\right) \tag{4}$$

where z without a subscript is the free field motion at the first segment, and τ_i is the phase delay across the i^{th} joint. For small values of τ_m,

$$\Delta z_m(t) = \tau_m \dot{z}\left(t - \sum_{i=1}^{m-1} \tau_i\right) = \tau_m \dot{z}_m(t) \tag{5}$$

The response $R_{\Delta z_m}^{k}$ is therefore

$$R_{\Delta z_m}^{k}(t) = \tau_m R_v^{k}(t_m) \tag{6}$$

where $R_v^{k}(t_m)$ is the solution to Eq. (2) with $\dot{z}_m(t)$ replacing $\Delta z_m(t)$, and where

$$t_m = t - \sum_{i=1}^{m-1} \tau_i \tag{7}$$

It can be shown that for $z_m(0) = 0$,

$$\dot{R}_z^{k}(t_m) = R_v^{k}(t_m) \tag{8}$$

where $R_z^{k}(t_m)$ is the response [i.e., the solution to Eq. (2)] when the input is $z_m(t)$. In words, the absolute velocity of the pipe segment due to a displacement input is the same as the absolute displacement due to the corresponding velocity input.

The total center joint displacement in the k^{th} mode is thus

$$\Delta x^{(k)}(t) = \sum_{m=1}^{N-1} D_m^{k} R_{\Delta z_m}^{k}(t) = \sum_{m=1}^{N-1} D_m^{k} \tau_m \dot{R}_z^{k}(t_m) \tag{9}$$

The response functions $\dot{R}_z^k(t_m)$ for all segments m are all the same, except for the phase delay. In the limiting case when (see Ref. [4], Appendix C)

$$\omega_k \sum_{m=1}^{N-1} \tau_m << \pi \tag{10}$$

and

$$\Omega \sum_{m=1}^{N-1} \tau_m << \pi \tag{11}$$

or the total transit time of the traveling wave is much less than a half period of the k^{th} mode, or of the dominant frequency of the input, then

$$\Delta x^{(k)}(t) \simeq \dot{R}_z^k(t_{N/2}) \sum_{m=1}^{N-1} D_m^k \tau_m \tag{12}$$

By definition (see Refs. [1] to [3]), the maximum absolute value of $\dot{R}_z^k(t)$ is the absolute velocity spectrum

$$S_V^A(\omega_k, \xi_k) \equiv \text{MAX}|\dot{R}_z^k(t)| \tag{13}$$

Therefore,

$$\text{MAX}|\Delta x^{(k)}(t)| \leq S_V^A(\omega_k, \xi_k) \sum_{m=1}^{N-1} D_m^k \tau_m \tag{14}$$

where the equal sign applies only when the maximum contribution from each segment occurs simultaneously, i.e., when Eqs. (10) and (11) hold.

In most practical cases of long pipes with many segments, Eqs. (10) and (11) will not hold. However, as was shown in Appendix B of Ref. [4], contributions from more than a few segments (say 3) away from the center have little effect on the total response of the center joint. (The individual modal contributions will be affected.)

With this in mind, SEGPIPE, the computer program described in Refs. [4] and [5] was altered to allow variable τ_m, and two additional runs were made. The assumed variation in τ_m is shown in Fig. 1. The transition

between two regions, with uniform wavespeeds or delay times τ_A and τ_B, respectively, was placed at the center joint. Since there is an odd number of joints (for an even number of links), and equal numbers of joints were assigned to the two regions, the center joint was assumed to have the average value $\bar{\tau} = (\tau_A + \tau_B)/2$. The ratio of delay times was taken as 2:1 and $\bar{\tau}$ was taken as 0.02 sec, the same as that of the previous uniform case to which the new runs were compared. Wave travel in both directions was considered.

For the configuration shown in Fig. 1, taking into account the symmetry of D_m^k, the contribution of the three centermost terms to Eq. (9) becomes

$$D_{\frac{N}{2}-1}^{k}\,\tau_{\frac{N}{2}-1}\,\dot{R}_z^k(t_{\frac{N}{2}-1}) + D_{\frac{N}{2}}^{k}\,\tau_{\frac{N}{2}}\,\dot{R}_z^k(t_{\frac{N}{2}}) + D_{\frac{N}{2}+1}^{k}\,\tau_{\frac{N}{2}+1}\,\dot{R}_z^k(t_{\frac{N}{2}+1})$$

$$= D_{\frac{N}{2}-1}^{k}\,\tau_A\,\dot{R}_z^k(t_{\frac{N}{2}}+\tau_A) + D_{\frac{N}{2}}^{k}\left(\frac{\tau_A+\tau_B}{2}\right)\dot{R}_z^k(t_{\frac{N}{2}}) + D_{\frac{N}{2}-1}^{k}\,\tau_B\,\dot{R}_z^k(t_{\frac{N}{2}}-\tau_B)$$

$$\simeq \dot{R}_z^k(t_{\frac{N}{2}})\left(\frac{\tau_A+\tau_B}{2}\right)\left(D_{\frac{N}{2}}^{k} + 2D_{\frac{N}{2}-1}^{k}\right) \tag{15}$$

for small values of τ_A and τ_B. The process may be continued until, for sufficiently small values of τ_A and τ_B, small enough to satisfy Eqs. (10) and (11),

$$\Delta x^{(k)}(t) \simeq \dot{R}_z^k(t_{N/2})\left(\frac{\tau_A+\tau_B}{2}\right)\sum_{m=1}^{N-1} D_m^k \tag{16}$$

and

$$\mathrm{MAX}\left|\Delta x^{(k)}(t)\right| \simeq S_V^A(\omega_k, \xi_k)\left(\frac{\tau_A+\tau_B}{2}\right)\sum_{m=1}^{N-1} D_m^k \tag{17}$$

Thus, to first order, the average phase delay $\bar{\tau}$ plays the key role, and results of all three calculations should be the same.

These conclusions are confirmed by Table I which compared the total center joint displacement, and the modal contributions to it, from Run 26 of Ref. [4], Appendix B, and the two new time history calculations. The largest

change in individual modal contributions is merely 2.4%, for mode 4. Most modal contributions change by much smaller amounts.(* The ± 6% variation in total response reflects the cumulative effect of the slight shifts in phase of the various modes, more than their change in magnitude. Nevertheless, for variations in delay time τ as large as 2 to 1, 6% changes in response are clearly second order. Moreover, via Eq. (9), a homogeneous soft site would lead to a larger response than one only half soft. Thus, other effects must be investigated as the possible cause of the pipe damage in the vicinity of local inhomogenuities.

*) The fact that mode 4 shows the largest relative change is no mere accident. Figure 4 of Refs. [4] and [5] shows that $D_m^4 \simeq 0$ for $m \simeq N/2$, while D_m^4 is maximum at $m = N/4, 3N/4$. The separation between these two contribution regions is sufficiently large for them not to occur simultaneously. Thus, mere addition along the line of Eq. (15) is not valid.

Table I: Effect of Variation in Phase Delay on Total Joint Displacement and Modal Contributions to it.

	Run 26 $\tau_A/\tau_B = 1.0$	Run 31 $\tau_B/\tau_A = 2.0$		Run 32 $\tau_B/\tau_A = 0.5$	
	Value (cm)	Value (cm)	% Increase	Value (cm)	% Increase
$MAX\|\Delta x\|$	1.874	1.766	-5.76	1.986	5.98
$MAX\|\Delta x^{(2)}\|$	3.294	3.276	-0.55	3.283	-0.33
$MAX\|\Delta x^{(4)}\|$	2.610	2.664	2.07	2.672	2.38
$MAX\|\Delta x^{(6)}\|$	2.109	2.099	-0.47	2.103	-0.28
$MAX\|\Delta x^{(8)}\|$	1.528	1.536	0.52	1.536	0.52
$MAX\|\Delta x^{(10)}\|$	1.145	1.140	-0.44	1.143	-0.17
$MAX\|\Delta x^{(12)}\|$	0.798	0.807	-1.12	0.807	-1.12
$MAX\|\Delta x^{(14)}\|$	0.570	0.576	1.05	0.575	0.88
$MAX\|\Delta x^{(16)}\|$	0.392	0.393	0.26	0.394	0.51
$MAX\|\Delta x^{(18)}\|$	0.231	0.227	-1.73	0.227	-1.73
$MAX\|\Delta x^{(20)}\|$	0.076	0.076	0	0.077	1.31
$MAX\|\Delta z_{N/2}\|$	0.658	0.658	-	0.658	-

In all cases, N = 20, $k_G/k_p = 4$, Damping Ratio = 5%, $t_{final} = 19.98$ sec, $\bar{\tau} = (\tau_A + \tau_B)/2 = 0.020$ sec.

Ground Input: El Centro May 1940 N-S

III. VARIATION IN FREE FIELD WAVEFORMS

Obviously, large local variations in the free field ground motion will lead to correspondingly large values of pipe joint displacement or pipe strain. Local inhomogenuities can cause focusing, reflections, etc., which will induce large variations in free field motion.

Even the simple situation illustrated in Fig. 2 of a non-uniform alluvium layer subjected to a vertically incident SH wave is worth examining. The baserock motion is assumed coherent. To the left of the transition region the surface motion will be $z_1(t)$, based on the rock motion and the characteristics of the layer (e.g., fundamental frequency $f_1 = c/4h_1$)(*. To the right of the transition region, the surface motion will be $z_2(t)$ (fundamental frequency $f_2 = c/4h_2$). The length of the transition region on the surface will be on the order of the horizontal extent of the change in layer thickness $\bar{\ell}$. A shallow buried pipe crossing the transition region at some angle would experience large strains even though the local soil properties would remain the same.

Wojcik, in a recent report, Ref. [13], presents an excellent survey of various analytic and numerical studies found in the seismological literature related to variation in ground motion caused by inhomogenuity. One study by Drake and Mal, Ref. [14], used the finite element method to model the northern portion of the San Fernando Valley and allowed Love waves to propagate from north to south. The thickness of the surface layer of alluvium increases substantially over the 16,000 ft included in their calculations. They found amplifications of the fundamental Love mode as

*) In Refs. [7] - [9], the fundamental frequency of the site was the means through which ground inhomogenuity was specified.

large as 5.5, and considerable variation in ground surface response along the cross section. While the scale of their problem is large (1000's of feet) relative to the length of pipe segments (~ 20 ft), their results suggest what might occur if the variation in ground properties were on a much smaller scale.

In a related problem of the analysis of SH waves in a dipping layer, Wojcik, Ref. [13], finds amplifications greater than 10 due to a harmonic input, see Fig. 3. The peak amplitude occurs at ~ 6 wavelengths from the vertex of the dipping layer. Moreover, a phase delay of π radians occurs across the peak, at a separation distance of approximately the wavelength in the layer λ. For example, if the layer shear wavespeed is 500 ft/sec, then the change in the 10 Hz components of the input will vary ~ 20 times that in the bedrock over a distance of only 50 ft. Such an effect is clearly relevant to a pipe with 20 ft segments crossing at an angle.

The general problem with a multifrequency input, and with many near surface layers of varying thickness is beyond the scope of the current paper. Nevertheless, one additional case, that of a vertical plane P-wave incident on a vertical plane interface, Fig. 4, is amenable to solution. As mentioned in the introduction, this was the case considered by Hindy and Novak, Ref. [12]. One must keep in mind, however, that it may be neither a realistic representation of what is found naturally, nor even a "worse case" situation.

Assume the incident wave (in material A) is traveling from left to right, i.e.,

$$z_I(y, t) = f(t - y/c_A) \tag{18}$$

Then, the reflected wave will be

$$z_R(y, t) = -\frac{\rho_B c_B - \rho_A c_A}{\rho_B c_B + \rho_A c_A} f(t + y/c_A) \tag{19}$$

while the transmitted wave will be given by

$$z_T(y, t) = \frac{2\rho_A c_A}{\rho_B c_B + \rho_A c_A} f(t - y/c_B) \tag{20}$$

In Eqs. (18) - (20), c_A, c_B and ρ_A, ρ_B are the wavespeeds and densities in the two materials, and the coordinate y is measured from the interface. The ground displacement in material A is the sum of the incident and reflected waves. It is noted that at the interface y = 0, the displacement is continuous. When the wave travels from a softer to a stiffer material ($\rho_A c_A < \rho_B c_B$), the reflected motion is in the opposite direction than the incident motion.

The interface is at the N_1^{th} joint in the pipe, see Fig. 4. The incident wave at the center of the m^{th} segment, where

$$y = (m - \frac{1}{2} - N_1)\ell \tag{21}$$

is given by

$$z_{Im}(t) = f[t + (N_1 + \frac{1}{2} - m)\tau_A] \quad , \qquad m \leq N_1 \tag{22}$$

where $\tau_A = \ell/c_A$. The reflected wave at the same location is

$$z_{Rm}(t) = -\frac{\rho_B c_B - \rho_A c_A}{\rho_B c_B + \rho_A c_A} f[t - (N_1 + \frac{1}{2} - m)\tau_A] \quad , \qquad m \leq N_1 \tag{23}$$

Expanding f in series, and retaining only the first two terms, the sum of incident and reflected motion is

$$z_m(t) = \frac{2\rho_A c_A}{\rho_B c_B + \rho_A c_A} f(t) + \frac{2\rho_B c_B}{\rho_B c_B + \rho_A c_A} (N_1 + \frac{1}{2} - m)\tau_A \dot{f}(t) \quad , \qquad m \leq N_1 \tag{24}$$

Similarly, the transmitted wave at segment m in material B is

$$z_m(t) = \frac{2\rho_A c_A}{\rho_B c_B + \rho_A c_A} [f(t) - (m - N_1 - \tfrac{1}{2})\tau_B \dot{f}(t)] \quad , \quad m > N_1 \tag{25}$$

The incoherent motion across the m^{th} joint, $\Delta z_m = z_m - z_{m+1}$, is thus

$$\Delta z_m = \frac{2\rho_B c_B \tau_A}{\rho_B c_B + \rho_A c_A} \dot{f}(t) \quad , \quad m < N_1 \tag{26}$$

$$\Delta z_m = \frac{2\rho_A c_A \tau_B}{\rho_B c_B + \rho_A c_A} \dot{f}(t) \quad , \quad m > N_1 \tag{27}$$

and at the joint across the interface

$$\Delta z_{N_1} = \frac{\rho_B c_B \tau_A + \rho_A c_A \tau_B}{\rho_B c_B + \rho_A c_A} \dot{f}(t) \tag{28}$$

It is worth considering the limiting cases of large differences in impedance. When the wave travels from very soft to very hard soil ($\rho_A c_A << \rho_B c_B$)

$$\left.\begin{aligned} \Delta z_m &\to 2\tau_A \dot{f}(t) \quad , \quad m < N_1 \quad \text{(in soft soil)} \\ \Delta z_m &\to 0 \quad , \quad m > N_1 \quad \text{(in hard soil)} \end{aligned}\right\} \tag{29}$$

Alternately, if the wave travels from hard to soft soil ($\rho_A c_A >> \rho_B c_B$)

$$\left.\begin{aligned} \Delta z_m &\to 0 \quad , \quad m < N_1 \quad \text{(in hard soil)} \\ \Delta z_m &\to 2\tau_B \dot{f}(t) \quad , \quad m > N_1 \quad \text{(in soft soil)} \end{aligned}\right\} \tag{30}$$

In either case, in the limit there is a doubling of the incoherent ground motion in the soft soil relative to what would occur at a homogeneous site of the same material.

Assuming the ground stiffness is uniform across the entire lifeline, the center joint displacement may be found as outlined in the previous section. With the Δz_m given by Eqs. (26) - (28), the elemental joint displacements in mode k may be found via Eqs. (1) - (3). Noting the Δz_m all

are proportional to f(t), expressions similar to Eqs. (12) and (14) may be derived for $\Delta x^{(k)}(t)$ and its maximum value. Of course, the same problem, the phasing of the different contributions, that was discussed previously would occur here too(*. Recalling the localized nature of the pipe response, one can consider the interface to be only a few (~ 3) joints from the "center joint" and that the response would be the same, i.e.,

$$\text{MAX}|\Delta x^{(k)}(t)| \leq \frac{2\rho_B c_B}{\rho_B c_B + \rho_A c_A} \tau_A \, S_V^A(\omega_k, \xi_k) \sum_{m=1}^{N-1} D_m^k \qquad (31)$$

where here material A is the softer material. Thus, regardless of the direction of wave propagation, the peak response will occur on the soft side of the interface, and the magnitude will be less than twice that of a pipe at a homogeneous soft site with the same input ground motion.

Finally, it is interesting to compare the present result with those of Ref. [12]. When the wave traveled from soft to firm material, Hindy and Novak assumed that f(t) was the incident wave. Their results for this case show the peak stress for an impedance ratio of 8 occurs in the soft material, close to the interface. However, the increase is only 35% larger than that which occurs in the homogeneous (soft) site, considerably less than the 78% increase suggested by Eq. (31). Moreover, their largest stress increase (50%) occurs directly at the interface and when the impedance ratio is only two. In that case, Eq. (31) gives only 33%.

The differences are even more striking when a wave traveling from firm to soft ground is considered. In that case, Ref. [12] assumed that the incident wave was $f(t)/c_T$ where c_T is the transmission coefficient defined

*) Actually, by retaining only first order terms in the expansions, Eqs. (24) and (25), it was tacitly assumed that the travel time to or from the interface was small.

by Eq. (20). Multiplying Eq. (27) by $1/c_T$,

$$\Delta z_m = \tau_B \, f(t) \, , \qquad m > N_1 \quad \text{(in soft soil, B)} \tag{32}$$

regardless of the impedance ratio, while Δz_m in material A will be smaller. Thus, for the assumption of Ref. [12], the current treatment gives the same result as that in a homogeneous soft site. The peak response will always occur on the soft side of the interface, and that caused by a wave traveling from hard to soft ground is less than that caused by wave motion in the opposite direction. This is in contrast to the results presented in Ref. [12] where large amplifications, > 100%, occur at the interface for all impedance ratios considered for wave motion from hard to soft ground.

One possible explanation of the variance between the conclusions reached in this section, and those of Ref. [12], is that the results derived up to this point assumed that the soil stiffness was uniform across the entire lifeline. In Ref. [12] the soil stiffness varied according to the square of the shear wave velocity, and thus differed in the two materials.

IV. VARIATION IN SOIL STIFFNESS

In the most general system, the soil stiffness k_G, the pipe/joint stiffness k_p and the mass of each segment could vary independently from one segment to the next. The program SEGPIPE was altered to treat just such a case, in addition to variations in the phase delay τ. The theory and discussion for the more general case, as well as the results from multi-segment calculations with real earthquake ground input, are given in a forthcoming report, Ref. [15]. For the current report, the discussion is limited to a simpler two degree of freedom system.

The simplest model which can include a variation in soil stiffness is the two degree of freedom system shown in Fig. 5. There, two pipe segments of mass m are attached to each other via a joint of stiffness k_p, and to the ground via soil stiffnesses k_{G1} and k_{G2}, respectively. For simplicity, free end conditions are assumed. It was shown in Refs. [4] and [5] that (when $k_{G1} = k_{G2}$) the analysis of a simple two degree of freedom model was relevant to much more complex systems for a wide range of small (but non-negligible) values of k_p/k_G. A similar conclusion is found in Ref. [15].

The equations of motion of the system, neglecting damping, are

$$\left.\begin{aligned} m\ddot{x}_1 + k_p(x_1 - x_2) + k_{G1}\, x_1 &= k_{G1}\, z_1 \\ m\ddot{x}_2 + k_p(x_2 - x_1) + k_{G2}\, x_2 &= k_{G2}\, z_2 \end{aligned}\right\} \tag{33}$$

The natural frequencies of free vibration ($\omega_1 < \omega_2$) are given by

$$m\omega_1^2,\ m\omega_2^2 = (k_{G1} + k_{G2})/2 + k_p \mp \sqrt{[(k_{G2} - k_{G1})/2]^2 + k_p^2} \tag{34}$$

If $k_{G1} = k_{G2}$, the two frequencies reduce to $\omega_1^2 = k_G/m$ and $\omega_2^2 = (k_G + 2k_p)/m$, respectively. Alternatively, if $k_{G1} < k_{G2}$, but $k_p \to 0$, then $\omega_1^2 = k_{G1}/m$ and $\omega_2^2 = k_{G2}/m$, and the two Eqs. (33) are completely uncoupled.

In general ($k_p > 0$), the mode shapes are given by

$$[\phi^1]^T = \left[1,\ \frac{k_{G1} - k_{G2}}{2k_p} + \sqrt{\left(\frac{k_{G2} - k_{G1}}{2k_p}\right)^2 + 1}\right] \tag{35}$$

$$[\phi^2]^T = \left[1,\ \frac{k_{G1} - k_{G2}}{2k_p} - \sqrt{\left(\frac{k_{G2} - k_{G1}}{2k_p}\right)^2 + 1}\right] \tag{36}$$

They are sketched in Fig. 6, mormalized so that the sum of the squares in each mode is unity. Also shown in Fig. 6 for each mode are components of the modal vector corresponding to the coherent motion, $\bar{\phi}$, and that corresponding to joint motion, $\Delta\phi$.

In general, both modes contribute to both $\bar{\phi}$ and $\Delta\phi$. the mode shapes, Eqs. (35) and (36), depend on a single parameter

$$\kappa = \frac{k_{G2} - k_{G1}}{2k_p} > 0 \tag{37}$$

When $\kappa << 1$, the mode shapes, Eqs. (35) and (36), approach [1, 1] and [1, -1], respectively; i.e., mode 1 becomes a rigid body translation ($\bar{\phi} = 1$, $\Delta\phi = 0$), while mode 2 becomes a pure extension ($\bar{\phi} = 0$, $\Delta\phi = 2$). On the other hand, when $k_p \to 0$ so that $\kappa >> 1$, the mode shapes become [1, 0] and [0 , 1], respectively, and both modes contribute equally to $\bar{\phi}$ and $\Delta\phi$.

It is interesting to rewrite the system, Eqs. (33), using the transformations

$$\left.\begin{aligned} \bar{x} &= (x_1 + x_2)/2 \\ \Delta x &= x_1 - x_2 \end{aligned}\right\} \tag{38}$$

and

$$\left.\begin{aligned} \bar{z} &= (z_1 + z_2)/2 \\ \Delta z &= z_1 - z_2 \end{aligned}\right\} \tag{39}$$

In terms of these new variables, Eqs. (33) become

$$\begin{bmatrix} 2m & 0 \\ 0 & \frac{m}{2} \end{bmatrix} \begin{bmatrix} \ddot{\bar{x}} \\ \Delta\ddot{x} \end{bmatrix} + \begin{bmatrix} \left(k_{G1}+k_{G2}\right) & \left(\frac{k_{G1}-k_{G2}}{2}\right) \\ \left(\frac{k_{G1}-k_{G2}}{2}\right) & \left(k_p + \frac{k_{G1}+k_{G2}}{4}\right) \end{bmatrix} \begin{bmatrix} \bar{x} \\ \Delta x \end{bmatrix} = \begin{bmatrix} \left(k_{G1}+k_{G2}\right) & \left(\frac{k_{G1}-k_{G2}}{2}\right) \\ \left(\frac{k_{G1}-k_{G2}}{2}\right) & \left(\frac{k_{G1}+k_{G2}}{4}\right) \end{bmatrix} \begin{bmatrix} \bar{z} \\ \Delta z \end{bmatrix} \tag{40}$$

The eigenvalues of the new system, Eq. (40), of course are the same as those found previously, Eq. (34). The transformed eigenvectors are

$$[\bar{\phi},\ \Delta\phi]^{1,2} = \left[1,\ \frac{2}{\kappa}\left(\pm\sqrt{\kappa^2+1}-1\right)\right] = \left[1,\ \frac{4k_p}{k_{G1}-k_{G2}} \pm \sqrt{4+\left(\frac{4k_p}{k_{G1}-k_{G2}}\right)^2}\ \right] \tag{41}$$

which are consistent with Eqs. (35) and (36). Following the approach used in Refs. [4] and [5], one may obtain an equation for $\Delta x^{(k)}$, the contribution of each mode k to the joint displacement, i.e.,

$$\Delta\ddot{x}^{(k)} + \omega_k^{\,2}\,\Delta x^{(k)} = \omega_k^{\,2}\,P_k\bar{z} + \omega_k^{\,2}\,Q_k\,\Delta z\ , \qquad k = 1,\ 2 \tag{42}$$

where the modal participation factors for the coherent and incoherent ground motion are given respectively by

$$P_k = \pm\frac{\kappa}{\sqrt{\kappa^2+1}} = \pm\frac{k_{G2}-k_{G1}}{\sqrt{(k_{G2}-k_{G1})^2+4k_p^{\,2}}} \tag{43}$$

and

$$\begin{aligned} Q_k &= \mp\frac{\kappa^2+\mu\left(1+\sqrt{\kappa^2+1}\right)}{2\sqrt{\kappa^2+1}\left(\mu+1\mp\sqrt{\kappa^2+1}\right)} \\ &= \mp\frac{(k_{G2}-k_{G1})^2+(k_{G1}+k_{G2})\left[2k_p \mp \sqrt{(k_{G2}-k_{G1})^2+4k_p^{\,2}}\right]}{2\sqrt{(k_{G2}-k_{G1})^2+4k_p^{\,2}}\left[k_{G1}+k_{G2}+2k_p \mp \sqrt{(k_{G2}-k_{G1})^2+4k_p^{\,2}}\right]} \end{aligned} \tag{44}$$

where

$$\mu = (k_{G1}+k_{G2})/2k_p \tag{45}$$

In the above, the upper signs refer to mode 1, and the lower ones to mode 2.

It is observed that as $\kappa \to 0$, i.e., for vanishing variation in soil stiffness, $P_k \to 0$. Thus, the coherent motion does not contribute then to the joint displacement. Also, as $\kappa \to 0$, $Q_1 \to 0$ while

$$\lim_{\kappa \to 0} \; Q_2 = \frac{\mu}{2 + \mu} = \frac{1}{1 + 2k_p / \left(\frac{k_{G1} + k_{G2}}{2} \right)} \tag{46}$$

which agrees with that found in Ref. [16]. Consequently, as was found more generally in Refs. [4] and [5], the first mode is symmetric for a symmetric system, and does not contribute at all to the center joint displacement.

It is noted that $k_{G2} > k_{G1} > 0$, so that κ must be less than μ. Thus, for $k_p > 0$, the other limiting values of Q_k occur as $\kappa \to \mu$, i.e.,

$$\lim_{\kappa \to \mu} \; Q_k = \mp \frac{\mu}{2\sqrt{\mu^2 + 1}} = - \frac{1}{2} P_k \tag{47}$$

Thus, Δz contributes equally to both modes in this limiting case. Alternately, when $\kappa < \mu$ but there is vanishingly small joint stiffness, i.e., $k_p \to 0$, $P_k \to \mp 1$ while both Q_1 and Q_2 approach + 1/2.

The variation in the modal participation factors, $P_1 = - P_2$, Q_1 and Q_2, with the parameters κ and μ is shown in Fig. 7. For a wide range of μ, it is seen that $|Q_1| < Q_2 < P_1$ for $1 < \kappa < \mu$.

Assuming that the addition of (modal) damping does not alter the above derivation, the solution to Eq. (42) (with damping ratio ξ_k included) is

$$\Delta x^{(k)}(t) = P_k \, R_{\bar{z}}^{\,k}(t) + Q_k \, R_{\Delta z}^{\,k}(t) \tag{48}$$

where $R_{\bar{z}}^{\,k}(t)$ and $R_{\Delta z}^{\,k}(t)$ are the solutions to Eq. (2) when the input ground motion is $\bar{z}(t)$ and $\Delta z(t)$, respectively. The frequency ω_k and damping ratio ξ_k appear as parameters. The actual joint displacement is the sum of the two modal contributions, or (noting $P_2 = - P_1$)

$$\Delta x(t) = \Delta x^{(1)} + \Delta x^{(2)} = P_1[R_{\bar{z}}(t, \omega_1, \xi_1) - R_{\bar{z}}(t, \omega_2, \xi_2)] + Q_1 R_{\Delta z}(t, \omega_1, \xi_1) + Q_2 R_{\Delta z}(t, \omega_2, \xi_2) \quad (49)$$

where the dependence of the R's on the ω_k and ξ_k is written explicitly.

Recalling from Refs. [1] to [3] the definition of the absolute displacement spectrum $S_D{}^A$ and the interference response spectrum S_I, the total joint displacement is bounded by

$$\text{MAX}|\Delta x(t)| \leq P_1[S_D{}^A(\omega_1, \xi_1) + S_D{}^A(\omega_2, \xi_2)] + |Q_1| S_I(\omega_1, \xi_1) + Q_2 S_I(\omega_2, \xi_2) \quad (50)$$

where the absolute spectra correspond to the coherent ground motion $\bar{z}(t)$, and where the interference spectra correspond to the incoherent ground motion $\Delta z(t)$. The equal sign will hold only when all the contributions are additive, and occur simultaneously. Alternately, by addition and subtraction of $\bar{z}(t)$ to the first term on the right side of Eq. (49), it becomes

$$\Delta x(t) = \Delta x^{(1)} + \Delta x^{(2)} = P_1[y_{\bar{z}}(t, \omega_1, \xi_1) - y_{\bar{z}}(t, \omega_2, \xi_2)] + Q_1 R_{\Delta z}(t, \omega_1, \xi_1) + Q_2 R_{\Delta z}(t, \omega_2, \xi_2) \quad (51)$$

where $y_{\bar{z}}(t, \omega_k, \xi_k)$ is the response, relative to the ground, of a single degree of freedom system of circular frequency ω_k and damping ξ_k to ground motion $\bar{z}(t)$. Consequently, the joint motion $\Delta x(t)$ is also bounded by

$$\text{MAX}|\Delta x(t)| \leq P_1[S_D{}^R(\omega_1, \xi_1) + S_D{}^R(\omega_2, \xi_2)] + |Q_1| S_I(\omega_1, \xi_1) + Q_2 S_I(\omega_2, \xi_2) \quad (52)$$

where $S_D{}^R(\omega_k, \xi_k)$ is the standard relative displacement spectrum. Whether Eq. (50) or Eq. (52) is more restrictive depends on the frequencies ω_1 and ω_2 and the frequency content of the coherent input $\bar{z}(t)$. In general, for sufficiently soft systems

$$S_D{}^A(\omega, \xi) < S_D{}^R(\omega, \xi) \quad \text{for } \omega << \Omega \quad (53)$$

while for stiff systems the opposite is true, i.e.,

$$S_D^{\,A}(\omega, \xi) > S_D^{\,R}(\omega, \xi) \qquad \text{for } \Omega << \omega \tag{54}$$

a) Joint Displacement Due To Coherent Input

First, let us consider the case when the ground motion is coherent, i.e., $\Delta z(t) \equiv 0$. In that case, only the first term on the right hand side of either Eq. (49) or Eq. (51) remains. Of course, the participation factor P_1 goes to zero for $\kappa \to 0$; however, for $\kappa > 1$, $P_1 \simeq 1$ (see Fig. 7), so that $|R_{\bar{z}}^{(1)} - R_{\bar{z}}^{(2)}|$ or $|y_{\bar{z}}^{(1)} - y_{\bar{z}}^{(2)}|$ must be examined.

It is useful to examine $\Delta x(t)$ in transform space, i.e.,

$$\Delta X(s) = P_1 \bar{Z}(s) \left[\frac{\omega_1^{\,2} + 2\omega_1\xi_1 s}{s^2 + 2\omega_1\xi_1 s + \omega_1^{\,2}} - \frac{\omega_2^{\,2} + 2\omega_2\xi_2 s}{s^2 + 2\omega_2\xi_2 s + \omega_2^{\,2}} \right] \tag{55}$$

where s is the transform variable, $\Delta X(s)$ and $\bar{Z}(s)$ are the Laplace transforms of $\Delta x(t)$ and $\bar{z}(t)$, respectively. The transforms of $R_{\bar{z}}(t, \omega_k, \xi_k)$ were obtained from Eq. (2), assuming rest initial conditions. Firstly, for very soft systems, where ω_2 is small but finite and $\omega_1 \to 0$,

$$\Delta X(s) \simeq - P_1 \bar{Z}(s) \frac{\omega_2^{\,2} + 2\omega_2\xi_2 s}{s^2 + 2\omega_2\xi_2 s + \omega_2^{\,2}} \quad , \omega_1 \to 0 \tag{56}$$

so that

$$\Delta x(t) \simeq - P_1 R_{\bar{z}}(t, \omega_2, \xi_2) \quad , \omega_1 \to 0 \tag{57}$$

Secondly, for very stiff systems where $\omega_2 >> \omega_1 > \Omega$, $\bar{Z}(s) \to 0$ as $s \to \omega_2$. Thus,

$$\Delta X(s) \simeq P_1 \bar{Z}(s) \left[\frac{\omega_1^{\,2} + 2\omega_1\xi_1 s}{s^2 + 2\omega_1\xi_1 s + \omega_1^{\,2}} - 1 \right] = - P_1 \bar{Z}(s) \left[\frac{s^2}{s^2 + 2\omega_1\xi_1 s + \omega_1^{\,2}} \right], \quad \omega_2 >> \omega_1 > \Omega \tag{58}$$

and

$$\Delta x(t) \simeq P_1 \; y_{\bar{z}}(t, \omega_1, \xi_1) \qquad , \omega_2 >> \omega_1 > \Omega \tag{59}$$

Obviously, as $\omega_1 \to \omega_2$ the difference in responses must vanish. While this may be intuitively true, the statement says nothing about the rate at which the difference in responses goes to zero. When $\Delta z = 0$, the Laplace transform of Eq. (51) becomes

$$\Delta X(s) = P_1 \; s^2 \; \bar{Z}(s) \left[\frac{1}{s^2 + 2\omega_2 \xi_2 \; s + \omega_2{}^2} - \frac{1}{s^2 + 2\omega_1 \xi_1 \; s + \omega_1{}^2} \right] \tag{60}$$

Assuming proportional damping ($\xi_1/\xi_2 = \omega_1/\omega_2$), and letting

$$\bar{\omega} = \frac{\omega_1 + \omega_2}{2} \qquad \text{and} \qquad \Delta\omega = \omega_2 - \omega_1 > 0 \tag{61}$$

as well as defining

$$\bar{\xi} = \xi_1 \; \bar{\omega}/\omega_1 = \xi_2 \; \bar{\omega}/\omega_2 = (\xi_1 + \xi_2)/2 \tag{62}$$

Eq. (60) may be written as

$$\Delta X(s) = P_1 \; s^2 \; \bar{Z}(s) \left[\frac{1}{s^2 + \left(2\bar{\xi}\bar{\omega}s + \bar{\omega}^2\right)\left(1 + \frac{\Delta\omega}{2\bar{\omega}}\right)^2} - \frac{1}{s^2 + \left(2\bar{\xi}\bar{\omega}s + \bar{\omega}^2\right)\left(1 - \frac{\Delta\omega}{2\bar{\omega}}\right)^2} \right] \tag{63}$$

For $\Delta\omega/\bar{\omega} << 1$, terms quadratic and higher in $\Delta\omega/\bar{\omega}$ may be dropped, so that

$$\underset{\text{for } \Delta\omega/\bar{\omega} << 1}{\Delta X(s)} = 2P_1 \frac{\Delta\omega}{\bar{\omega}} \left[\frac{-s^2 \; \bar{Z}(s)}{s^2 + 2\bar{\xi}\bar{\omega}s + \bar{\omega}^2} \right] \left[\frac{2\bar{\xi}\bar{\omega}s + \bar{\omega}^2}{s^2 + 2\bar{\xi}\bar{\omega}s + \bar{\omega}^2} \right] \tag{64}$$

The first bracket is recognized as the transform of the relative response $y_{\bar{z}}(t, \bar{\omega}, \bar{\xi})$, while the second bracket is the transform of the absolute response if $\bar{Z}(s)$ were unity, i.e., if $\bar{z}(t)$ were a Dirac delta function. Thus, by convolution,

$$\underset{\text{for } \Delta\omega/\bar{\omega} << 1}{\Delta x(t)} = 2P_1 \frac{\Delta\omega}{\bar{\omega}} \int_0^t y_{\bar{z}}(\tau, \bar{\omega}, \bar{\xi}) \; r_\delta(t - \tau, \bar{\omega}, \bar{\xi}) \; d\tau \tag{65}$$

where $r_\delta(t, \bar{\omega}, \bar{\xi})$ is the absolute response of a single degree of freedom system (of frequency $\bar{\omega}$ and damping $\bar{\xi}$) to a ground motion $\delta(t)$. One may find r_δ analytically, i.e.,

$$r_\delta(t, \bar{\omega}, \bar{\xi}) = \bar{\omega} e^{-\xi\omega t} \left[2\bar{\xi} \cos \bar{\omega}\sqrt{1 - \bar{\xi}^2}\, t + \frac{\left(1 - 2\bar{\xi}^2\right)}{\sqrt{1 - \bar{\xi}^2}} \sin \bar{\omega}\sqrt{1 - \bar{\xi}^2}\, t \right] \tag{66}$$

It is noted that

$$r_\delta(0^+) = 2\bar{\xi}\bar{\omega} \neq 0 \tag{67}$$

and

$$\dot{r}_\delta(0^+) = \bar{\omega}^2(1 - 4\bar{\xi}^2) \tag{68}$$

The joint response is seen in Eq. (65) to go to zero linearly as $\Delta\omega/\bar{\omega}$ goes to zero. The actual variation in $\Delta\omega/\bar{\omega}$ with κ and μ is shown in Fig. 8.

While it is possible to obtain numerically first $y_{\bar{z}}(t, \bar{\omega}, \bar{\xi})$ for a real earthquake input, and then numerically integrate Eq. (65), it would be a formidable task. However, if the ground motion were a haversine function,

$$\bar{z}(t) = \frac{1}{2}(1 - \cos \Omega t) \tag{69}$$

and the damping were neglected, then Eq. (65) may be integrated analytically, i.e.,

$$\begin{matrix} \Delta x(t) \\ \frac{\Delta\omega}{\bar{\omega}} << 1 \end{matrix} = \frac{\frac{P_1}{2}\left(\frac{\Delta\omega}{\bar{\omega}}\right)\left(\frac{\Omega}{\bar{\omega}}\right)^2}{1 - \left(\Omega/\bar{\omega}\right)^2} \left\{ \begin{aligned} &\sin \bar{\omega}t \left[\bar{\omega}t - \frac{\sin(\bar{\omega} - \Omega)\, t}{1 - \Omega/\bar{\omega}} - \frac{\sin(\bar{\omega} + \Omega)\, t}{1 + \Omega/\bar{\omega}} \right] \\ &+ \cos \bar{\omega}t \left[\frac{2}{1 - (\Omega/\bar{\omega})^2} - \frac{\cos(\bar{\omega} - \Omega)\, t}{1 - \Omega/\bar{\omega}} - \frac{\cos(\omega + \Omega)\, t}{1 + \Omega/\bar{\omega}} \right] \end{aligned} \right\} \tag{70}$$

Figure 9 shows that Eq. (70) is an excellent approximation to the actual computed joint response for early times ($\bar{\omega}t < 20$) for $\Delta\omega/\bar{\omega}$ as large as 0.1. The limit $\bar{\omega}t < 20$ was not chosen arbitrarily. Real earthquake motions are not sinusoids. It is rare for there to be more than approximately three major cycles of a dominant frequency.

Equation (70) is still a rather complicated expression. Moreover, it is not valid as $\Omega \to \bar{\omega}$ (or more accurately ω_1 or ω_2). It can be shown (after much algebra!) for sufficiently small values of $\Delta\omega/\bar{\omega} <<< 1$ and

$$\psi = 1 - \Omega/\bar{\omega} << 1 \tag{71}$$

that

$$\Delta x(t) = -\frac{\Delta\omega}{\bar{\omega}} \frac{\bar{\omega}t}{8} P_1 \sqrt{1 + \tan^2 \theta}\, \sin(\bar{\omega}t - \theta) \tag{72}$$

where

$$\tan \theta = \frac{\psi^2 \bar{\omega}t}{\psi^2 - (\Delta\omega/2\bar{\omega})^2} \tag{73}$$

The computed joint response and the approximation Eq. (72) are compared in Fig. 10 for $\Delta\omega/\bar{\omega} = 0.01$ and $\Omega/\bar{\omega} = 0.95$; viz, $\psi = 0.05$. Again, an excellent early time approximation has been obtained, one which is proportional to $\Delta\omega/\bar{\omega}$.

The actual values of $\Delta\omega/\bar{\omega}$ are almost certainly beyond the range for which Eq. (72) holds (see Fig. 8), and may be beyond the range for which Eq. (70) holds as well. Calculations were made for various values of $\Delta\omega/\bar{\omega}$ and $\Omega/\bar{\omega}$. The joint displacement, or difference in response, was normalized with respect to its maximum possible value, i.e.,

$$Y(t, \Delta\omega/\bar{\omega}, \Omega/\bar{\omega}) = \frac{R_{\bar{z}}(t, \omega_1) - R_{\bar{z}}(t, \omega_2)}{\text{MAX}|R_{\bar{z}}(t, \omega_1)| + \text{MAX}|R_{\bar{z}}(t, \omega_2)|} \tag{74}$$

An example of Y versus $\bar{\omega}t$ is shown in Fig. 11 for $\Delta\omega/\bar{\omega} = 0.3$ and $\Omega/\bar{\omega} = 0.6$. Other plots are given in the Appendix.

The maximum values of $|Y(t)|$ from all the undamped calculations are shown as the various symbols in Fig. 12. Not much credence should be given to the solid symbols, which are connected with dashed lines. They correspond to cases in which $R_{\bar{z}}(t, \omega_1)$ was "resonant-like", and still did not reach its eventual maximum by $\bar{\omega}t = 20$. For all values of $\Omega/\bar{\omega}$, MAX$|Y|$ increases with

$\Delta\omega/\bar{\omega}$, at first linearly as suggested by Eq. (70). In all cases, $\text{MAX}|R_{\bar{z}}(t, \omega_1) - R_{\bar{z}}(t, \omega_2)|$ was smaller than the maximum of the larger response, $|R_{\bar{z}}(t, \omega_1)|$. In all non-"resonant-like" cases, it was less than the smaller one as well. The largest value of $\text{MAX}|Y|$, ignoring the "resonant-like" solid symbols, was 0.369 at $\Omega/\bar{\omega} = 0.7$ and $\Delta\omega/\bar{\omega} = 0.2$, a point close to being "resonant-like". Most values shown in Fig. 12 are considerably less than that.

One should try to interpret the parameter $\Omega/\bar{\omega}$ in terms of real earthquake ground motion input. For a given value of $\Delta\omega/\bar{\omega}$, $\text{MAX}|Y|$ decreases as $\Omega/\bar{\omega}$ decreases. As $\Omega/\bar{\omega} \to 0$, both $R_{\bar{z}}(t, \omega_1)$ and $R_{\bar{z}}(t, \omega_2)$ will approach the ground input, $\bar{z}(t)$; i.e., each response will be quasistatic. The difference between the two responses will approach zero. Adding damping to the system will have a similar effect. Thus, in viewing Fig. 12, most credence should be given to the smaller values of $\Omega/\bar{\omega}$.

The effect of damping on the joint displacement is shown in Fig. 13, drawn for $\Delta\omega/\bar{\omega} = 0.3$ and $\Omega/\bar{\omega} = 0.6$. The undamped case is the same, except for a scale factor, as the curve in Fig. 11. Also shown is the coherent haversine input, $\bar{z}(t)$. While the addition of damping changes the magnitude and frequency of the response, the basic character of the solution is not changed.

Only so much can be ascertained from calculations with sinusoidal type imput. A total of ten calculations were made using the first 20 seconds of the May 1940 El Centro North-South record as the coherent ground motion $\bar{z}(t)$. The calculations are listed in Table II. In all the calculations the mass m of each segment was held constant, and equal to $1/\pi^2$. The values of k_{G1}, k_{G2} and k_p, and consequently κ and μ, were varied as shown in the table. The computed (undamped) natural frequencies f_1 and f_2 which could be obtained

Table II: Two Degree of Freedom Calculations Made Using El Centro N-S as the Coherent Ground Motion Input

Run	$k_{G1}/k_{G2}/k_p$	κ	μ	f_1(Hz)	f_2(Hz)	ξ_1(%)	ξ_2(%)	$\Delta\omega/\bar{\omega}$	P_1	MAX$\lvert\Delta x(t)\rvert$ (cm)
1	2.9267/5.0733/1	1.0733	4	0.9398	1.2715	0	0	0.3000	0.73166	27.2376
2	2.9267/5.0733/1	1.0733	4	0.9398	1.2715	5.0	6.765	0.3000	0.73166	10.8056
3	2.9267/5.0733/1	1.0733	4	0.9398	1.2715	10.0	13.53	0.3000	0.73166	6.8753
4	3.5 / 4.5 /1	0.50	4	0.9851	1.2367	10.0	12.55	0.2265	0.44721	3.7318
5	4.0 / 8.0 /1	2.00	6	1.0913	1.5195	10.0	13.92	0.3280	0.89443	7.6352
6	5.0 / 7.0 /1	1.00	6	1.1817	1.4504	10.0	12.27	0.2041	0.70711	4.5042
7	5.0 / 7.0 /1	1.00	6	1.1817	1.4504	20.0	24.55	0.2041	0.70711	2.3916
8	9.5 / 10.5 /1	0.50	10	1.5718	1.7405	20.0	22.15	0.1019	0.44721	0.7149
9	6.0 / 10.0 /1	2.00	8	1.3004	1.6760	20.0	25.78	0.2524	0.89443	3.1224
10	16.0 / 36.0 /2	5.00	13	2.1096	3.0902	20.0	29.30	0.3772	0.98058	1.8691

Note: $m = 1/\pi^2$ and $t_f = 20.0$ sec for all calculations

via Eq. (34)(* are listed, as is the assumed damping ratio ξ_1, $\xi_2 = \xi_1(f_2/f_1)$, $\Delta\omega/\bar{\omega}$ and the modal participation factor P_1 computed from Eq. (43)(*. The final column shows the computed maximum joint displacement, $MAX|\Delta x(t)|$. The time histories of the joint displacement for each of the ten calculations are shown in the Appendix.

Runs 1 to 3 correspond to the same two segment systems, with various damping ratios, which was subjected to the haversine input discussed above. For the undamped case, Run 1, the maximum response occurs at late times and is greater than the maximum value of $R_{\bar{z}}^{(1)}$. For that case, the square root of the sum of the squares of the maximum modal responses is a good approximation to the maximum total response. However, Run 1 is atypical in that for all the other cases, the maximum total response occurs relatively early, and is less than $MAX|R_{\bar{z}}^{(1)}(t)|$. In fact, except for Run 2, the maximum total response is less than $MAX|R_{\bar{z}}^{(2)}(t)|$ as well. Of course, assuming no damping is totally unrealistic for a buried pipeline.

Some of the calculations were run for a specific purpose. For example, the effect of damping (in a more realistic range) may be seen by comparing the results of Runs 6 and 7. The mode 1 contribution to joint displacement for both Runs are shown in Fig. 14. The modal response is computed via Eq. (48), but where $R_{\Delta z}^{k}(t) \equiv 0$ for a coherent input. Also shown in the figure is the coherent ground motion $\bar{z}(t)$. The two modal responses follow one another very closely, and follow $\bar{z}(t)$ generally as well. The major discrepancy in magnitude between the $\Delta x^{(1)}$ and $\bar{z}$ can be explained by the value of P_1. The total joint response for the same two calculations is shown in Fig. 15. Except for the obvious reduction in magnitude caused by the increased damping, the two curves are very similar. Moreover, they

*) The frequencies, participation factor P_1, as well as the modal and total response $\Delta x(t)$, for each calculation were actually computed with a more general program SEGPIP2. The program is applicable to multilink systems and will be described in Ref. [15].

differ greatly from the modal responses shown in Fig. 14. All the low frequency motion has been eliminated.

This apparent paradox may be explained by recalling that $\Delta x(t)$ may be expressed in terms of absolute responses $R_{\bar{z}}^{(k)}$, Eq. (49) or relative responses $y_{\bar{z}}^{(k)}$, Eq. (51). The maximum absolute values of these two quantities, i.e., the absolute and relative displacement spectra, are plotted against frequency in Fig. 16 for 15% of critical damping. It is observed that except for extremely low frequencies, $S_D^R < S_D^A$. Thus, Eq. (51) is more apropos for the current problem. Moreover, even at frequencies as low as 1 Hz, $S_D^A \simeq D_{max}$, i.e., the peak modal response is quasistatic, as was seen in Fig. 14.

However, even at higher frequencies, where $R_{\bar{z}}(t, \omega, \xi)$ follows $\bar{z}(t)$ almost exactly, the total joint response is still not zero. Figure 17 compares the mode 1 contribution to joint displacement from Run 10, in which $f_1 = 2.11$ Hz, and the coherent El Centro input. Here, $P_1 = 0.98$, so that except at isolated peaks (the largest difference being the negative peak at $t \simeq 2.2$ sec), the two curves essentially coincide. The difference between the two, $y_{\bar{z}}(t, \omega_1, \xi_1)$, is plotted as the dashed curve in Fig. 18. Again, except at the large negative peak at $t \simeq 2.2$ sec and at several smaller peaks, the dashed curve follows closely the solid curve which represents the total joint response for this case. Thus, for Run 10, Eq. (59) appears to hold except at the isolated peaks. The reason why Eq. (59) is not accurate at the peaks may be seen in Fig. 19 in which $y_{\bar{z}}^{(1)}(t)$ and $y_{\bar{z}}^{(2)}(t)$ are compared. Although $y_{\bar{z}}^{(2)}(t)$ is generally a third the magnitude of $y_{\bar{z}}^{(1)}(t)$, the minimum of each curve occurs at $t = 2.2$ sec, so that the total response at $t = 2.2$ sec $[y_{\bar{z}}^{(1)} - y_{\bar{z}}^{(2)} = -1.84$ cm] is less than the positive peak total response of 1.87 cm at $t = 2.4$ sec. At this later time the local maxima in $y_{\bar{z}}^{(1)}$ and $y_{\bar{z}}^{(2)}$ do not occur simultaneously.

Returning to Table II, other runs were made to compare with multi-degree of freedom systems. For the most part, these comparisons will be shown in Ref. [15]. For example, the multi-link calculations described in Section I all had a uniform ground stiffness $k_G = 4k_p$. Run 4 results were compared with those from a 12 segment calculation in which the ratio k_G/k_p was 3.5 over half the pipe, and 4.5 over the other half. The total center joint response of both systems are compared in Fig. 20. A similar trend is shown in Fig. 21 in which the Run 5 results are compared with those from a 12 segment calculation which has the same $k_{G1}:k_{G2}:k_p$ ratio, i.e., 4:8:1. The corresponding value of κ in this case is considerably larger than in the previous case. Nevertheless, in both Figs. 20 and 21, the two link system response is seen to be an excellent model for the response of the corresponding more complicated multi-link system.

Run 8 was made specifically to examine a case in which $\Delta\omega/\bar{\omega}$ was small, i.e., $\simeq 0.10$. Run 9 tried to establish a limiting case for "closely spaced" frequencies; i.e., $\Delta\omega/\bar{\omega} \simeq 0.25$. Finally, Run 10 was a case in which both f_1 and f_2 were shifted, considerably higher than those in the other cases, to a range so that $S_D{}^R(\omega_2) \simeq S_D{}^R(\omega_1)/3$, see Fig. 16.

b) Joint Displacement When Incoherent Ground Motion Is Due To A Phase Delay

If in addition to the change in ground stiffness, there is a phase delay τ in the ground motion, then

$$\Delta z(t) = \tau\, \dot{\bar{z}}(t) \tag{75}$$

and recalling Eq. (8),

$$R_{\Delta z}(t, \omega_k, \xi_k) = \tau\, R_V(t, \omega_k, \xi_k) = \tau\, \dot{R}_{\bar{z}}(t, \omega_k, \xi_k) \tag{76}$$

Thus, Eq. (49) becomes

$$\Delta x(t) = P_1\left[R_{\bar{z}}(t, \omega_1, \xi_1) + \tau \frac{Q_1}{P_1} \dot{R}_{\bar{z}}(t, \omega_1, \xi_1)\right]$$
$$- P_1\left[R_{\bar{z}}(t, \omega_2, \xi_2) - \tau \frac{Q_2}{P_1} \dot{R}_{\bar{z}}(t, \omega_2, \xi_2)\right] \quad (77)$$

For small values of τ, the first and second brackets represent $R_{\bar{z}}(t + \tau\, Q_1/P_1, \omega_1, \xi_1)$ and $R_{\bar{z}}(t - \tau\, Q_2/P_1, \omega_2, \xi_2)$, respectively. Consequently,

$$\text{MAX}|\Delta x(t)| \leq P_1[S_D{}^A(\omega_1, \xi_1) + S_D{}^A(\omega_2, \xi_2)] \quad (78)$$

becomes a lower upper bound than Eq. (50), even for the case when there is an incoherent component to the input.

In Fig. 16, the dotted curve shows the interference response spectrum S_I for the EL CENTRO record corresponding to a phase delay $\tau = 0.020$ sec. Larger values of τ (within limits) would shift the curve upward proportionately. In the limited region in which $S_D{}^A < S_D{}^R$, so that Eq. (50) is more restrictive than Eq. (52), Eq. (78) would hold. However, in that region ($f < 0.1$ Hz), S_I is two orders of magnitude smaller than $S_D{}^A$, so that the difference between Eqs. (50) and (78) is negligible. For $f > 0.1$ Hz, Eq. (52), which cannot be simplified, is more restrictive. However, again referring to Fig. 16, $S_I << S_D{}^R$ and may be neglected as long as $f < 2$ Hz. For $f \simeq 4$ Hz, $S_I \simeq S_D{}^R$ so that the complete Eq. (52) must be evaluated. Finally, for very stiff systems ($f > 6$ Hz) where $S_I \simeq \tau V_{MAX}$, the quasistatic relative displacement, $S_D{}^R << S_I$ so that the top line of Eq. (52) may be neglected.

c) Maximum Joint Displacement In Terms Of Spectra

In general, the joint displacement is given by the sum of two or more time varying terms, i.e., Eq. (49) or (51). The maximum joint displacement, of course, is bounded by the absolute sum of the individual terms, i.e., Eq. (78) or (52). However, this maximum would only be achieved if all the individual maxima were to occur simultaneously, and were additive.

In similar situations in conventional structures, the square root of the sum of the squares of the modal contributions is used to estimate the total response, Ref. [17]. A similar approach was tried for the current problem when the input was coherent. The results are shown in Table III for each of the ten cases. Except for the unrealistic case of zero damping, Run 1, it appears that

$$\text{MAX}|\Delta x(t)| < P_1 \sqrt{\left[S_D{}^R(\omega_1, \xi_1)\right]^2 + \left[S_D{}^R(\omega_2, \xi_2)\right]^2} \tag{79}$$

where error in using Eq. (79) runs from 0.6% for case 2 (with $\xi_1 = 5\%$), up to almost 300% for case 8. Using only the fundamental frequency appears to give a better estimate (again excluding Run 1), i.e.,

$$\text{MAX}|\Delta x(t)| \simeq P_1 \, S_D{}^R(\omega_1, \xi_1) \tag{80}$$

While Eq. (80) would follow directly from Eq. (59), which was derived assuming a very stiff system with widely spaced frequencies, none of the ten cases satisfy these restrictions. With the possible exception of Run 10, all the frequencies are in the earthquake range (see Fig. 16) and the ratios f_2/f_1 are all less than 1.5. Nevertheless, Eq. (80) is a reasonably good estimate except for those cases in which $\Delta\omega/\bar{\omega} < \sim 0.25$; in such cases (i.e., Runs 4, 6, 7, 8 and 9) the estimate given by Eq. (80) is too high. It is especially too high for the case with closest frequencies, Run 8.

For limitingly small values of $\Delta\omega/\bar{\omega}$, from Eq. (65), one may write

$$\text{MAX}|\Delta x(t)| = 2P_1 \frac{\Delta\omega}{\bar{\omega}} G(\bar{\omega}, \bar{\xi}, \bar{z}) \tag{81}$$

where the function G, the maximum value of the integral in Eq. (65), depends implicitly on $\bar{z}(t)$ and the average parameters $\bar{\omega}$ and $\bar{\xi}$, but not on $\Delta\omega/\bar{\omega}$. If it is assumed that Eq. (80) holds for $\Delta\omega/\bar{\omega} \geq 0.25$ and Eq. (81) for $\Delta\omega/\bar{\omega} \leq 0.25$, one may obtain by equating the two expressions at $\Delta\omega/\bar{\omega} = 0.25$

$$G(\bar{\omega}, \bar{\xi}, \bar{z}) = 2S_D{}^R(\omega_1, \xi_1) \tag{82}$$

Table III: Estimates of Joint Displacement for Two Degree of Freedom System Using Computed Relative Spectra for El Centro N-S Record

Run	f_1 (Hz)	f_2 (Hz)	ξ_1 (%)	ξ_2 (%)	$\Delta\omega/\bar{\omega}$	$S_D^R(\omega_1,\xi_1)$ (cm)	$S_D^R(\omega_2,\xi_2)$ (cm)	MAX$\lvert\Delta x\rvert$ (cm)	$P_1\sqrt{S_1^2+S_2^2}$ (cm)	Error (%)	P_1S_1 (cm)	Error (%)
1	0.9398	1.2715	0	0	0.300	21.99	17.01	27.24	20.34	-25.3	16.09	-40.9
2	0.9398	1.2715	5	6.76	0.300	12.61	7.86	10.81	10.87	0.6	9.22	-14.6
3	0.9398	1.2715	10	13.53	0.300	8.78	5.83	6.88	7.71	12.2	6.42	- 6.6
4	0.9851	1.2367	10	12.55	0.226	8.84	6.32	3.73	4.86	30.2	3.95	5.9
5	1.0913	1.5195	10	13.92	0.328	7.83	5.78	7.64	8.71	14.1	7.01	- 8.2
6	1.1817	1.4504	10	12.27	0.204	7.37	6.10	4.50	6.76	50.1	5.21	15.6
7	1.1817	1.4504	20	24.55	0.204	5.05	4.42	2.39	4.75	98.5	3.57	49.4
8	1.5718	1.7405	20	22.15	0.102	4.83	4.14	0.71	2.84	298	2.16	202
9	1.3004	1.6760	20	25.78	0.252	4.93	3.94	3.12	5.64	80.8	4.41	41.2
10	2.1096	3.0902	20	29.30	0.377	2.82	0.965	1.87	2.92	56.5	2.77	48.1

Using Eq. (82) and $S_D^R(\omega_1, \xi_1) \simeq S_D^R(\bar{\omega}, \bar{\xi})$ for small $\Delta\omega/\bar{\omega}$, Eq. (81) becomes

$$\text{MAX}|\Delta x(t)| \simeq 4P_1 \frac{\Delta\omega}{\bar{\omega}} S_D^R(\bar{\omega}, \bar{\xi}) \quad , \Delta\omega/\bar{\omega} < 0.25 \tag{83}$$

The values given by Eq. (83) for Runs 4, 6, 7, 8 and 9 are given in Table IV, along with the previous results given by Eq. (80). It is seen that the relative error for Run 8, which has the smallest value of $\Delta\omega/\bar{\omega}$, is reduced substantially.

Thus, for the limited number of cases considered, one may conclude that by using Eq. (80) when $\Delta\omega/\bar{\omega} > 0.25$, and Eq. (83) for $\Delta\omega/\bar{\omega} < 0.25$, the maximum joint displacement may be estimated to within about 30%. The exception is Run 10 in which the cause for the poor estimate was examined earlier in Fig. 19. In absolute terms, the difference is less than 1 cm.

The natural frequencies for all the cases considered were in the range $0.9 < f < 3.1$ Hz. Referring to Fig. 16, this is in the range in which $S_D^R < S_D^A$ and $S_D^R >> S_I$. For very soft systems (which are not realistic for pipelines), the "sum" of the absolute spectra, following Eq. (78), would produce a lower bound. Following Eq. (57), one suspects that a reasonable estimate might be

$$\text{MAX}|\Delta x(t)| \simeq P_1 S_D^A(\omega_2, \xi_2) \tag{84}$$

in the range $f_1 < f_2 < 0.1$ Hz. Finally, for very stiff systems (say $f_2 > 6$ Hz), $S_D^R << S_I$, so that the difference in stiffness is unimportant and the joint displacement is given in terms of the interference spectra only. Noting that for very stiff systems both $R_{\Delta z}(t, \omega_1, \xi_1)$ and $R_{\Delta z}(t, \omega_2, \xi_2)$ approach $\Delta z(t)$, one may write

$$\text{MAX}|\Delta x(t)| \simeq Q_1 S_I(\omega_1, \xi_1) + Q_2 S_I(\omega_2, \xi_2) \simeq (Q_1 + Q_2) \tau V_{max} \tag{85}$$

where Eq. (75) has been used.

Table IV: Estimates of Joint Displacement for Two Degree of Freedom System with Closely Spaced Frequencies (Coherent El Centro N-S Input)

Run	f_1 (Hz)	f_2 (Hz)	ξ_1 (%)	Eq. (80) (cm)	Error (%)	MAX$\|\Delta x\|$ (cm)	$\bar{f}$ (Hz)	$\bar{\xi}$ (%)	$\frac{\Delta\omega}{\bar{\omega}}$	Eq. (83) (cm)	Error (%)
4	0.9851	1.2367	10	3.95	5.9	3.73	1.1109	11.3	0.226	3.026	-18.9
6	1.1817	1.4504	10	5.21	15.6	4.50	1.3161	11.1	0.204	3.868	-14.1
7	1.1817	1.4504	20	3.57	49.4	2.39	1.3161	22.3	0.204	2.828	+18.3
8	1.5718	1.7405	20	2.16	202	0.71	1.6562	21.1	0.102	0.7473	+ 4.5
9	1.3004	1.6760	20	4.41	41.2	3.12	1.4882	22.9	0.252	4.126	32.1

V. SUMMARY AND CONCLUSIONS

Transition zones between soil types are locations in which disproportionate pipe damage occurs due to seismic shaking. In the present report, the various possible effects of local inhomogeneities on the axial response of pipelines were considered individually. While in reality all may occur simultaneously, by examining the effects separately, their importance may be determined.

If the ground inhomogeneity results in a local variation in phase delay, the variation does not cause a major change in the pipe response. If the average phase delay remains constant, the effect on pipe response is of second order. Moreover, the response due to phase delay is always less than that which would occur at a soft homogeneous site.

Not surprisingly, amplification of the pipe joint response occurs when there is a large variation in the incoherent component of the free field ground motion due to changes in the waveforms caused by inhomogeneities. The general case is beyond the scope of this paper. However, for the case of a plane P-wave travelling horizontally incident on a vertical plane interface, amplifications as large as two occur, relative to that in a homogeneous soft site. In general, it appears as if the amplification in joint response is proportional to that in the incoherent free field ground motion.

A major cause of large joint motion results from the change in local soil stiffness caused by local inhomogeneities. A simplified two degree of freedom model was examined, and significant joint motion can result even for a coherent input. This joint motion can be several times that which would occur due to a phase delay only. Various special cases were considered. For coherent input, it was shown that the joint response approaches zero linearly as $\Delta\omega/\bar{\omega} \to 0$. Relatively simple expressions, e.g.,

Eqs. (80) and (83), were developed to estimate the joint response in terms of spectra. Finally, it was shown that the response of a two degree of freedom system closely corresponds to that of a multi-link system.

REFERENCES

[1] Weidlinger, P. and Nelson, I., "Seismic Analysis of Lifelines with Interference Response Spectra," Grant Report No. 7, prepared for National Science Foundation (RANN), Grant Nos. ENV P76-9838 and PFR 78-15049, Weidlinger Associates, New York, New York, June 1978.

[2] Weidlinger, P. and Nelson, I., "Seismic Analysis of Lifelines with Interference Response Spectra," presented at ASCE Fall Convention, Preprint No. 3312, Chicago, Illinois, October 16 - 20, 1978.

[3] Nelson, I., "Interference Response Spectra - A Tool for Lifeline Seismic Analysis," EERI Newsletter, Vol. 13, No. 2, March 1979, pp. 62-63.

[4] Nelson, I. and Weidlinger, P., "Dynamic Seismic Analysis of Long Segmented Lifelines," Grant Report No. 10, prepared for National Science Foundation (ASRA), Grant No. PFR 78-15049, Weidlinger Associates, New York, New York, November 1978.

[5] Nelson, I. and Weidlinger, P., "Dynamic Seismic Analysis of Long Segmented Lifelines," presented at ASME Annual Winter Meeting, Paper No. 78-WA/PVP-4, San Francisco, California, December 10 - 15, 1978; also, J. Pressure Vessel Technology, ASME, Vol. 101, No. 1, February 1979, pp. 10 - 20.

[6] Kubo, K., Katayama, T. and Ohashi, A., "Present State of Lifeline Earthquake Engineering in Japan," The Current State of Knowledge of Lifeline Earthquake Engineering, Proceedings of TCLEE Specialty Conference, University of California, ASCE, August 30-31, 1977, p. 121.

[7] Shinozuka, M. and Kawakami, H., "Underground Pipe Damages and Ground Characteristics," The Current State of Knowledge of Lifeline Earthquake Engineering, Proceedings of TCLEE Specialty Conference, University of California, ASCE, August 30-31, 1977, pp. 293 - 307.

[8] Shinozuka, M. and Kawakami, H., "Underground Pipe Damages and Ground Characteristics," Technical Report No. CU-1, prepared for National Science Foundation (RANN), Grant No. ENV 76-09838, Columbia University, New York, New York, June 1977.

[9] Shinozuka, M. and Kawakami, H., "Ground Characteristics and Free Field Strains," Technical Report No. CU-2, prepared for National Science Foundation (RANN), Grant No. ENV 76-09838, Columbia University, New York, New York, August 1977.

[10] Wang, L.R.-L. and Cheng, K.-M., "Seismic Response Behavior of Buried Pipelines," presented at ASME Annual Winter Meeting, Paper No. 78-WA/PVP-5, San Francisco, California, December 5 - 10, 1978; also, J. Pressure Vessel Technology, ASME, Vol. 101, No. 1, February 1979, pp. 21 - 30.

[11] Wang, L.R.-L and Cheng, K.-M, "Seismic Response Behavior of Buried Pipelines," Technical Report (SVBDUPS Project) No. 5, prepared for National Science Foundation (RANN), Grant No. ENV 76-14884, Rensselaer Polytechnic Institute, Troy, New York, June 1978.

[12] Hindy, A. and Novak, M., "Earthquake Response of Underground Pipelines," GEOT-1-1978, Faculty of Engineering Science, University of Western Ontario, London, Ontario, 1978.

[13] Wojcik, G.L., "Resonance Zones on the Surface of a Dipping Layer Subjected to Plane SH Seismic Input," Grant Report No. 11, prepared for National Science Foundation (ASRA), Grant No. PFR 78-15049, Weidlinger Associates, Menlo Park, California, January 1979.

[14] Drake, L.A. and Mal, A.K., "Love and Rayleigh Waves in the San Fernando Valley," Bulletin of the Seismological Society of America, Vol. 62, No. 6, December 1972, pp. 1673 - 1690.

[15] Nelson, I., "Seismic Response of Segmented Pipelines with Varying Stiffness and End Conditions," forthcoming technical report, prepared for National Science Foundation (ASRA), Grant No. PFR 78-15049, Weidlinger Associates, New York, New York.

[16] Nelson, I. and Weidlinger, P., "Development of Interference Response Spectra for Lifelines Seismic Analysis," Interim Grant Report No. IR-2, prepared for National Science Foundation (RANN), Grant No. ENV P76-9838, Weidlinger Associates, New York, New York, July 1, 1977.

[17] Newmark, N.M. and Rosenbleuth, E., Fundamentals of Earthquake Engineering, Prentice-Hall, Inc., Englewood Cliffs, New Jersey, 1971.

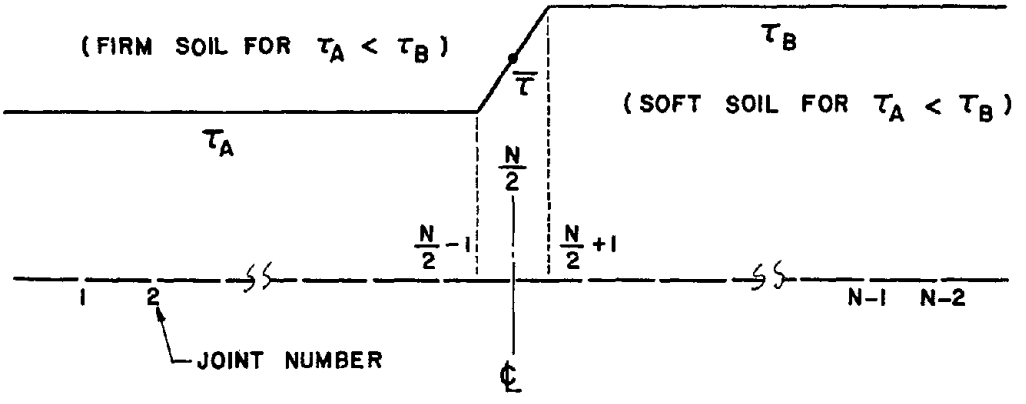

FIG. 1 VARIATION IN PHASE DELAY τ

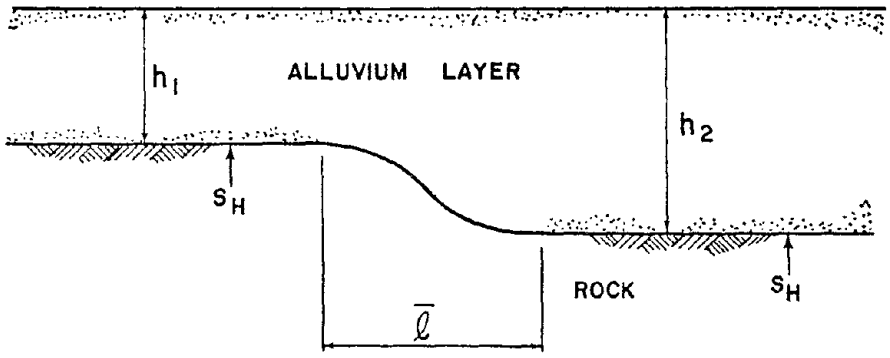

FIG. 2 NON UNIFORM LAYER SUBJECTED TO A VERTICALLY INCIDENT SH WAVE

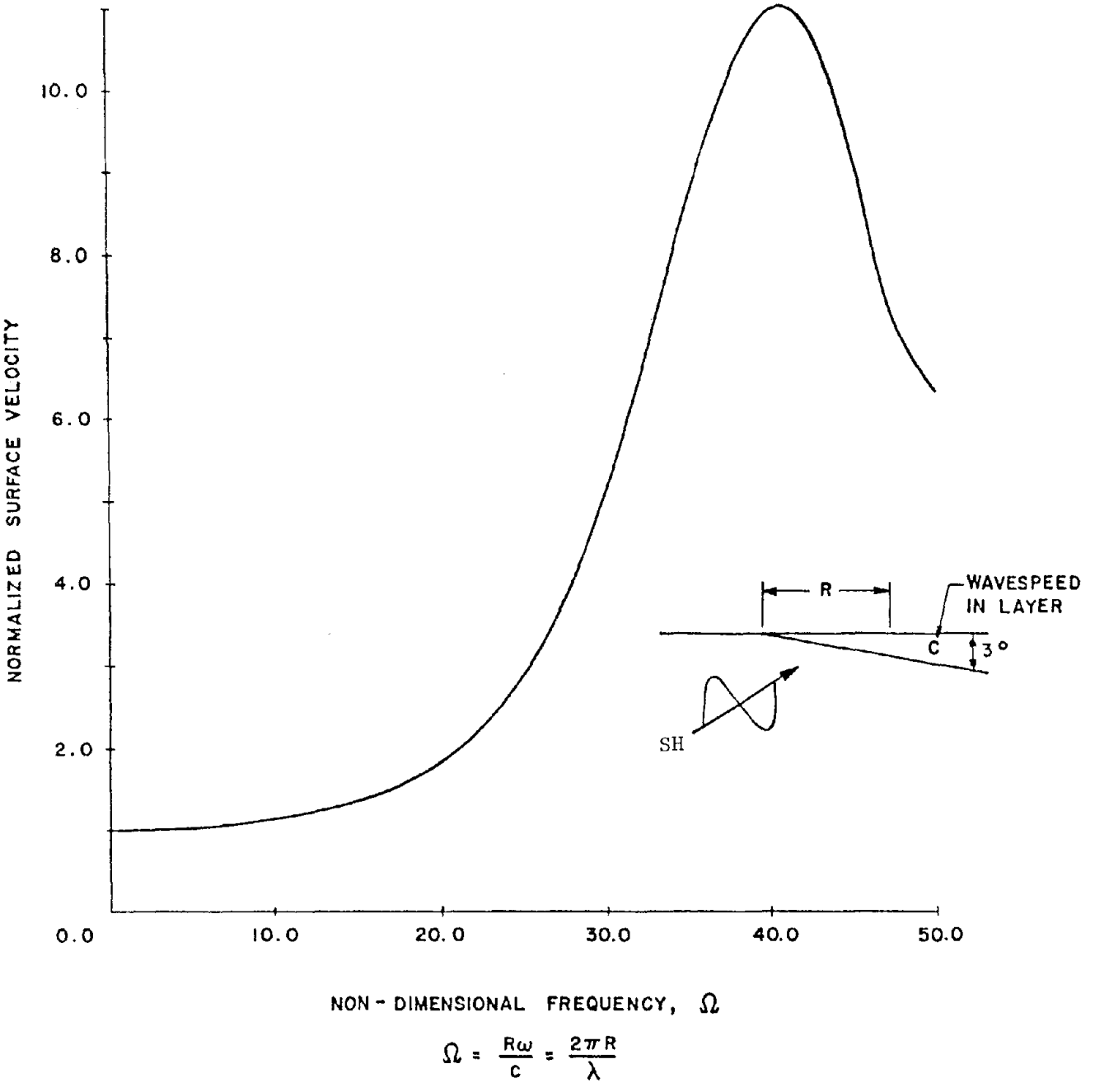

FIG. 3 HARMONIC AMPLITUDE OF SURFACE VELOCITY AS A FUNCTION OF NON-DIMENSIONAL FREQUENCY (AFTER WOJCIK, REF [13])

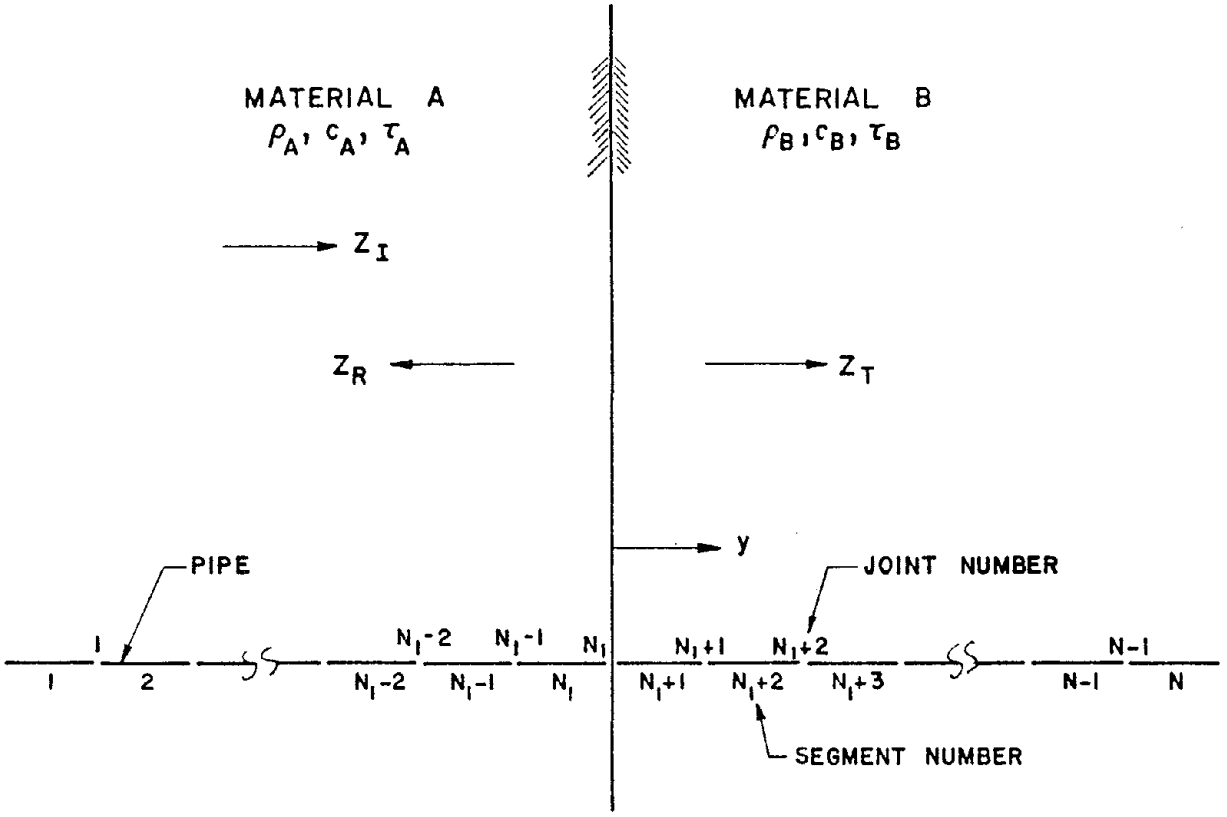

FIG. 4 PLANE P-WAVE INCIDENT ON A VERTICAL INTERFACE

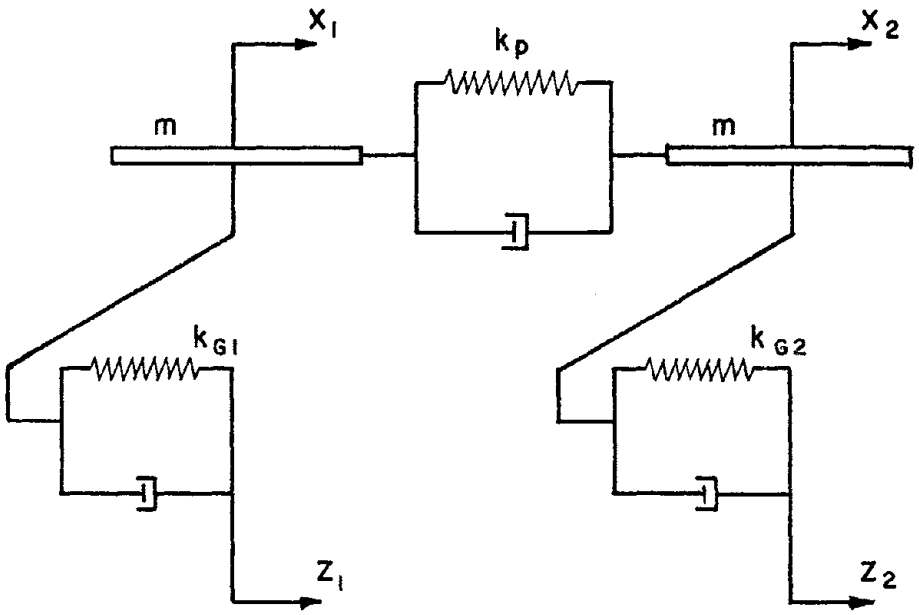

FIG. 5 TWO DEGREE OF FREEDOM SYSTEM

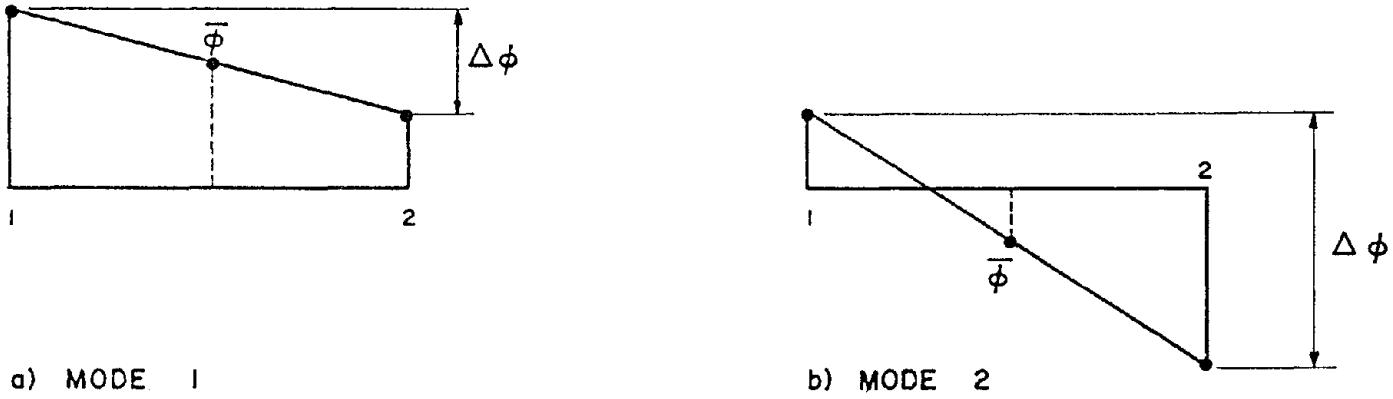

FIG. 6 NORMALIZED MODE SHAPES OF TWO DEGREE OF FREEDOM SYSTEM (DRAWN FOR $\kappa=(k_{G2}-k_{G1})/2k_p = 1$)

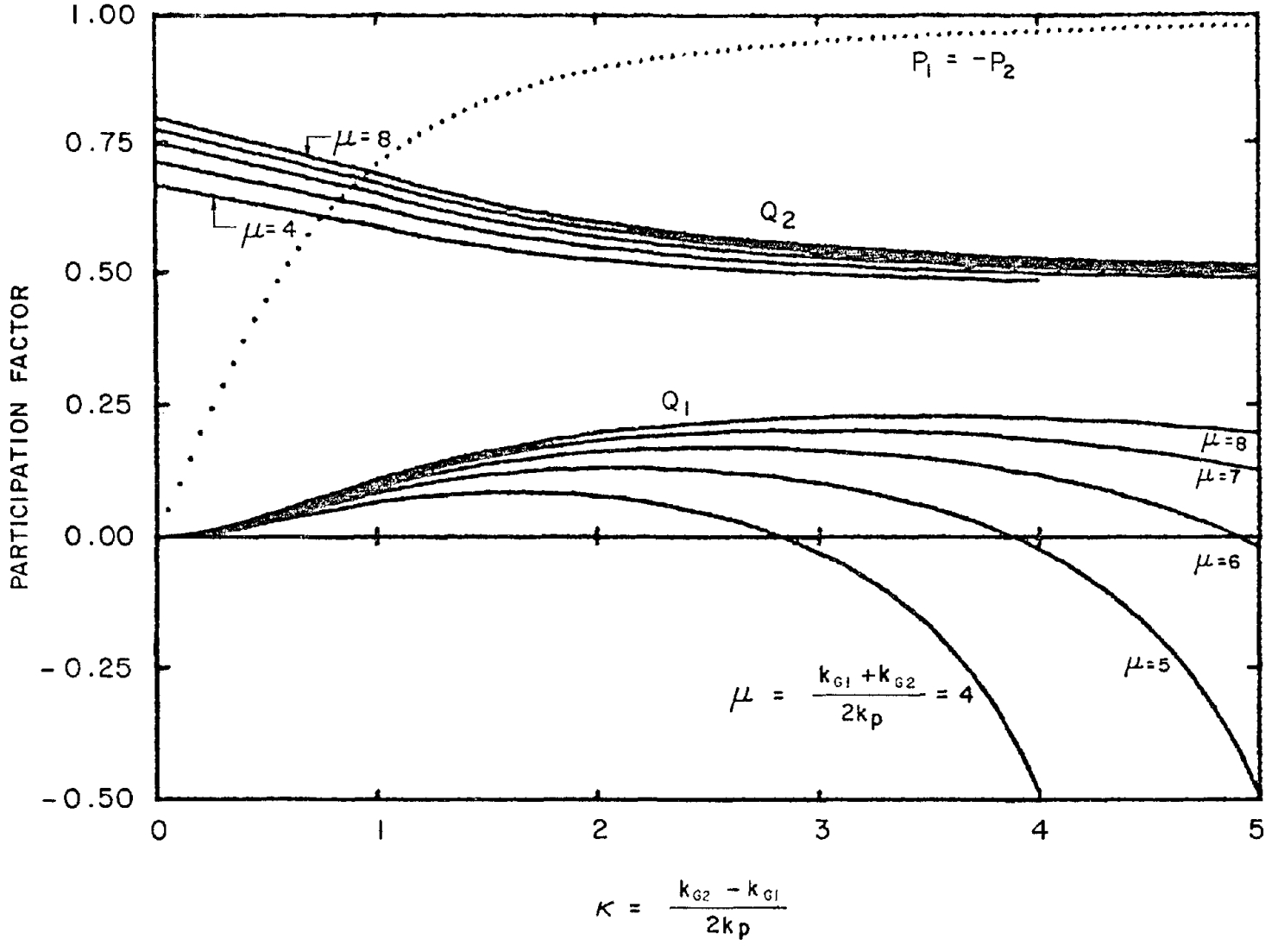

FIG. 7 VARIATION OF PARTICIPATION FACTORS WITH KAPPA AND MU

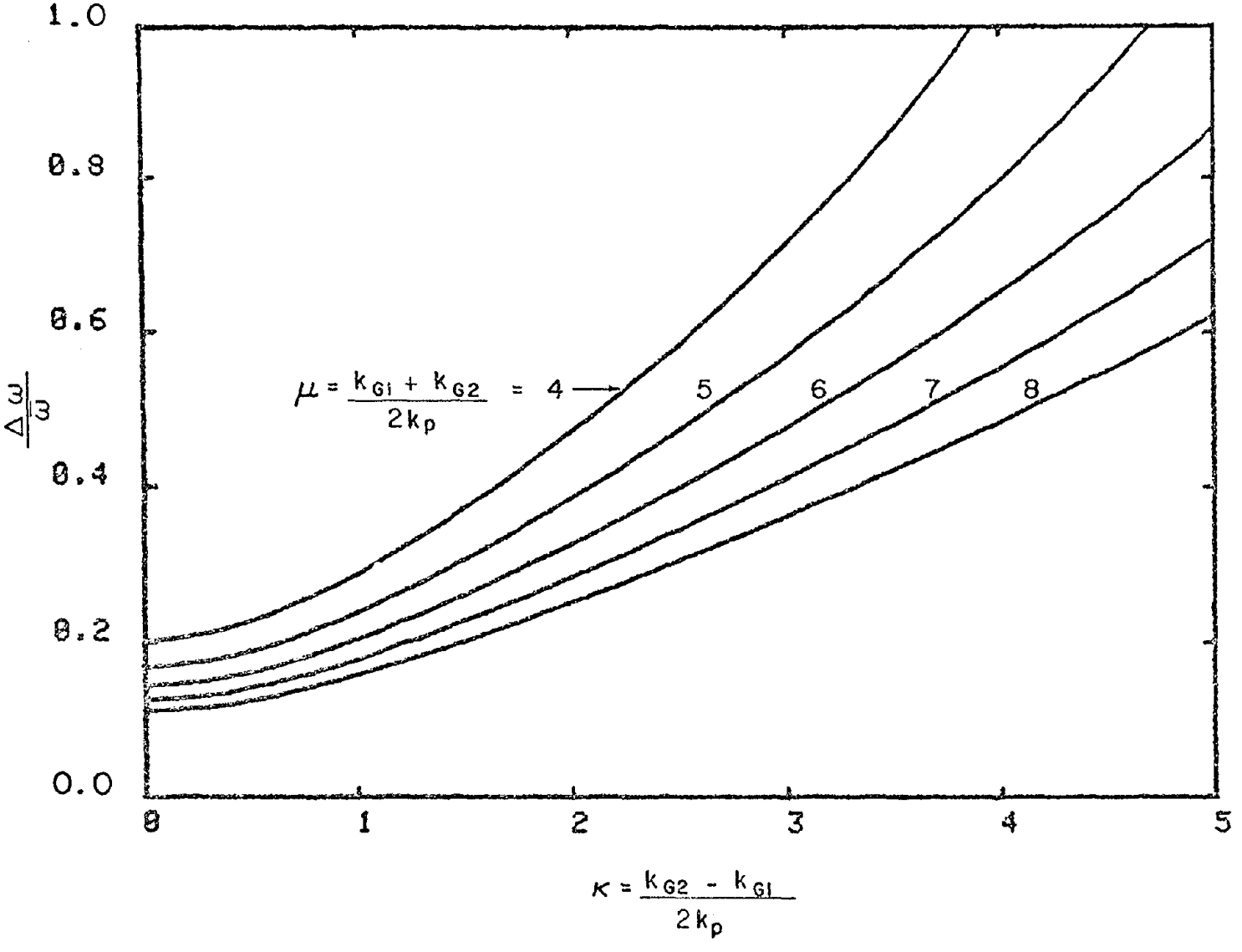

FIG. 8 VARIATION IN $\Delta\omega/\bar{\omega} = 2(\omega_2 - \omega_1)/(\omega_1 + \omega_2)$ WITH κ AND μ

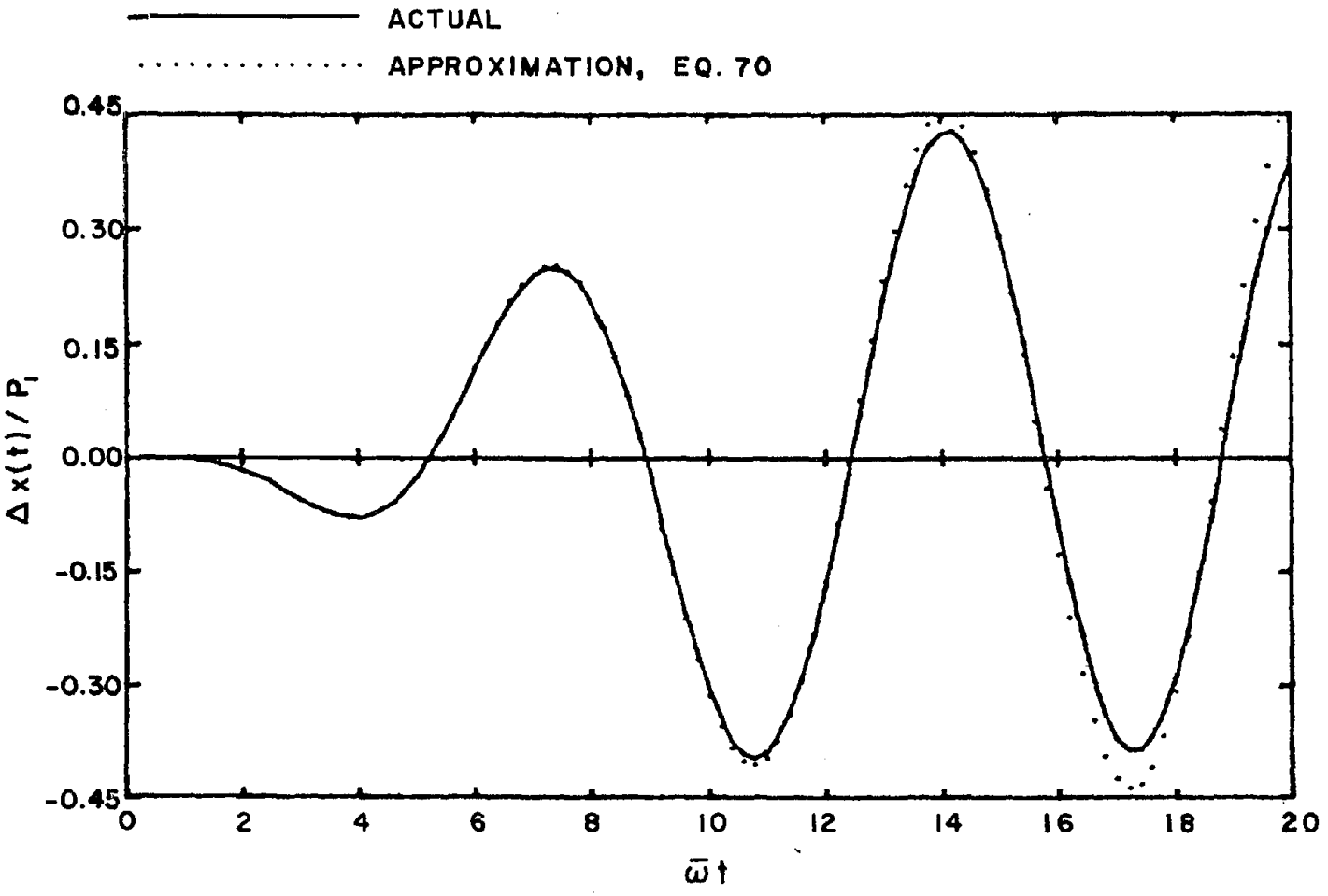

FIG. 9 JOINT DISPLACEMENT DUE TO COHERENT HAVERSINE INPUT $\bar{z}(t) = (1-\cos \Omega t)/2$, FOR $\Delta\omega/\bar{\omega} = 0.1$ AND $\Omega/\bar{\omega} = 0.6$, DAMPING NEGLECTED

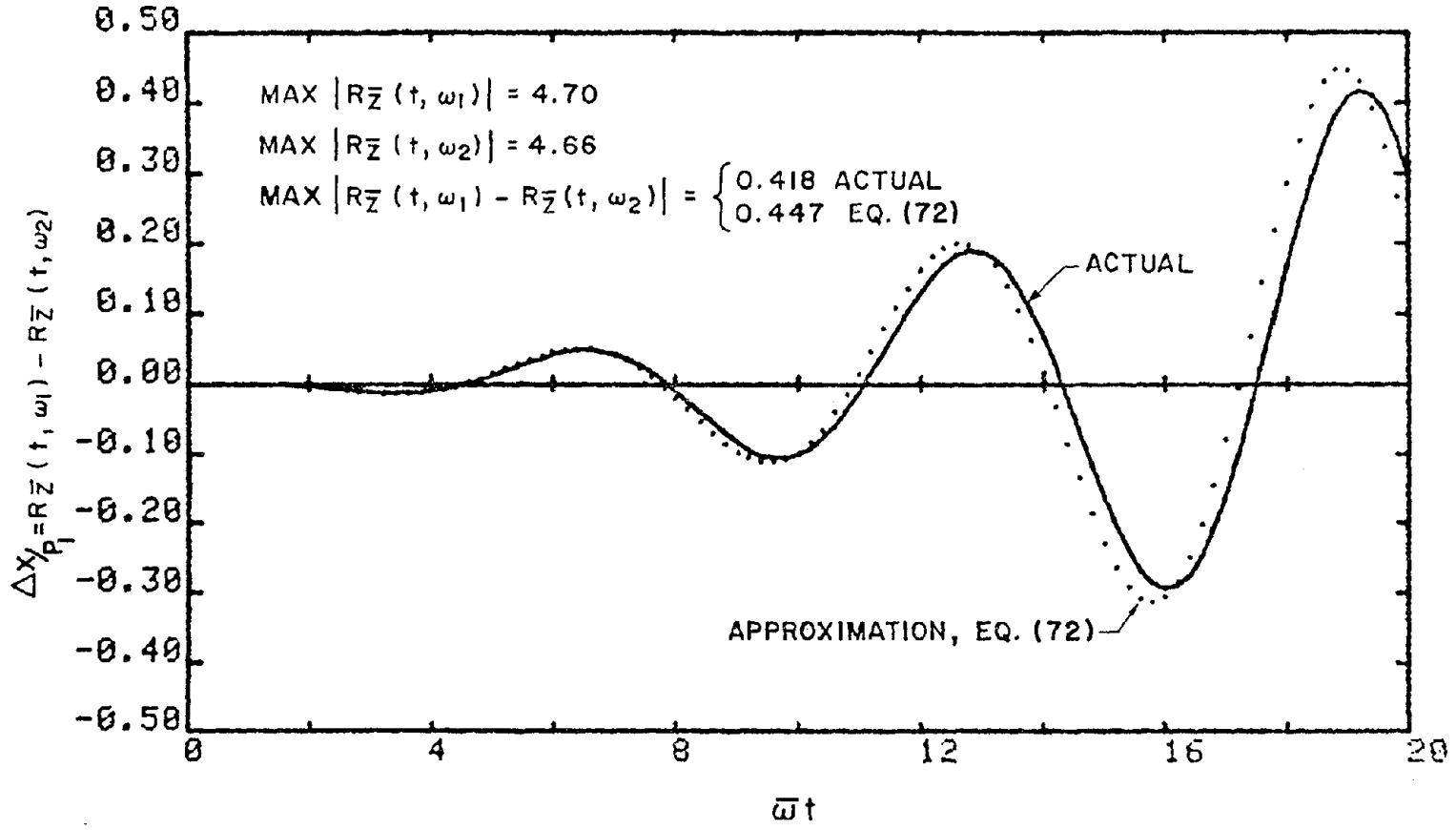

FIG.10 DIFFERENCE IN RESPONSE $R_{\bar{Z}}(t,\omega_1) - R_{\bar{Z}}(t,\omega_2)$ WHEN $\bar{Z}(t) = (1 - \cos \Omega t)/2$ FOR $\Delta\omega/\bar{\omega} = 0.01$ AND $\Omega/\bar{\omega} = 0.95$ (NO DAMPING)

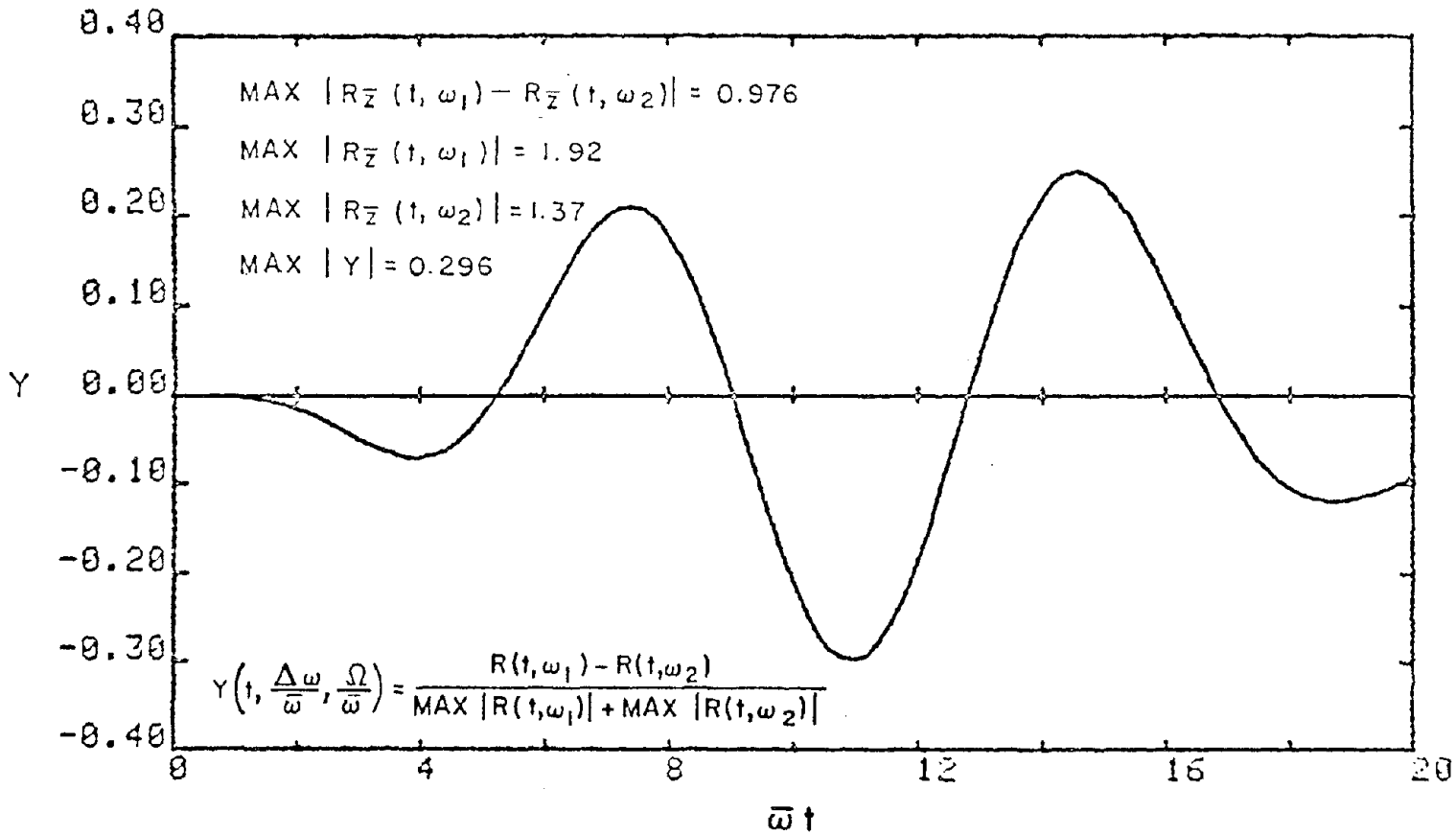

FIG. II NORMALIZED DIFFERENCE IN UNDAMPED RESPONSE WHEN $\bar{Z} = (1 - \cos \Omega t)/2$, $\Delta\omega/\bar{\omega} = 0.3$ AND $\Omega/\bar{\omega} = 0.6$

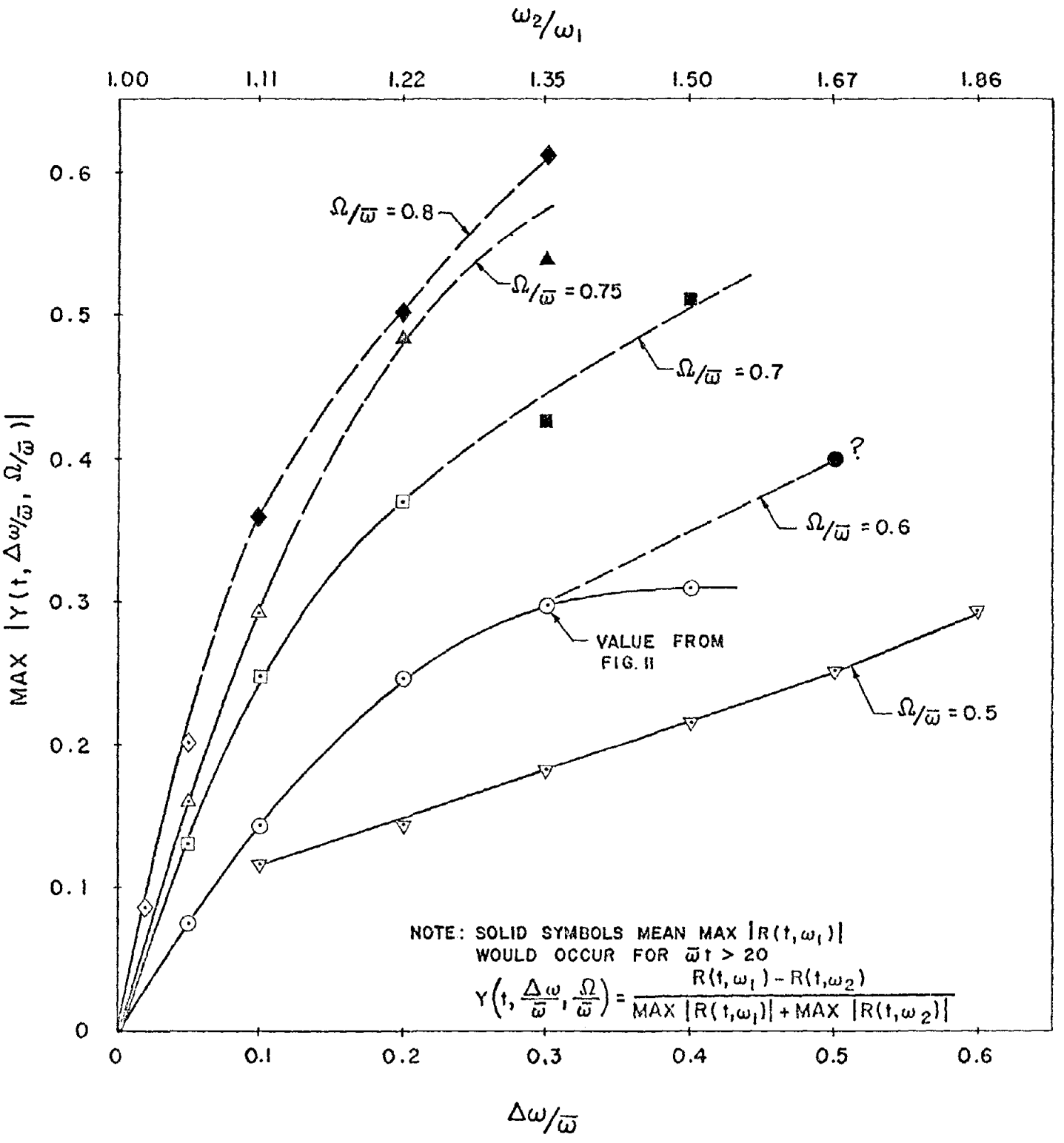

FIG. 12 MAXIMUM NORMALIZED DIFFERENCE IN UNDAMPED RESPONSE Y FOR HAVERSINE GROUND MOTION AND $\bar{\omega}t \leq 20$

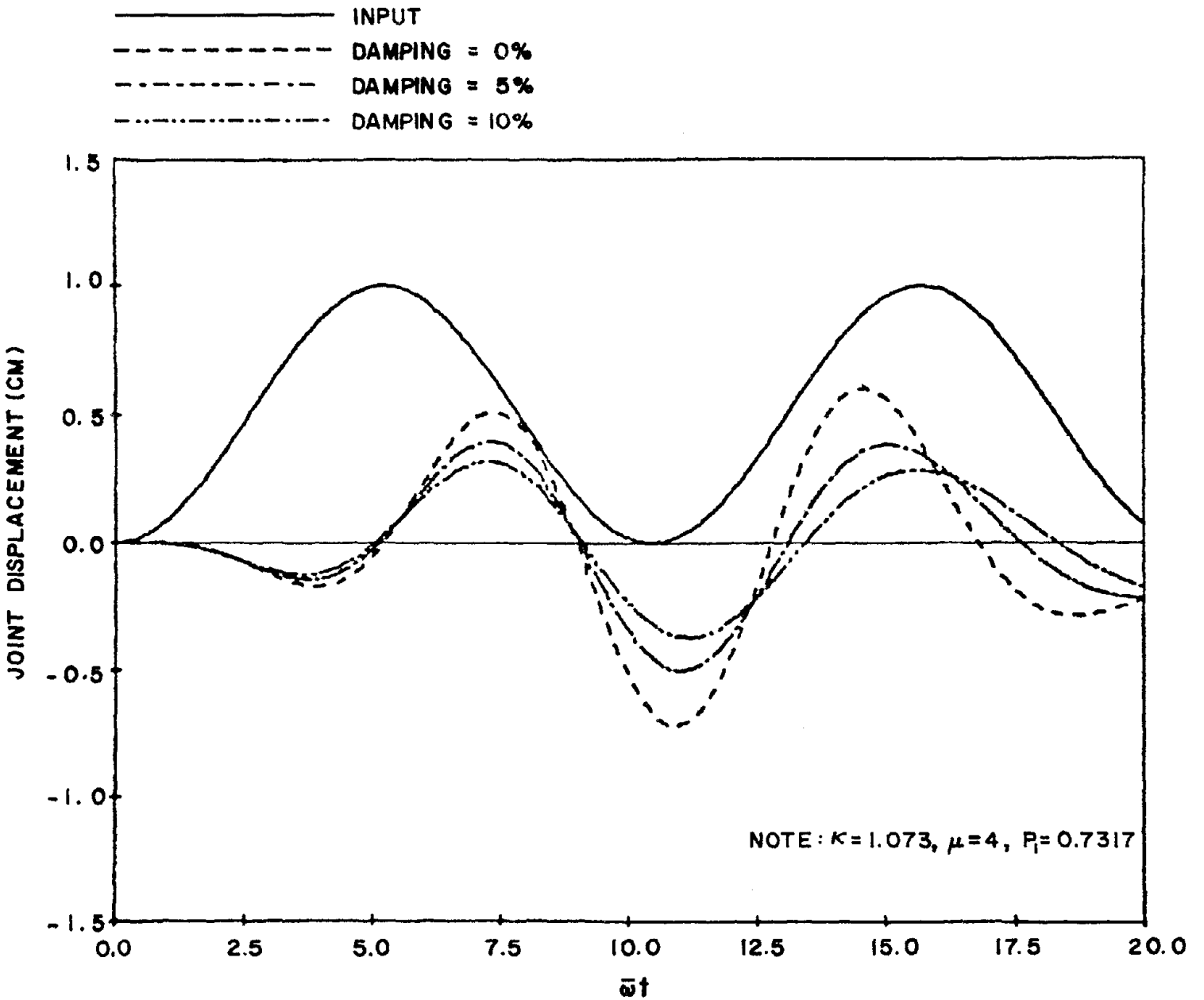

FIG.13 EFFECT OF DAMPING ON JOINT DISPLACEMENT DUE TO COHERENT HAVERSINE INPUT $\bar{z}(t) = (1-\cos \Omega t)/2$ (DRAWN FOR $\Delta\omega/\bar{\omega} = 0.3$ AND $\Omega/\bar{\omega} = 0.6$)

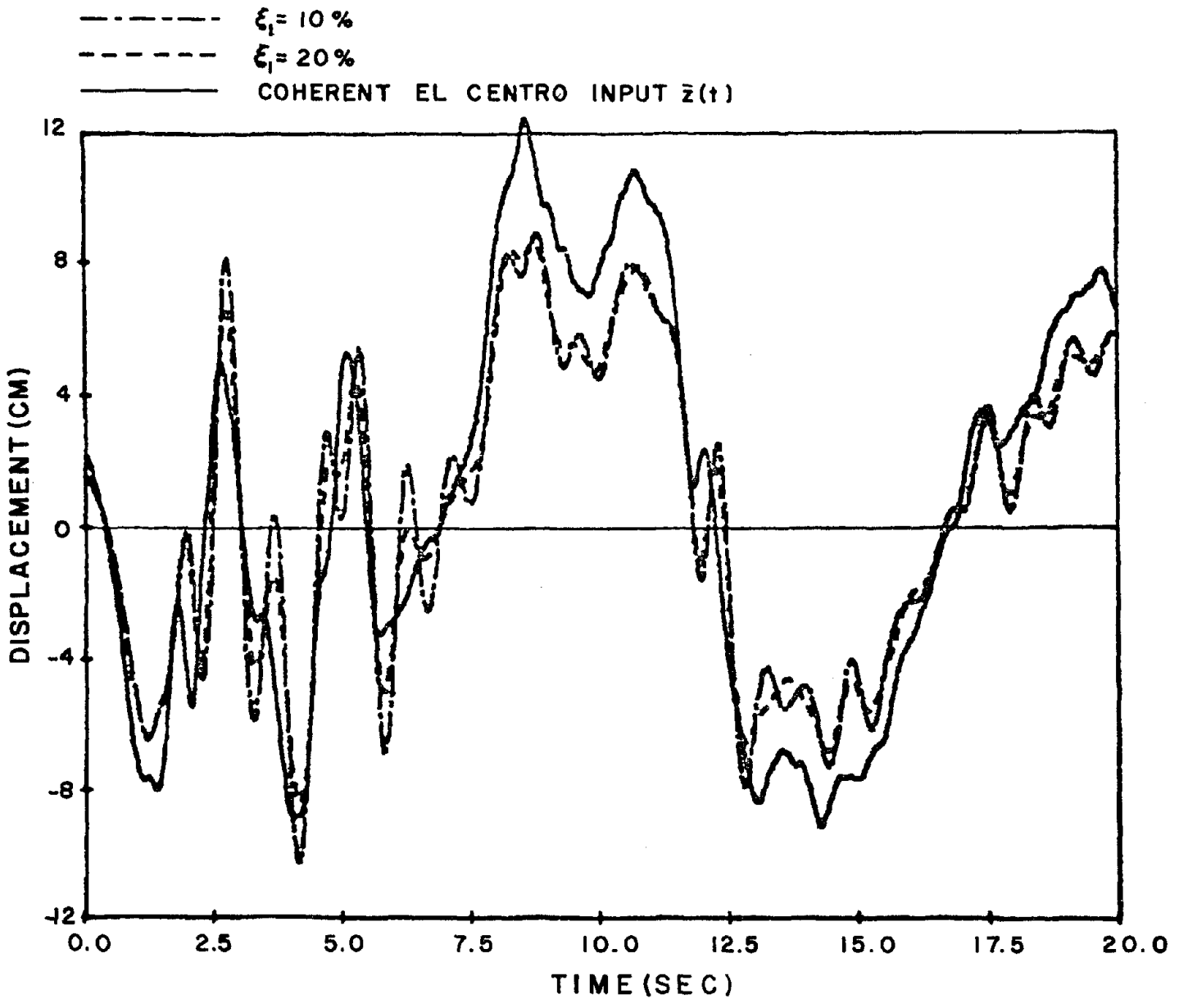

FIG.14 MODE I CONTRIBUTION TO JOINT DISPLACEMENT FOR $K_{G1}/K_{G2}/K_p$= 5/7/1 AND FOR 10% AND 20% DAMPING

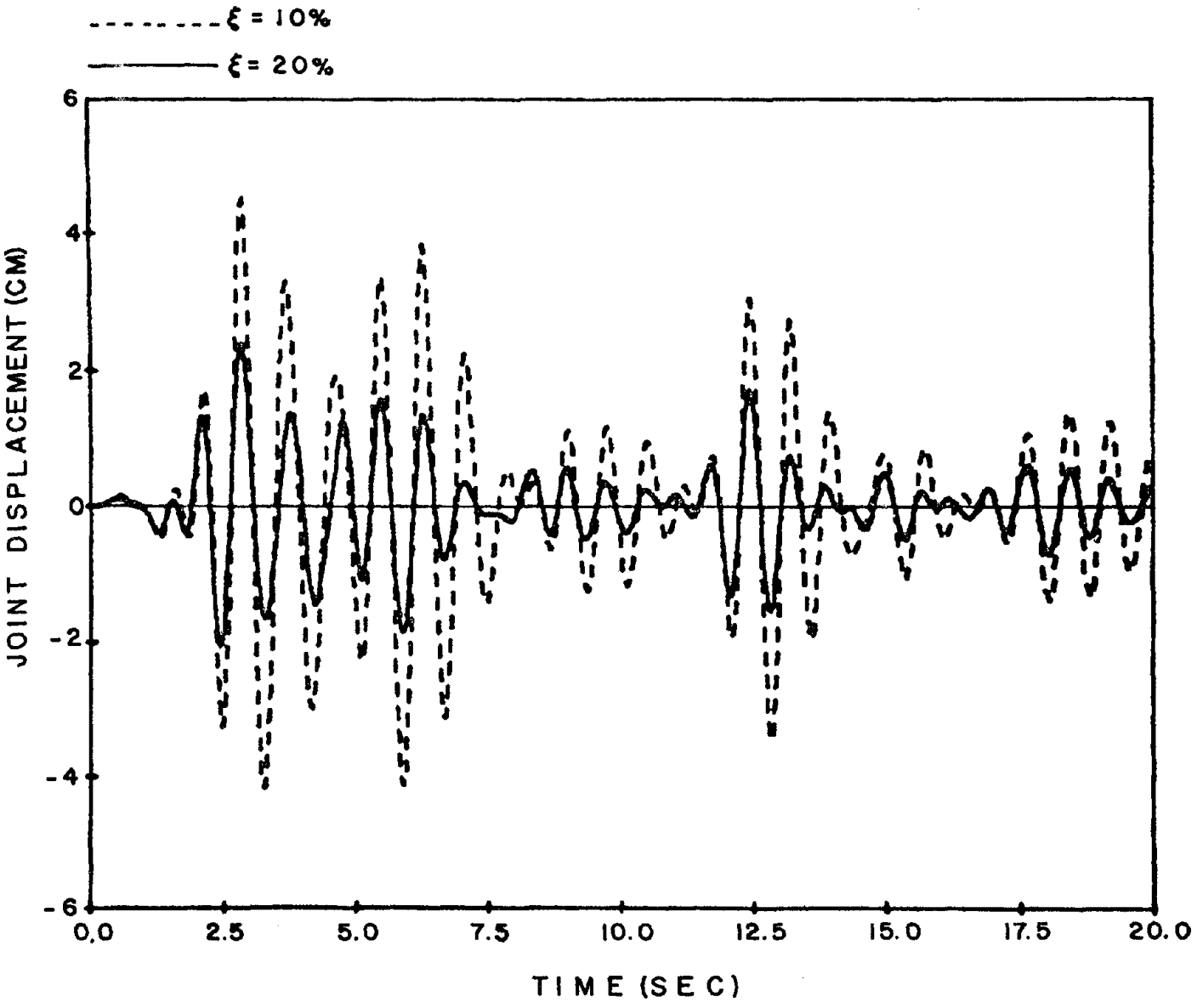

FIG.15 TOTAL JOINT DISPLACEMENT $\Delta x(t)$ DUE TO COHERENT EL CENTRO N-S INPUT FOR $K_{G1} / K_{G2} / K_p = 5/7/1$ AND FOR 10% AND 20 % DAMPING

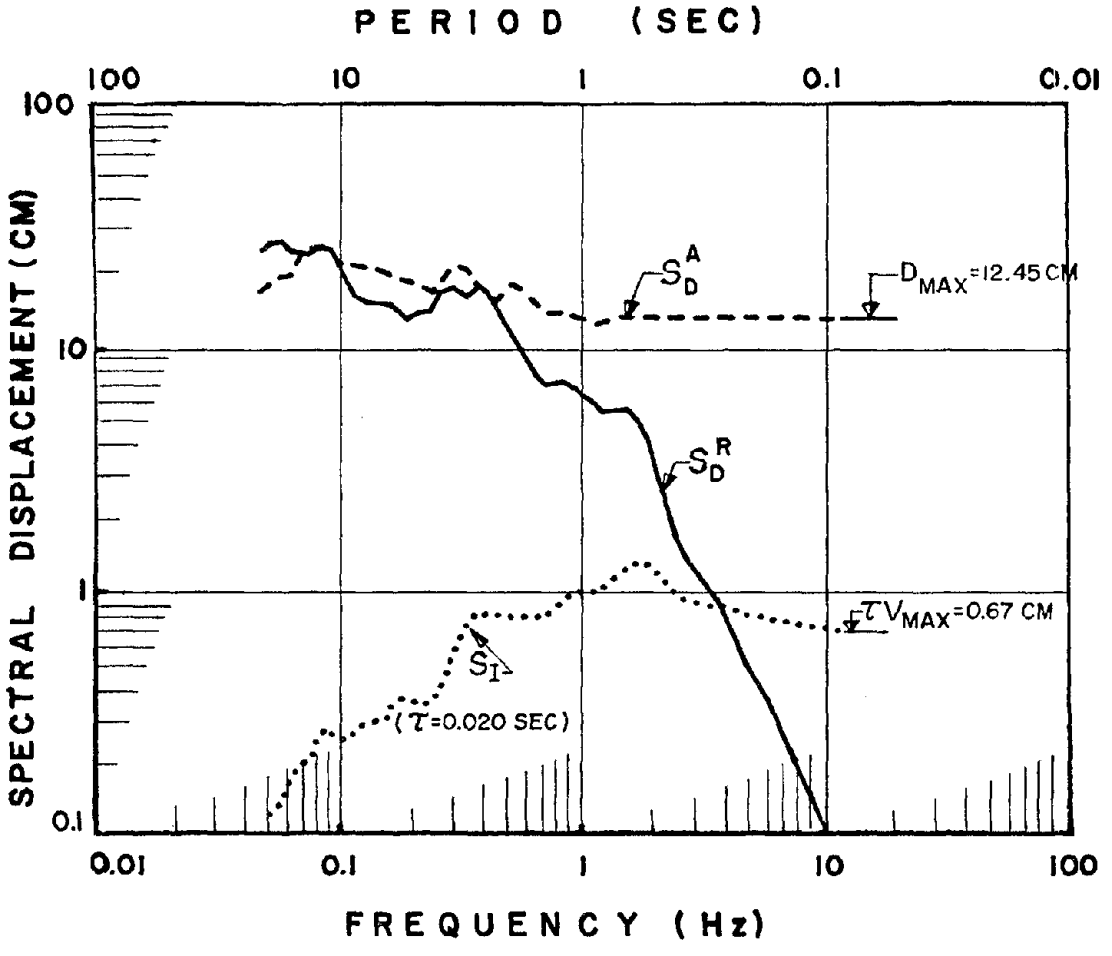

FIG.16 RELATIVE, ABSOLUTE AND INTERFERENCE RESPONSE SPECTRA FOR EL CENTRO N-S RECORD (DAMPING RATIO=0.15)

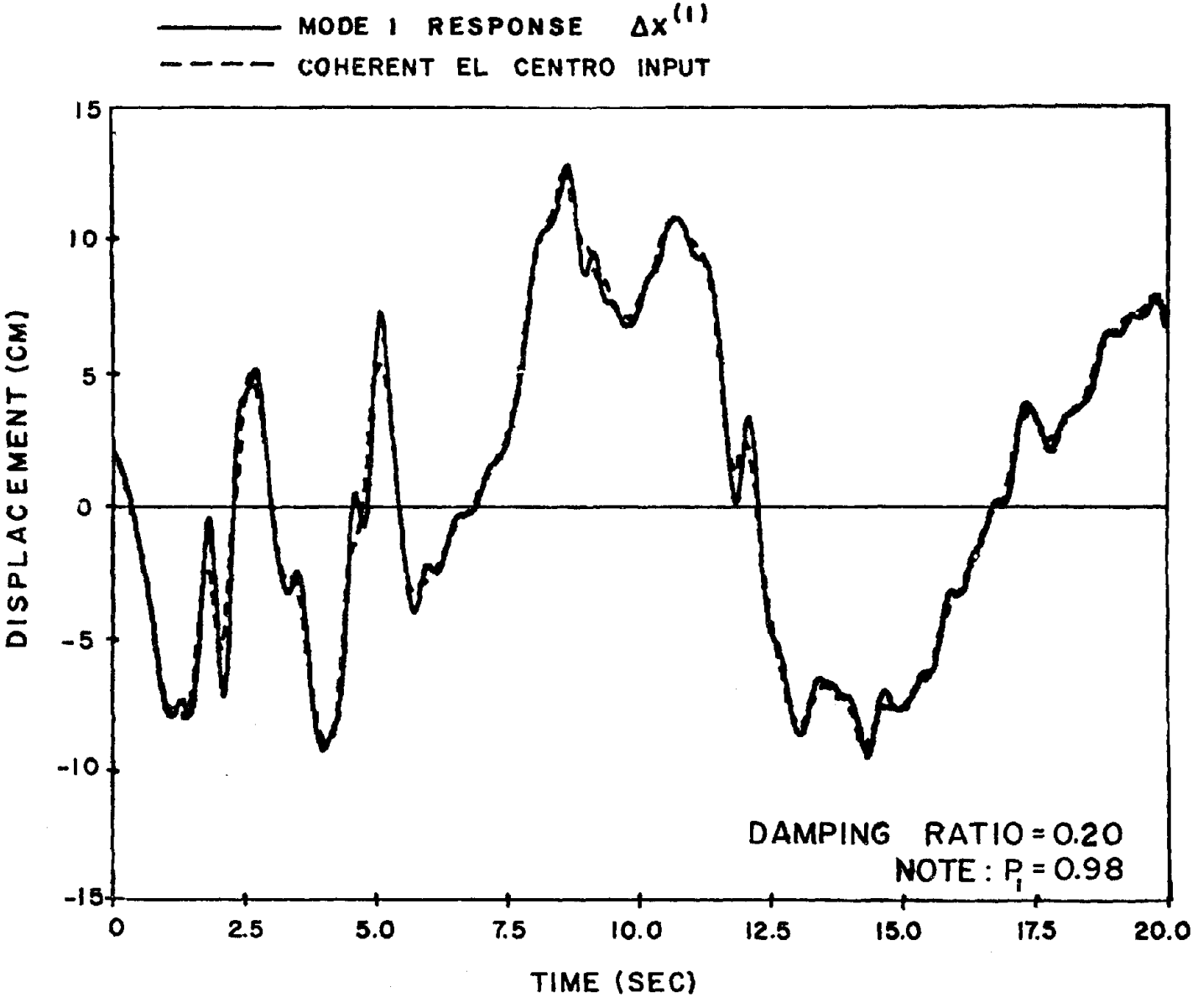

FIG.17 MODE 1 CONTRIBUTION TO JOINT DISPLACEMENT FOR 2 SEGMENT SYSTEM WITH $k_{G1}=16$, $k_{G2}=36$ AND $k_p=2$ AND COHERENT EL CENTRO N-S INPUT

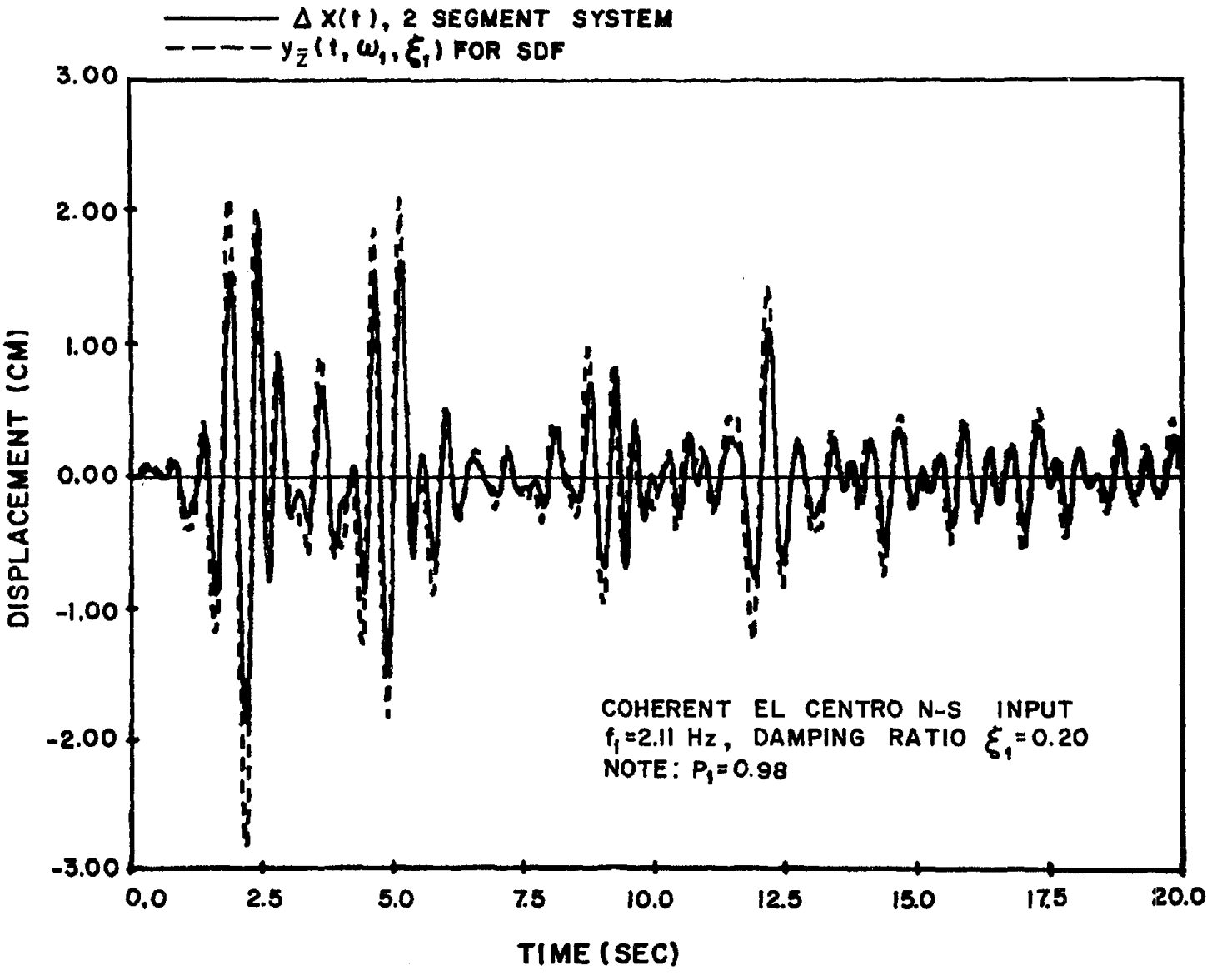

FIG.18 TOTAL JOINT RESPONSE FOR 2 SEGMENT SYSTEM WITH k_{G1}=16, k_{G2}=36 AND k_p=2 AND RELATIVE DISPLACEMENT OF A SDF REPRESENTING THE FIRST MODE.

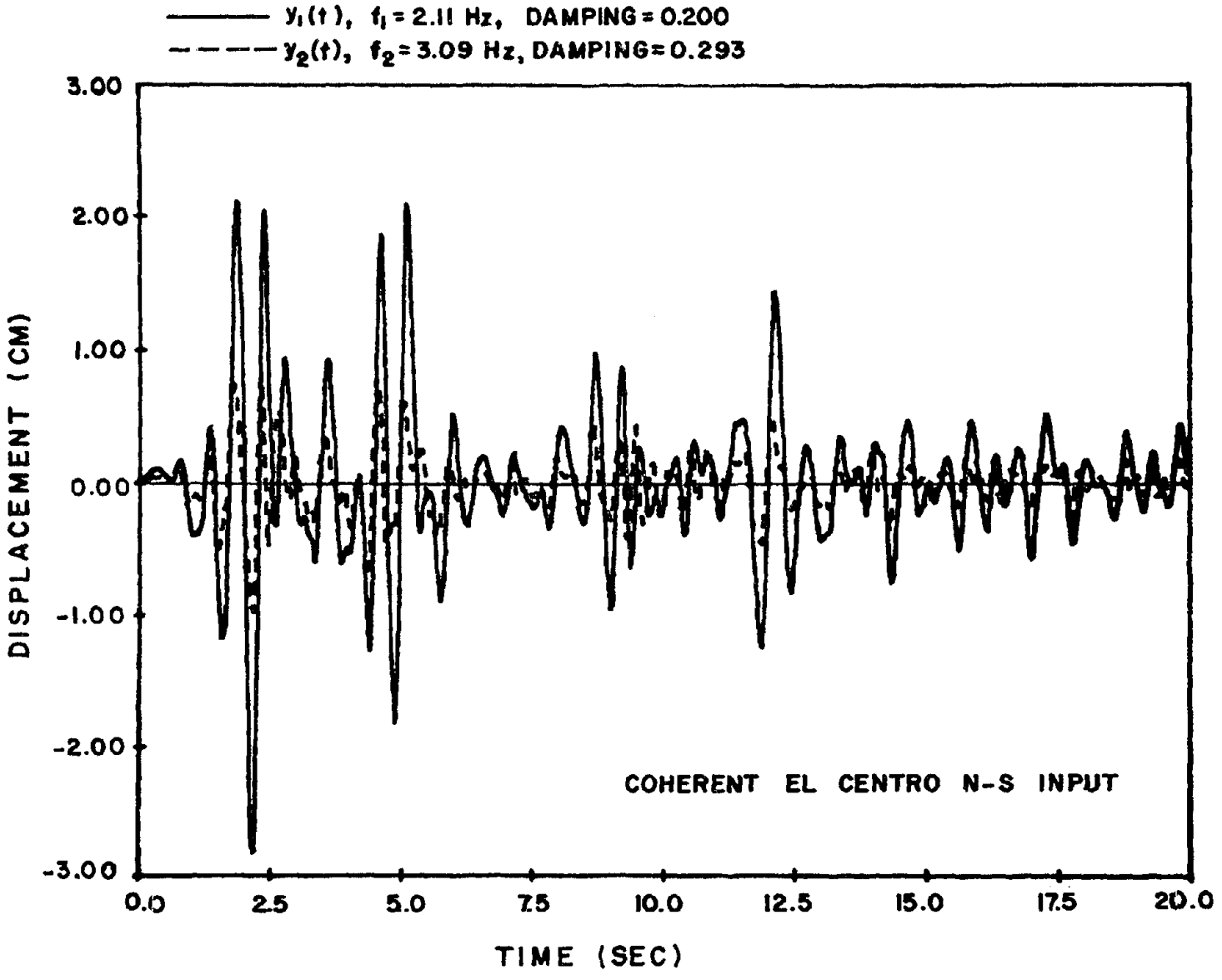

FIG.19 RELATIVE DISPLACEMENT OF THE TWO SDF OSCILLATORS CORRESPONDING TO THE TWO NORMAL MODES OF THE TWO SEGMENT SYSTEM WITH k_{G1}=16, k_{G2}=36 AND k_p=2

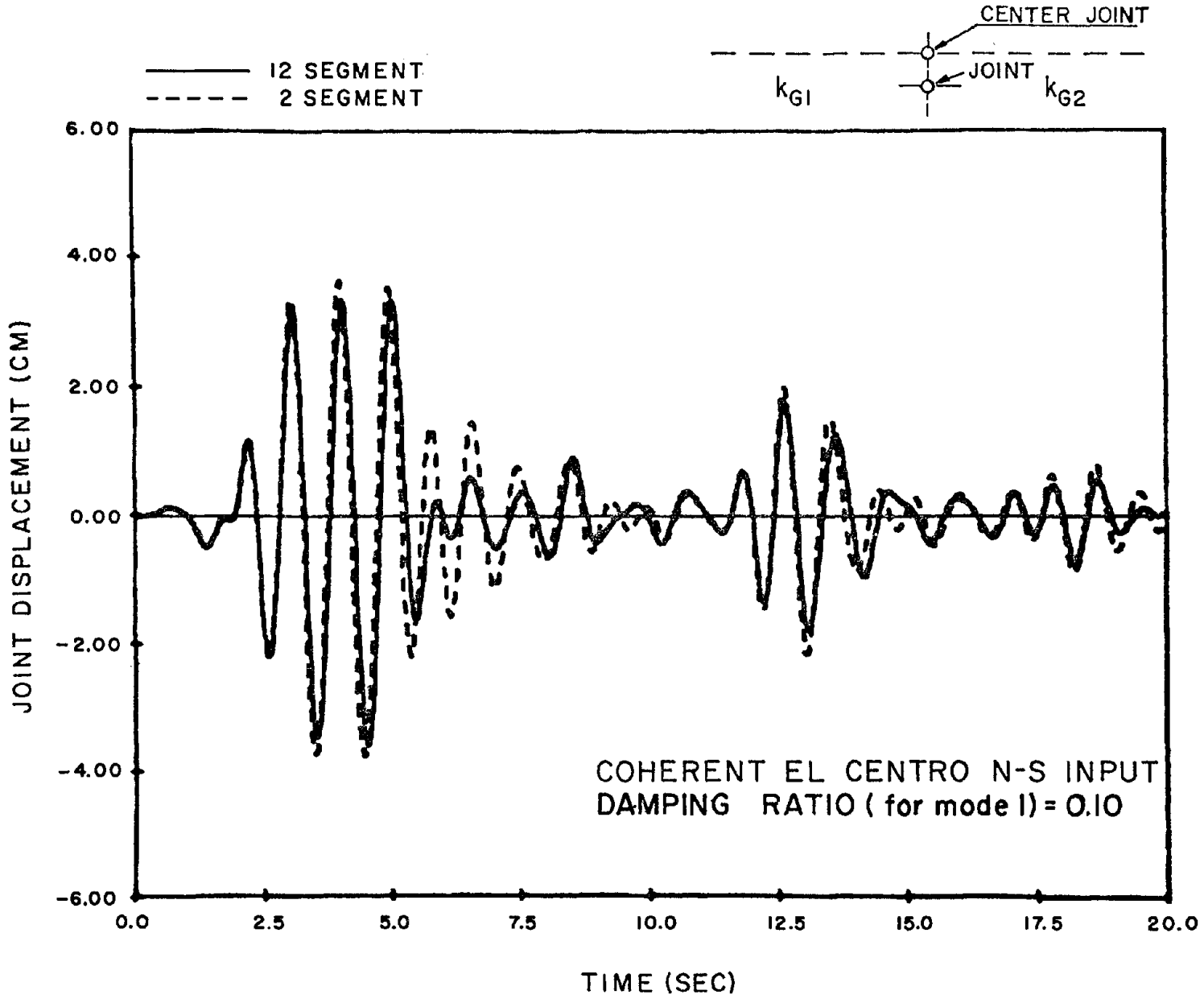

FIG. 20 TOTAL CENTER JOINT RESPONSE OF 12 SEGMENT SYSTEM AND 2 SEGMENT SYSTEM; k_{G1}= 3.5, k_{G2}= 4.5 AND k_p= 1 FOR BOTH SYSTEMS

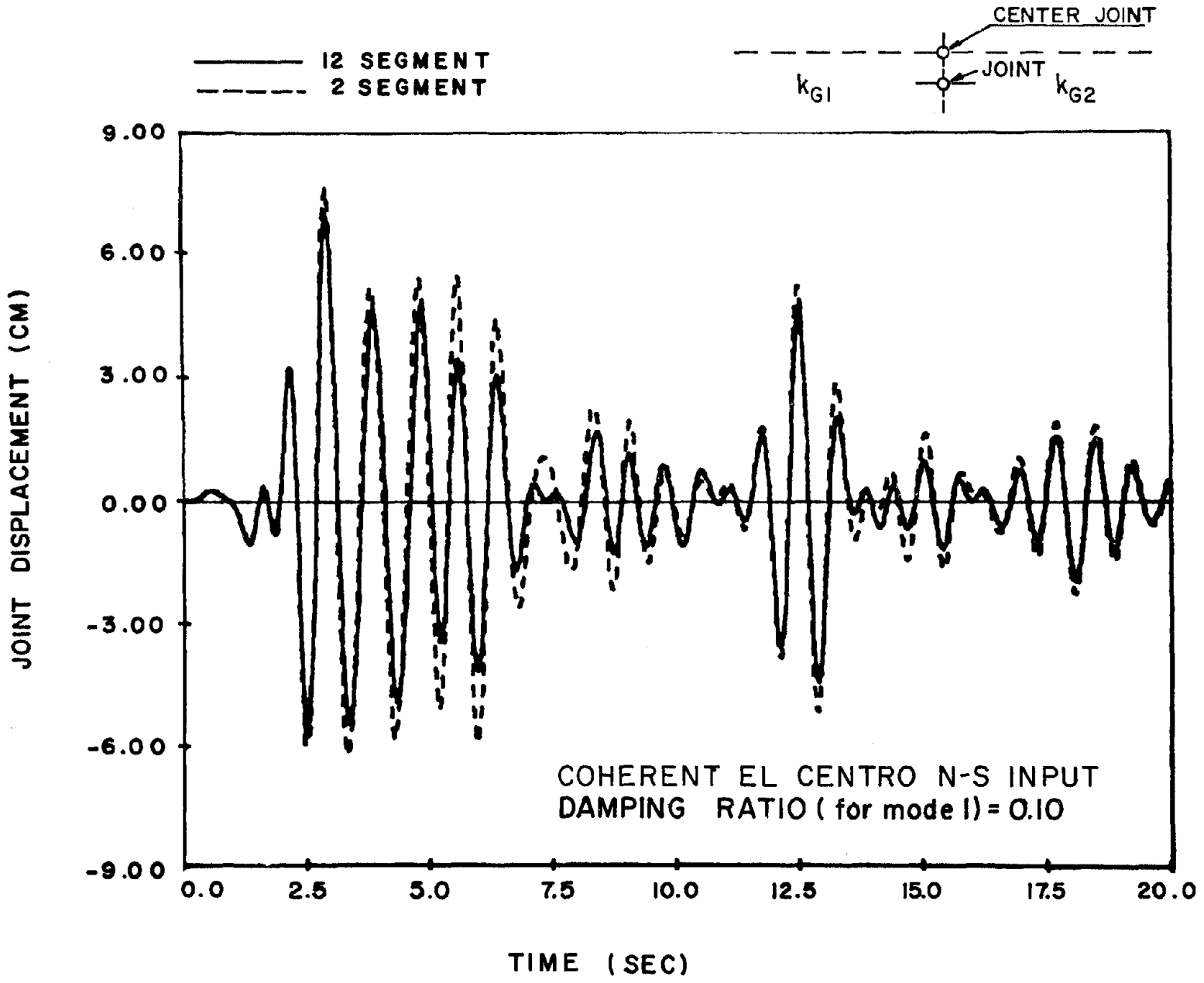

FIG 21-TOTAL CENTER JOINT RESPONSE OF 12 SEGMENT SYSTEM AND 2 SEGMENT SYSTEM; $k_{G1} = 4$, $k_{G2} = 8$ AND $k_p = 1$ FOR BOTH SYSTEMS

APPENDIX

In this appendix the response, i.e., the joint relative displacement, of a two degree of freedom system to a coherent ground motion is shown for the various cases studied. The first 26 figures show the normalized response $Y(t, \Delta\omega/\bar{\omega}, \Omega/\bar{\omega})$ [see Eq. (74) in the text] for an undamped system when the coherent ground motion is a haversine function. The figures correspond to the 26 data points plotted in Fig. 12. (Note, Fig. A-10 is identical to Fig. 11 in the text, and is included here for completeness.) On each figure, the relevant maximum values are shown.

Figures A-27 through A-36 show the response of the two degree of freedom system to a coherent earthquake motion, i.e., the first 20 seconds of the EL CENTRO May 1940 North-South record. The ten figures correspond to the ten cases listed in Table II of the text. The input ground displacement is included in Figs. A-27 to A-31.

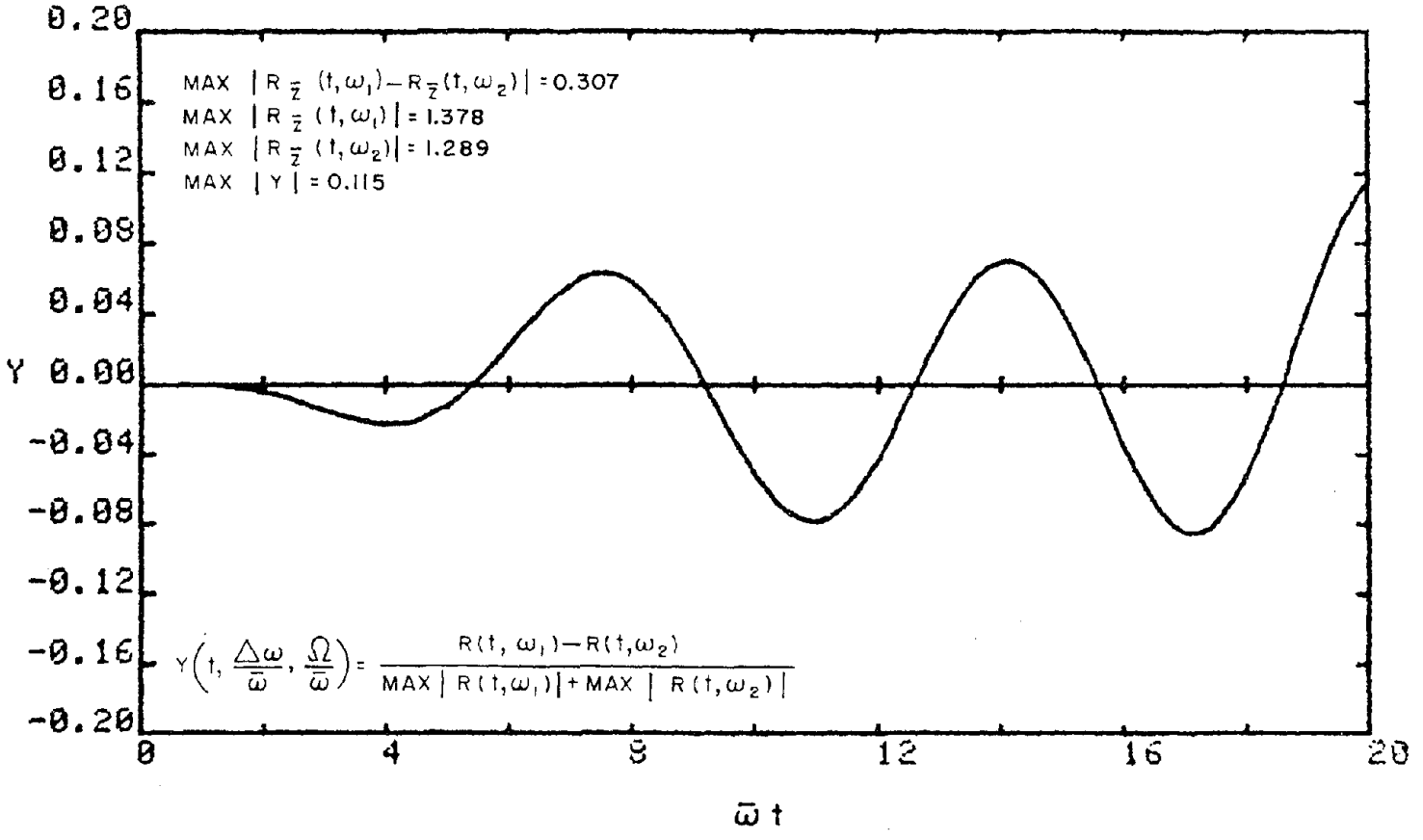

FIG. A1 – NORMALIZED DIFFERENCE IN UNDAMPED RESPONSE WHEN $\bar{Z} = (1-\cos \Omega t)/2$, $\Delta\omega/\bar{\omega} = 0.1$ AND $\Omega/\bar{\omega} = 0.5$

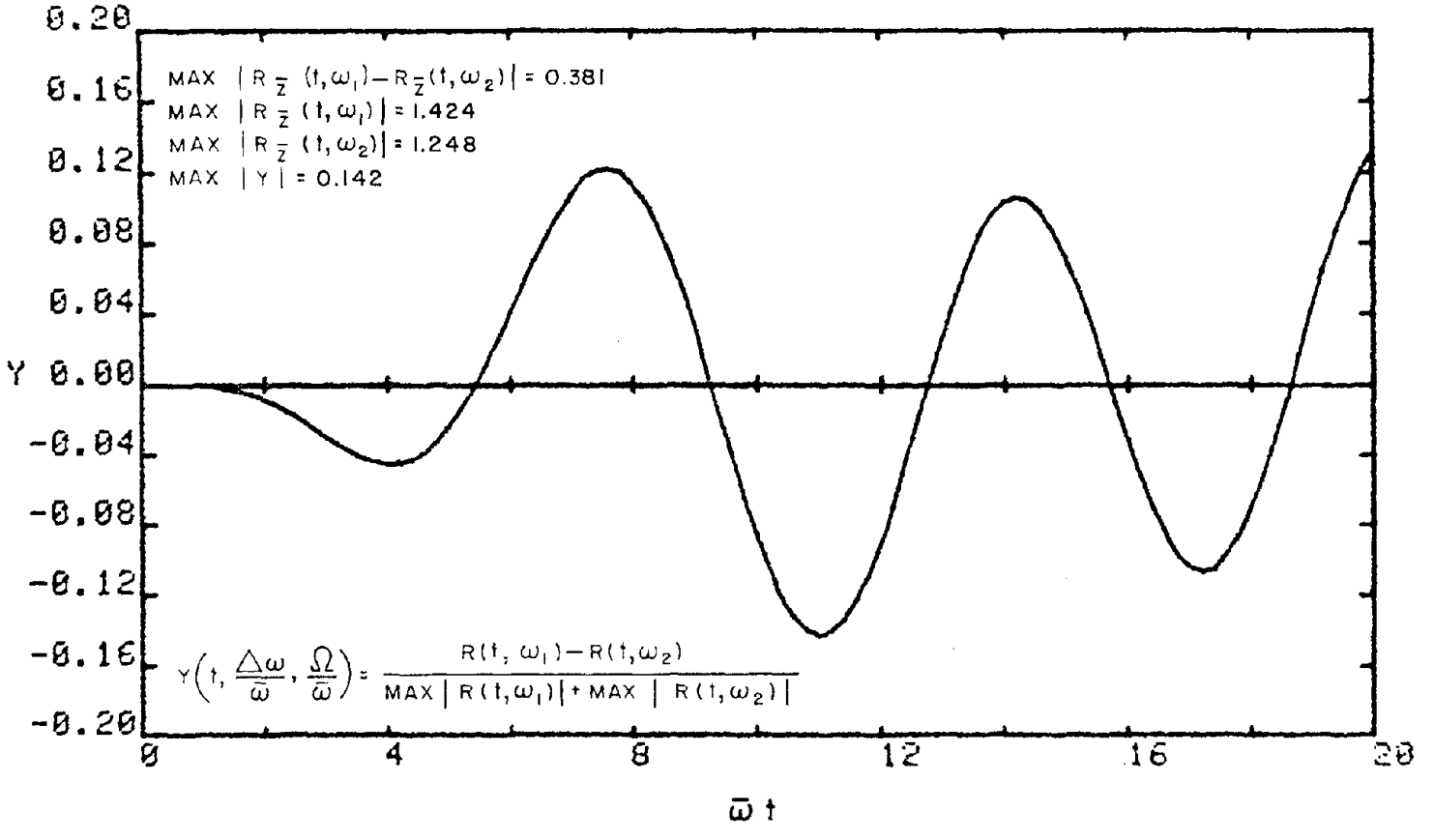

FIG. A2 NORMALIZED DIFFERENCE IN UNDAMPED RESPONSE WHEN $\bar{Z} = (1 - \cos \Omega t)/2$, $\Delta\omega/\bar{\omega} = 0.2$ AND $\Omega/\bar{\omega} = 0.5$

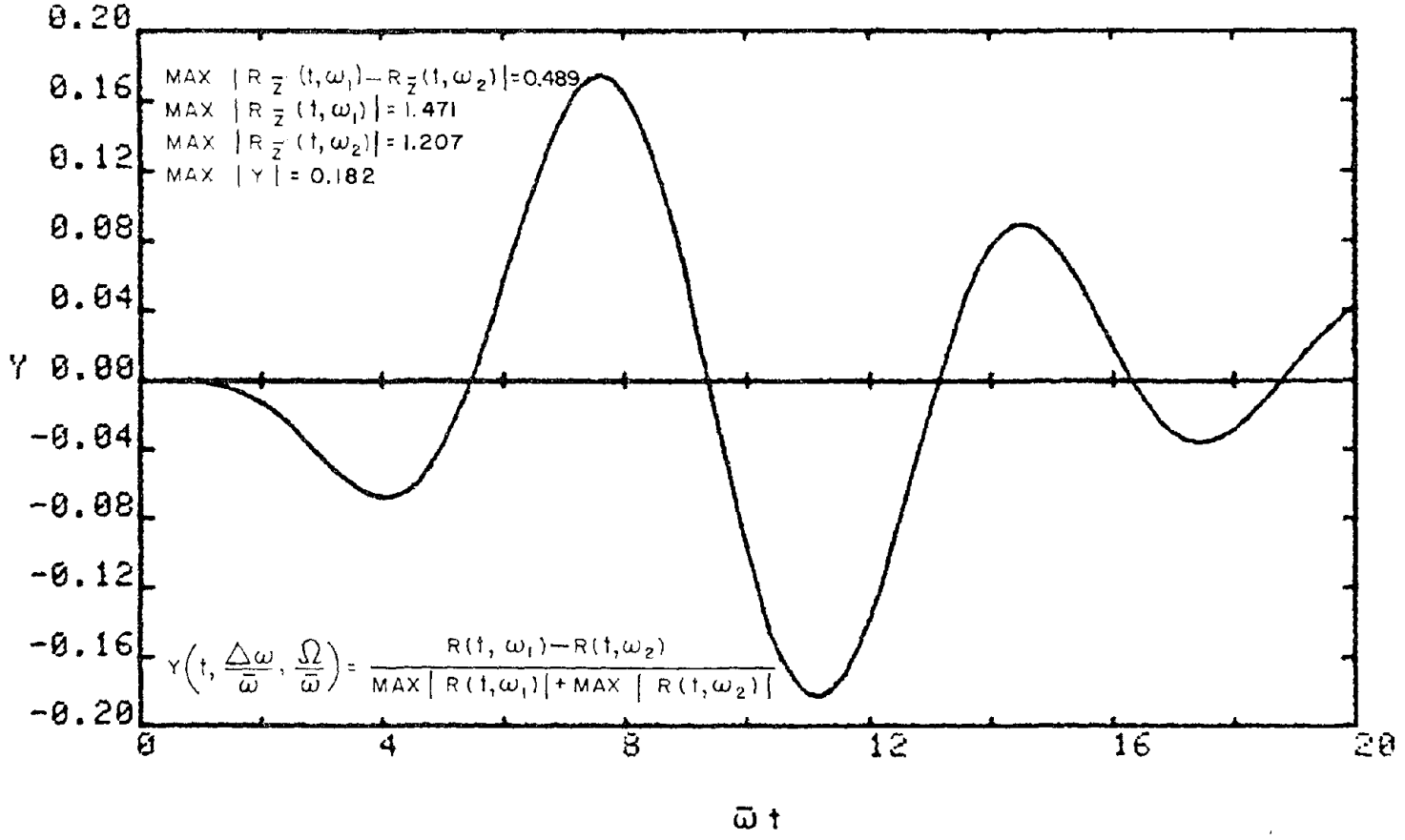

FIG. A3 NORMALIZED DIFFERENCE IN UNDAMPED RESPONSE WHEN $\bar{Z} = (1 - \cos \Omega t)/2$, $\Delta\omega/\bar{\omega} = 0.3$ AND $\Omega/\bar{\omega} = 0.5$

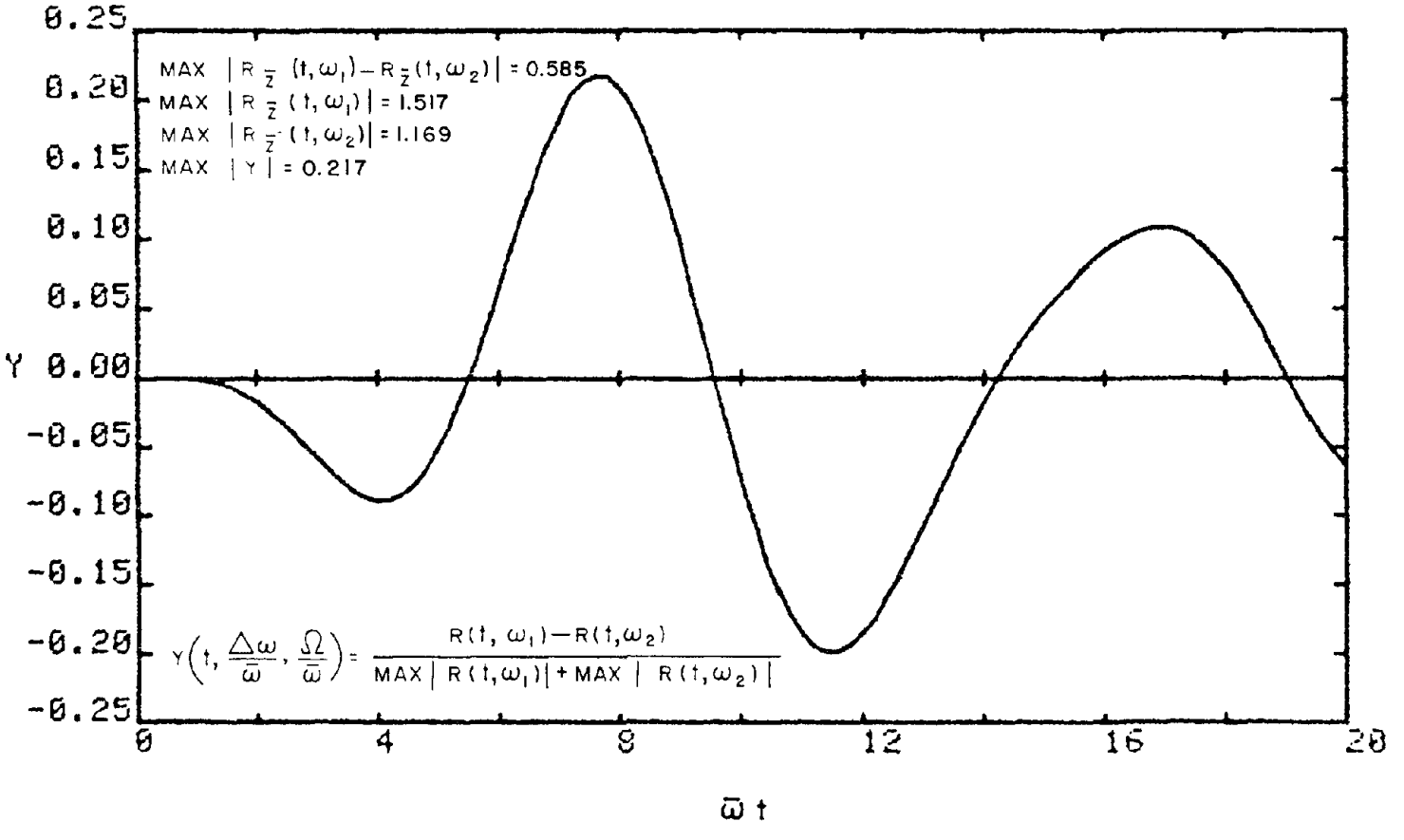

FIG. A4 NORMALIZED DIFFERENCE IN UNDAMPED RESPONSE WHEN $\bar{Z} = (1 - \cos \Omega t)/2$, $\Delta\omega/\bar{\omega} = 0.4$ AND $\Omega/\bar{\omega} = 0.5$

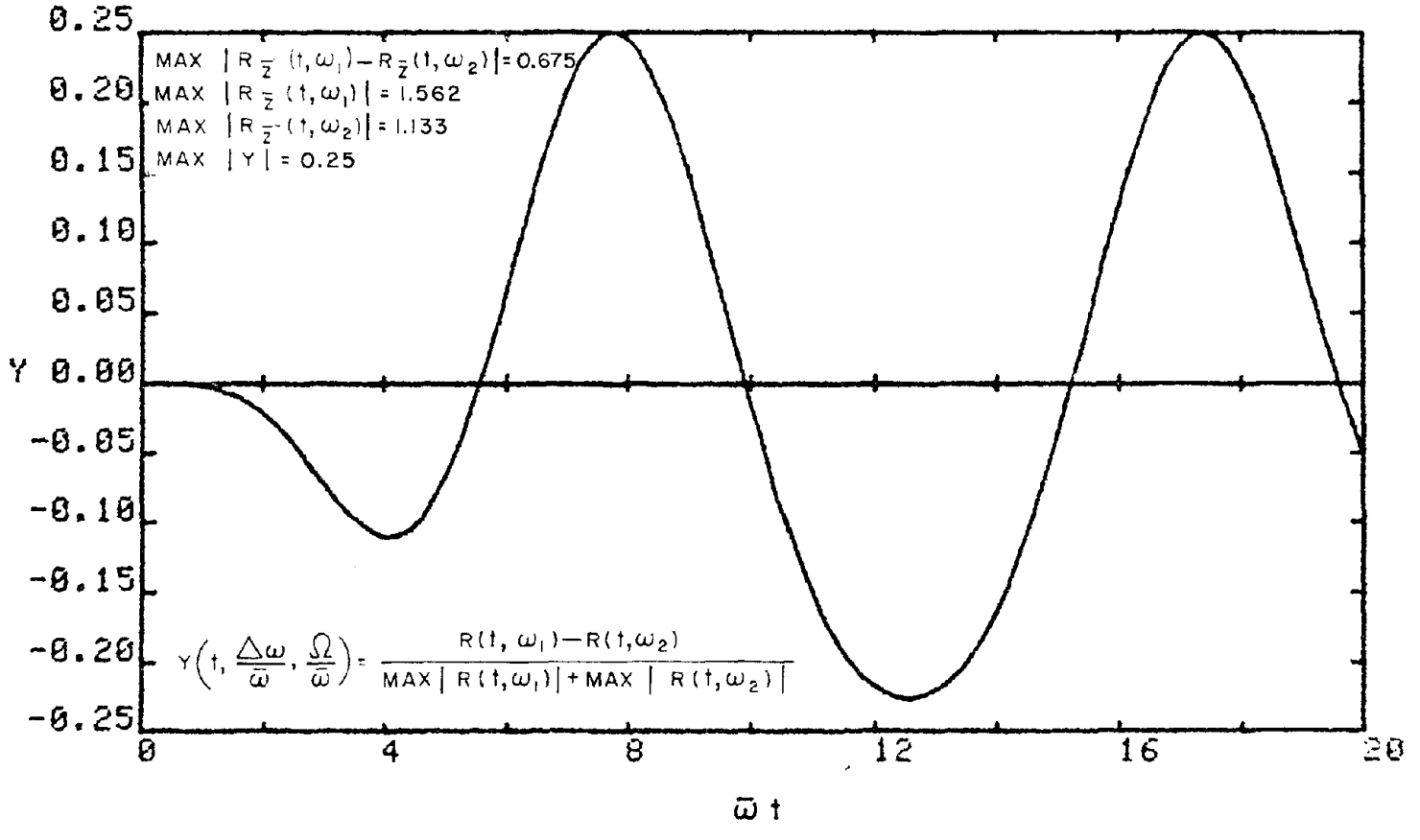

FIG. A5 NORMALIZED DIFFERENCE IN UNDAMPED RESPONSE WHEN $\bar{Z} = (1 - \cos \Omega t)/2$, $\Delta\omega/\bar{\omega} = 0.5$ AND $\Omega/\bar{\omega} = 0.5$

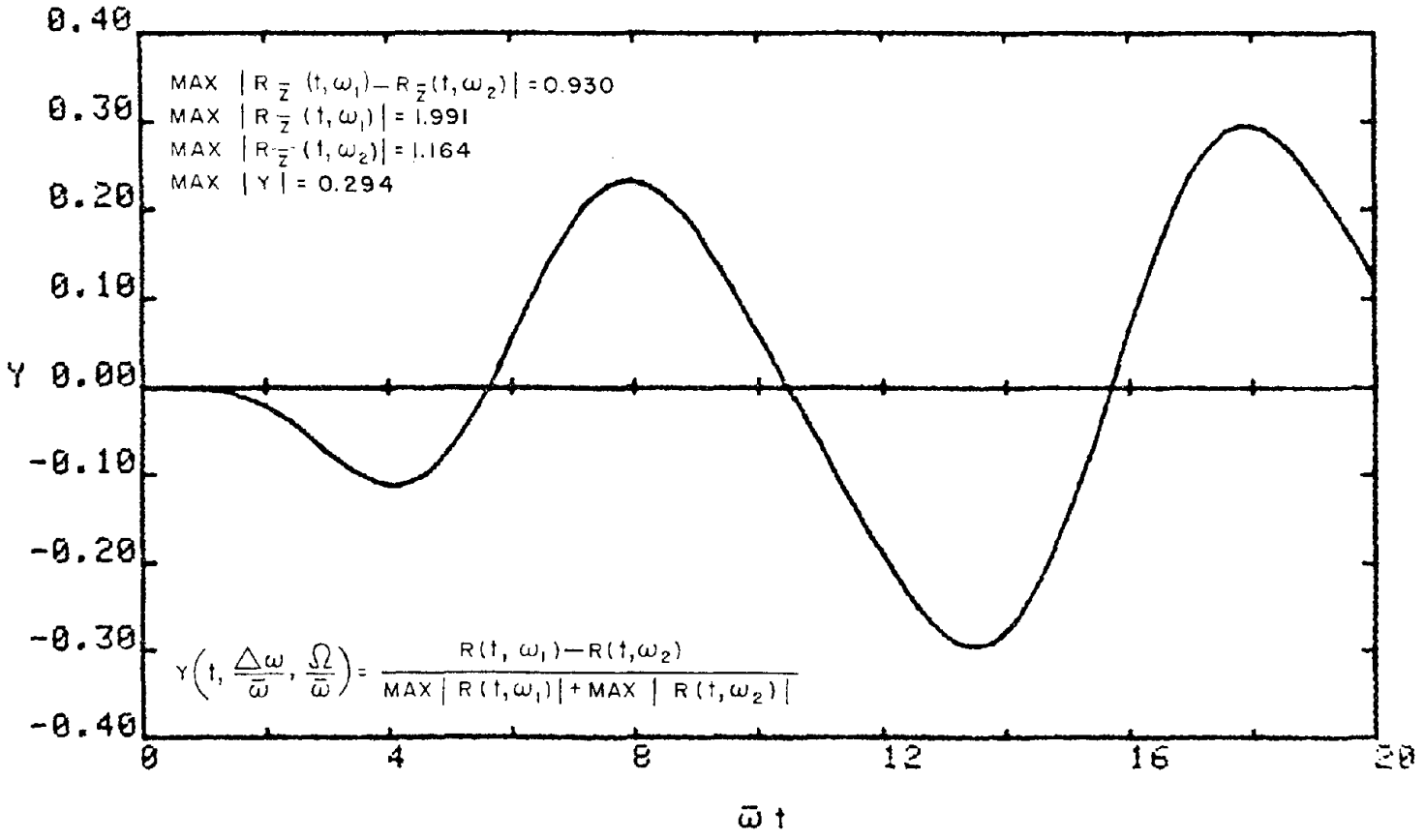

FIG. A6 NORMALIZED DIFFERENCE IN UNDAMPED RESPONSE WHEN $\bar{Z} = (1 - \cos \Omega t)/2$, $\Delta\omega/\bar{\omega} = 0.6$ AND $\Omega/\bar{\omega} = 0.5$

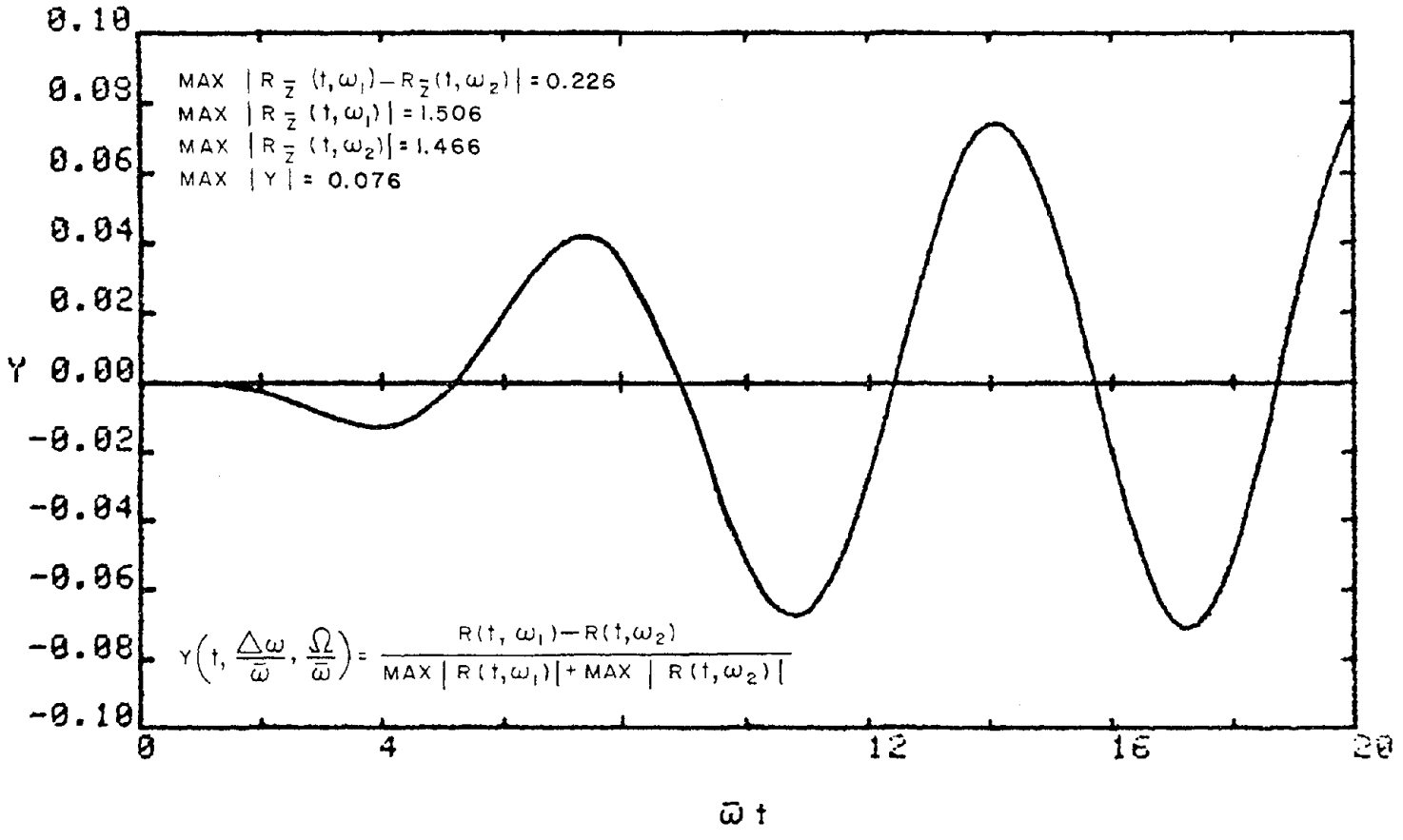

FIG. A7 NORMALIZED DIFFERENCE IN UNDAMPED RESPONSE WHEN $\bar{Z} = (1-\cos \Omega t)/2$, $\Delta\omega/\bar{\omega} = 0.05$ AND $\Omega/\bar{\omega} = 0.6$

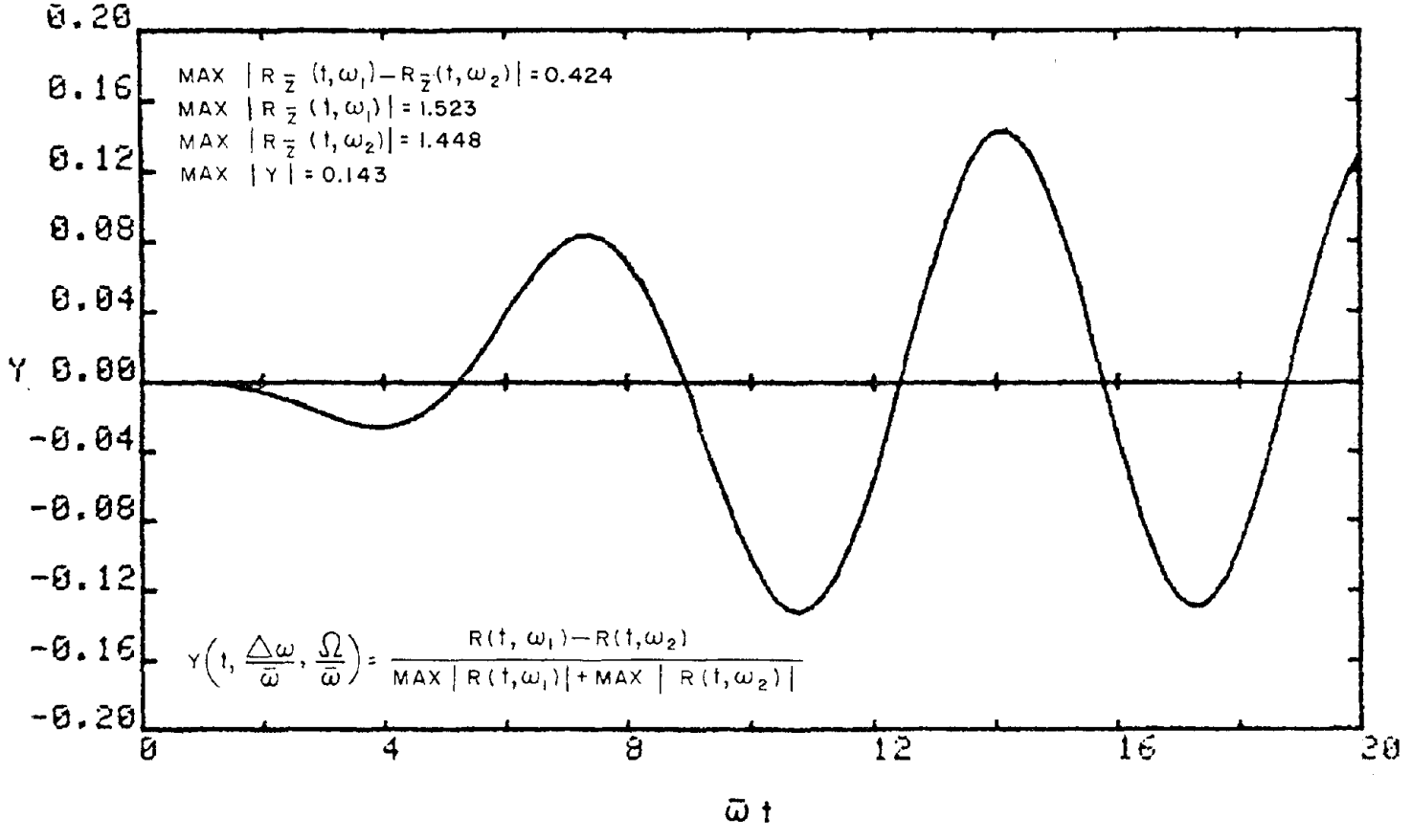

FIG. A8 NORMALIZED DIFFERENCE IN UNDAMPED RESPONSE WHEN $\bar{Z} = (1-\cos \Omega t)/2$, $\Delta\omega/\bar{\omega} = 0.1$ AND $\Omega/\bar{\omega} = 0.6$

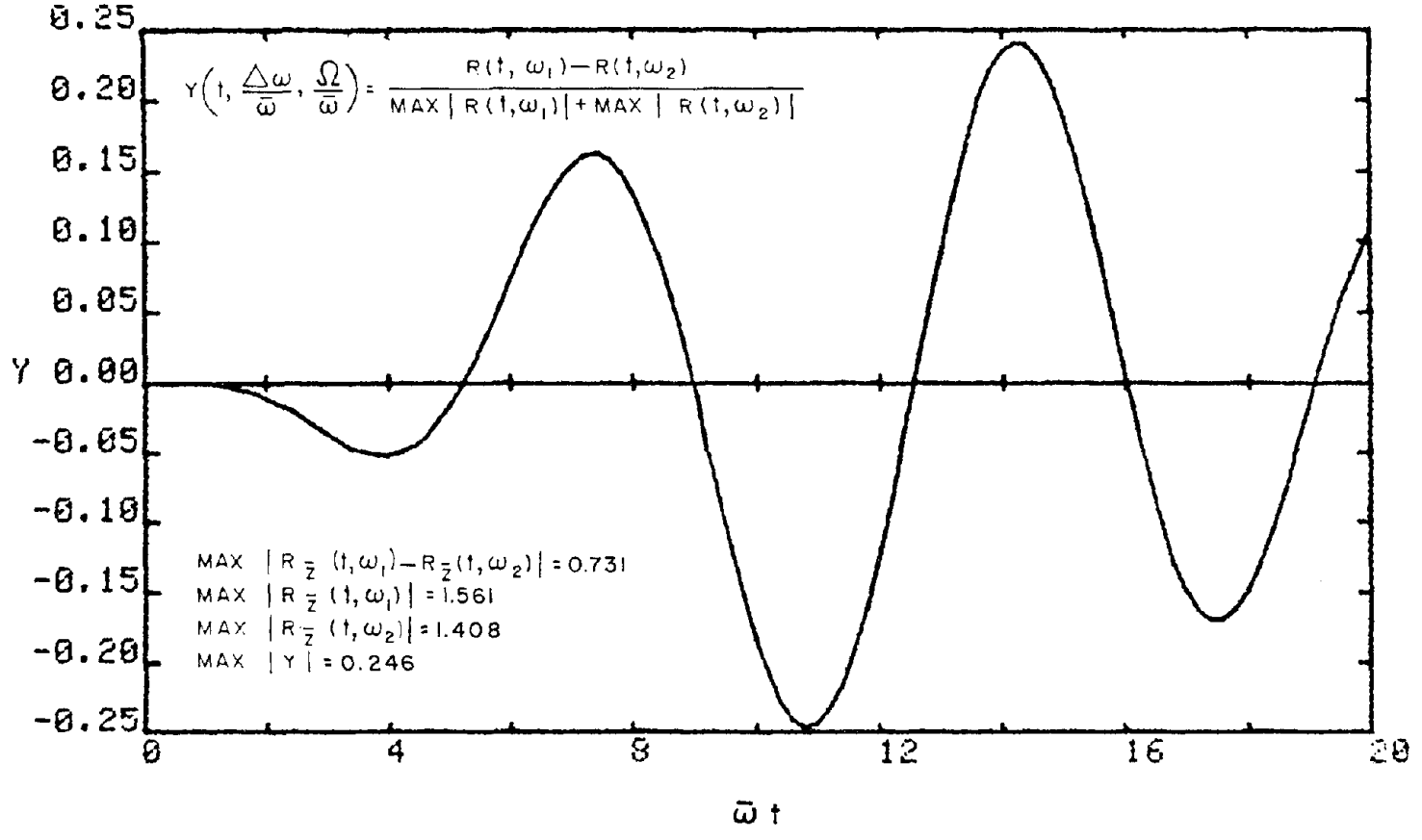

FIG. A9 NORMALIZED DIFFERENCE IN UNDAMPED RESPONSE WHEN $\bar{Z} = (1 - \cos \Omega t)/2$, $\Delta\omega/\bar{\omega} = 0.2$ AND $\Omega/\bar{\omega} = 0.6$

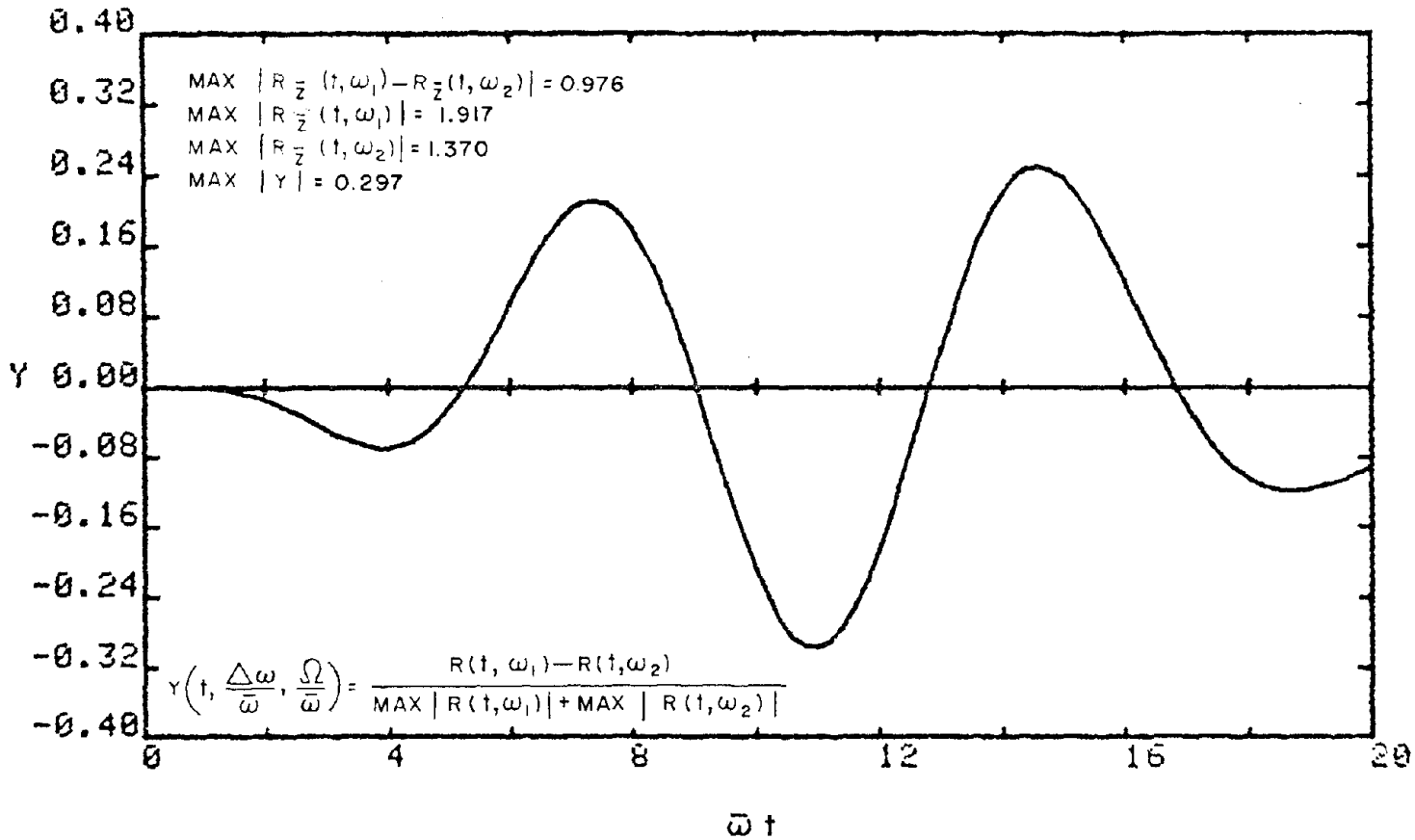

FIG.A10 NORMALIZED DIFFERENCE IN UNDAMPED RESPONSE WHEN $\bar{Z} = (1-\cos \Omega t)/2$, $\Delta\omega/\bar{\omega} = 0.3$ AND $\Omega/\bar{\omega} = 0.6$

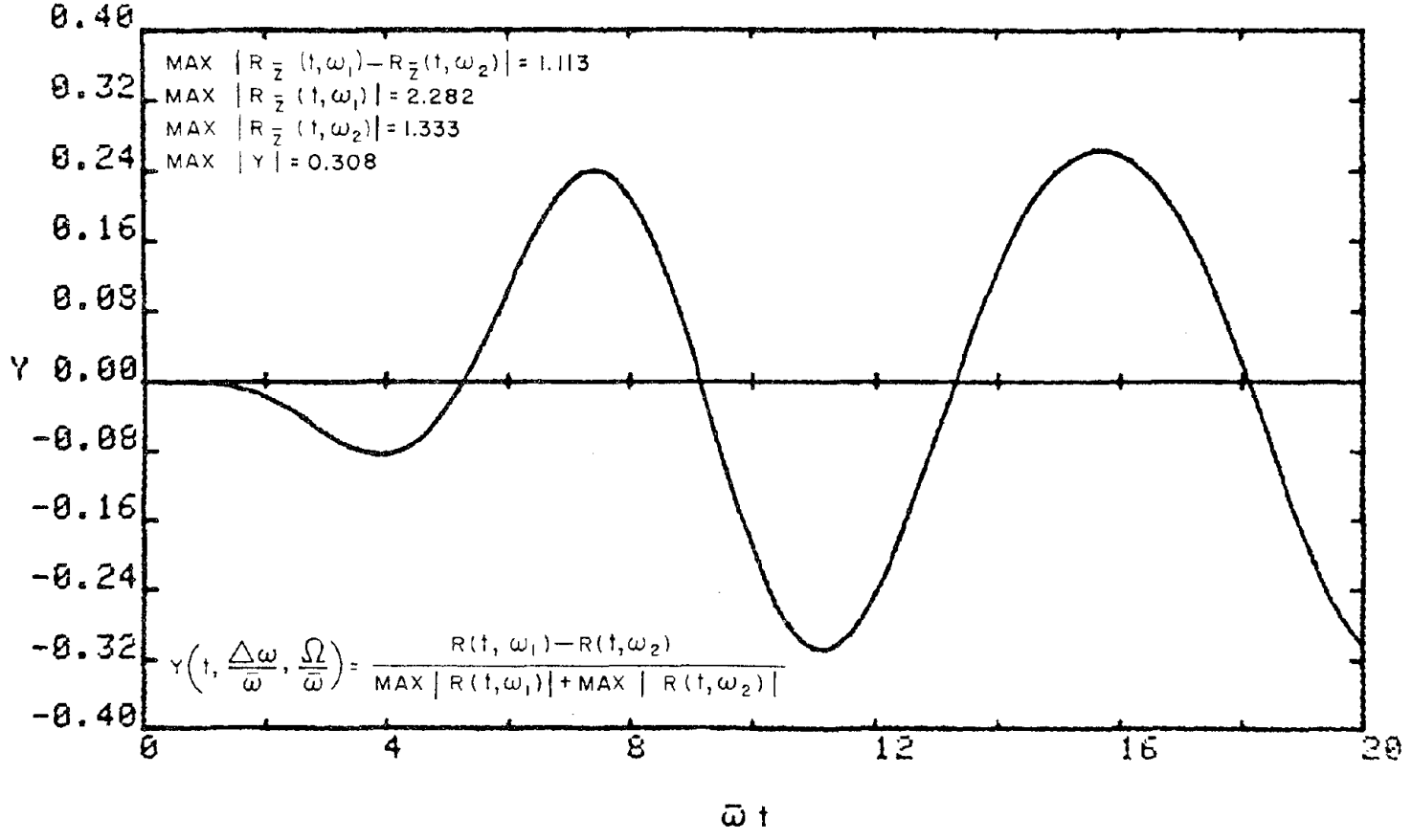

FIG.AII NORMALIZED DIFFERENCE IN UNDAMPED RESPONSE WHEN $\bar{Z} = (1-\cos \Omega t)/2$, $\Delta\omega/\bar{\omega} = 0.4$ AND $\Omega/\bar{\omega} = 0.6$

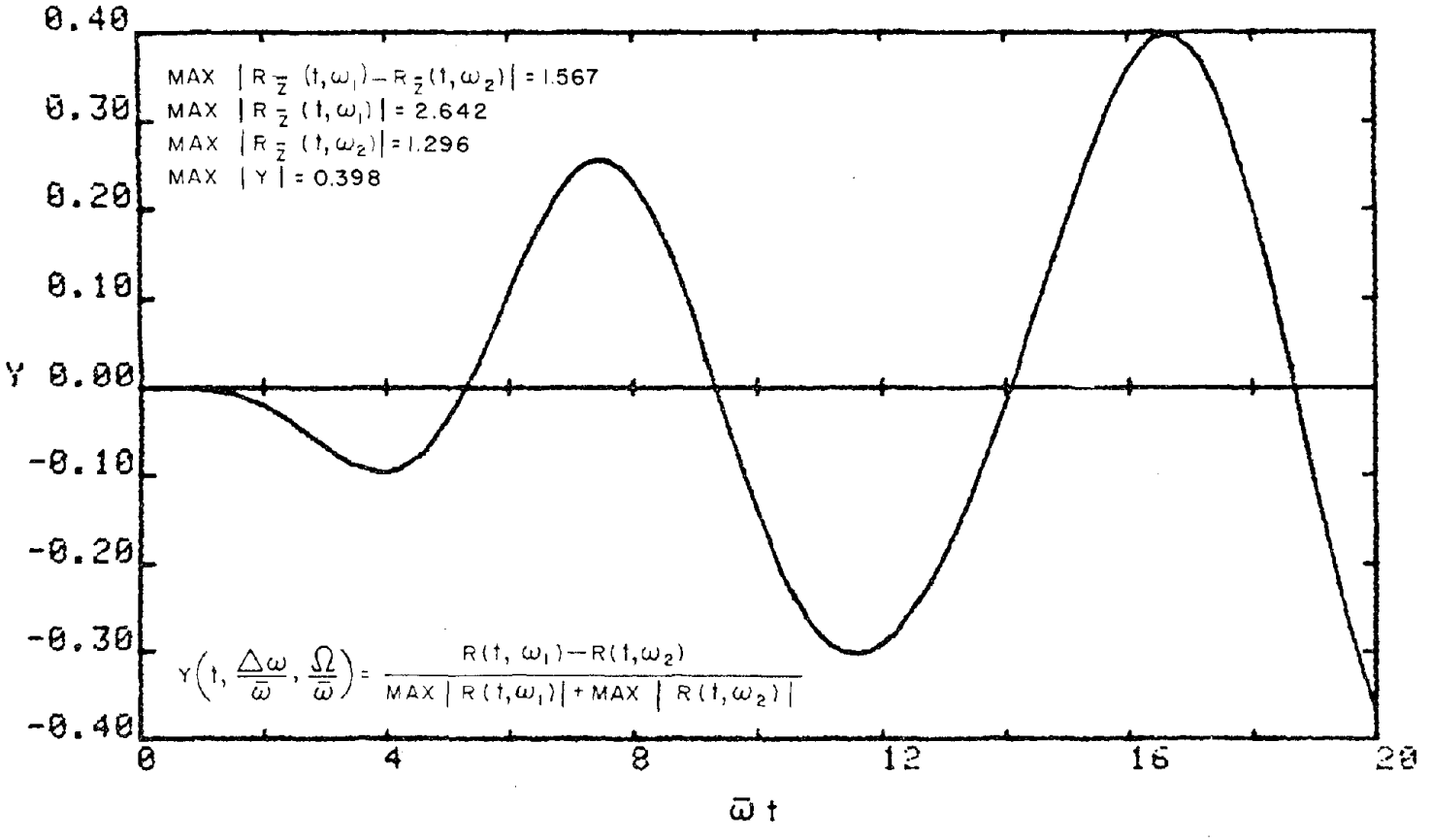

FIG.A12 NORMALIZED DIFFERENCE IN UNDAMPED RESPONSE WHEN $\bar{Z} = (1-\cos \Omega t)/2$, $\Delta\omega/\bar{\omega} = 0.5$ AND $\Omega/\bar{\omega} = 0.6$

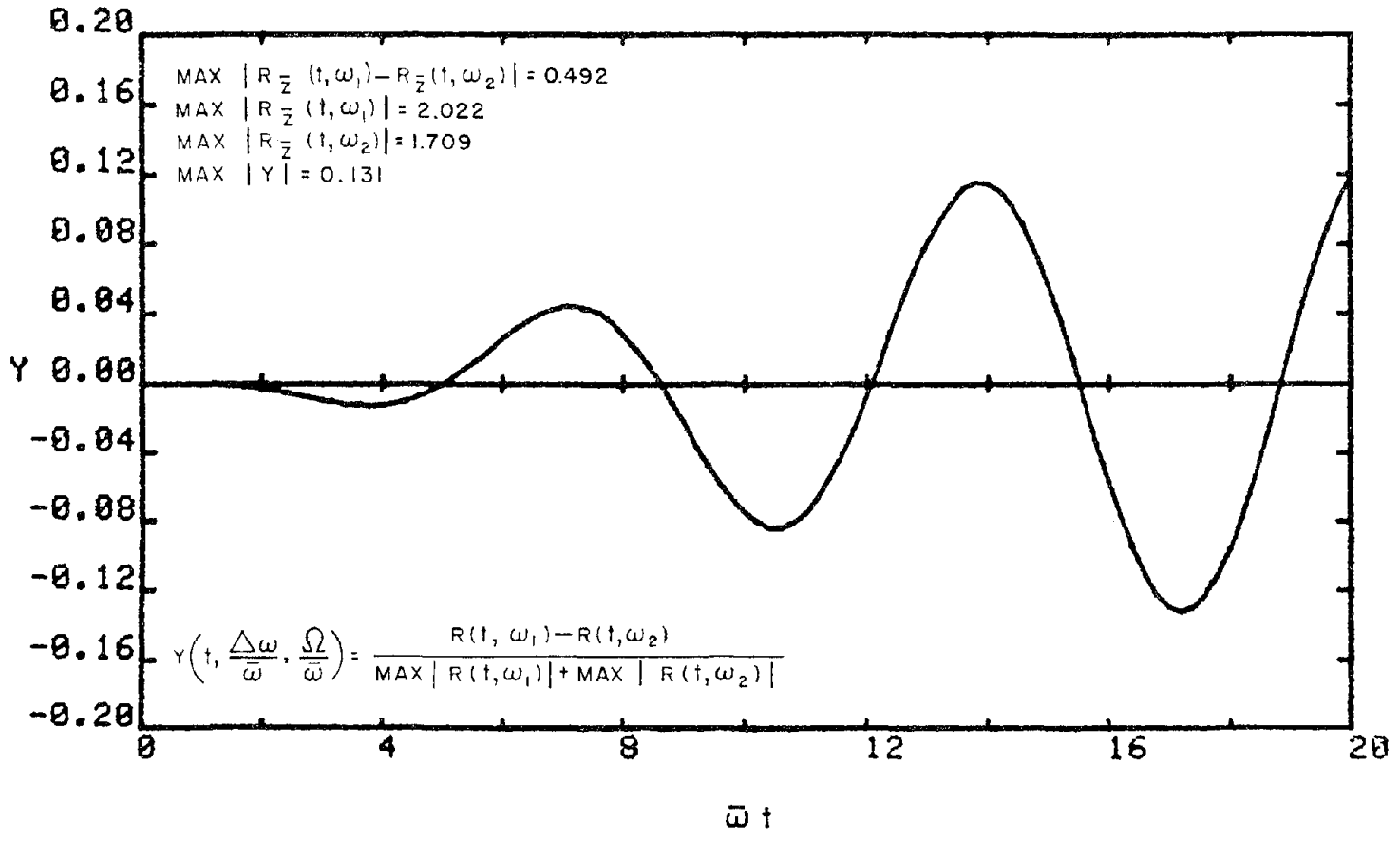

FIG.A13 NORMALIZED DIFFERENCE IN UNDAMPED RESPONSE WHEN $\bar{Z} = (1-\cos \Omega t)/2$, $\Delta\omega/\bar{\omega} = 0.05$ AND $\Omega/\bar{\omega} = 0.7$

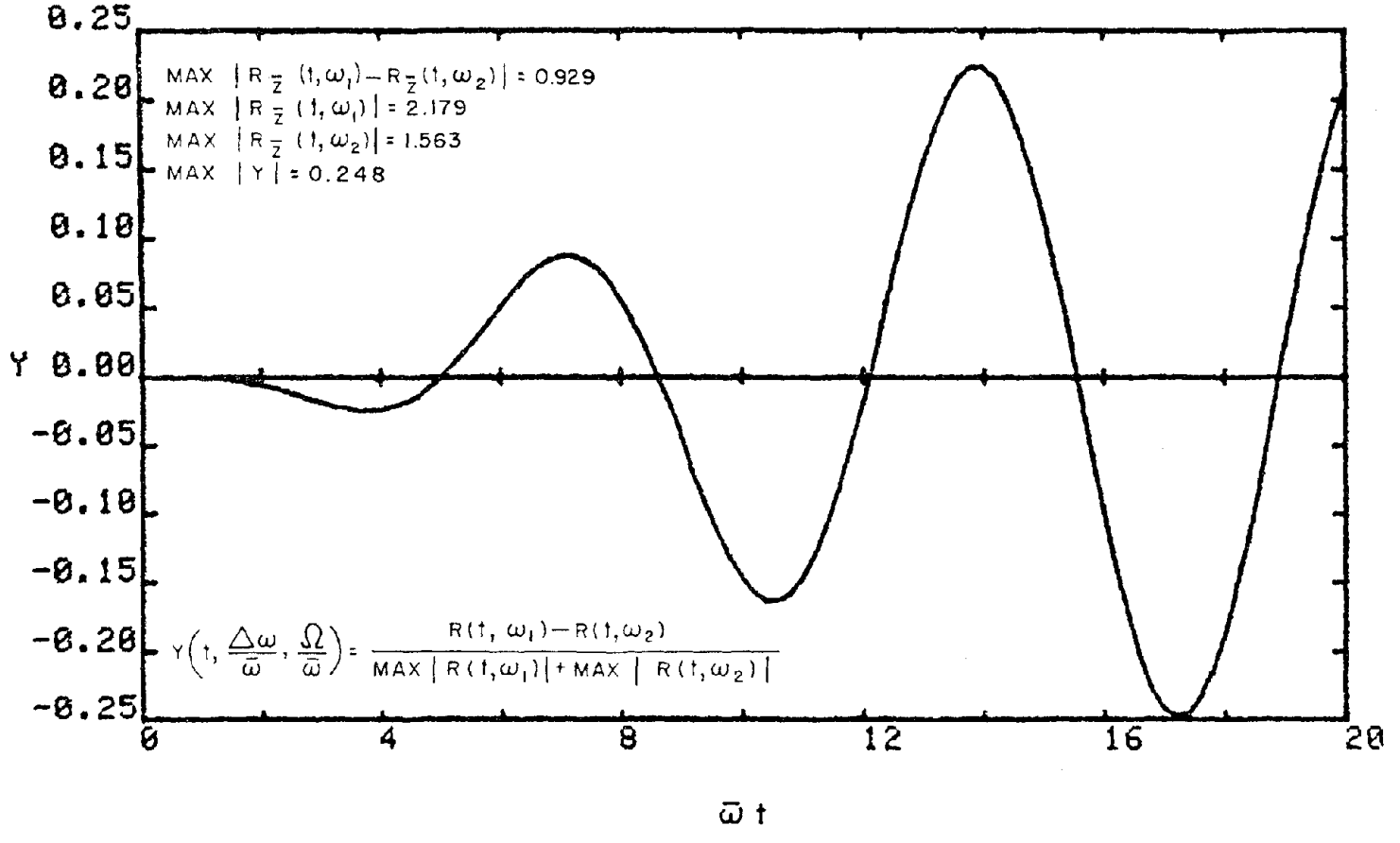

FIG.AI4 NORMALIZED DIFFERENCE IN UNDAMPED RESPONSE WHEN $\bar{Z} = (1-\cos \Omega t)/2$, $\Delta\omega/\bar{\omega} = 0.1$ AND $\Omega/\bar{\omega} = 0.7$

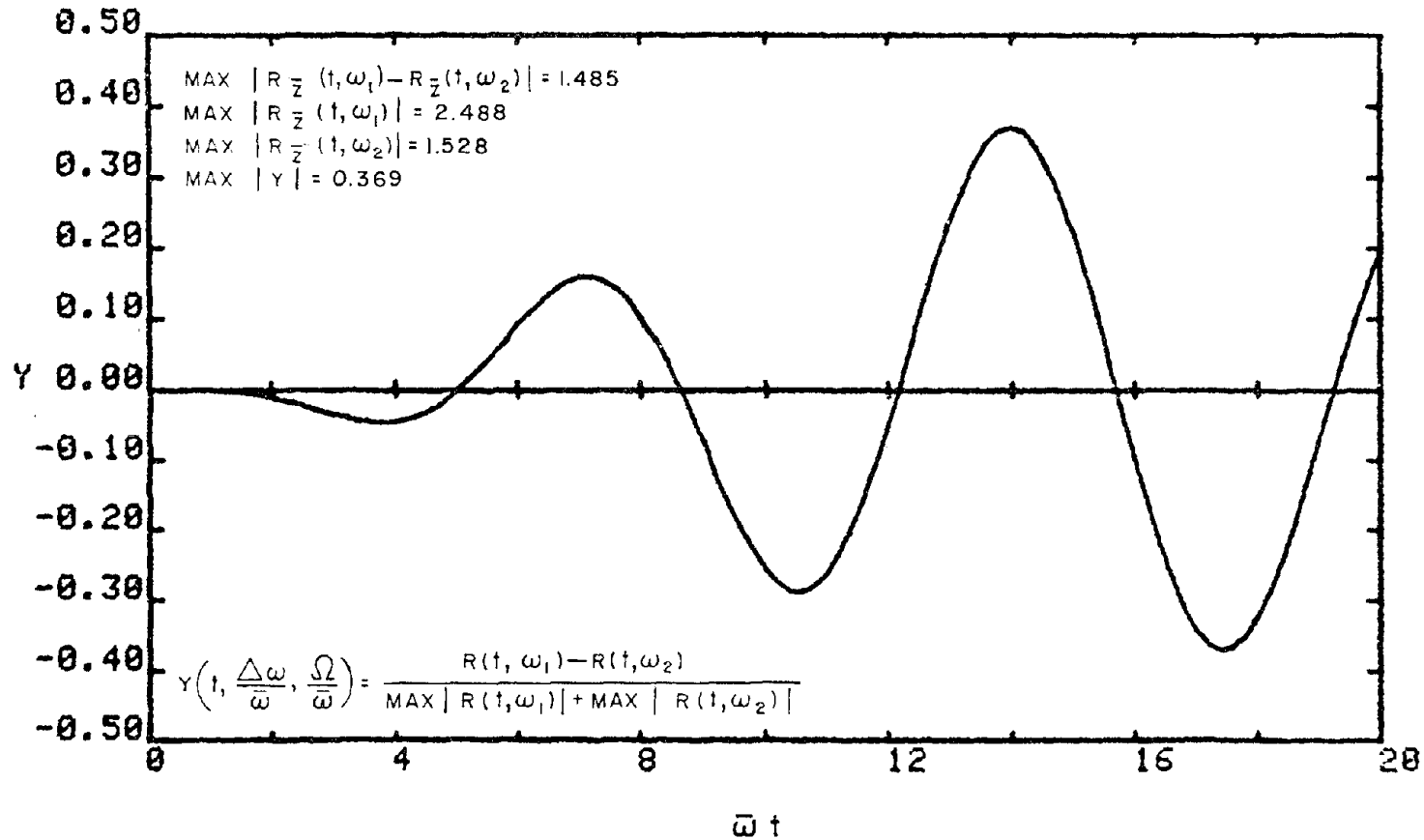

FIG.AI5 NORMALIZED DIFFERENCE IN UNDAMPED RESPONSE WHEN $\bar{Z} = (1 - \cos \Omega t)/2$, $\Delta\omega/\bar{\omega} = 0.2$ AND $\Omega/\bar{\omega} = 0.7$

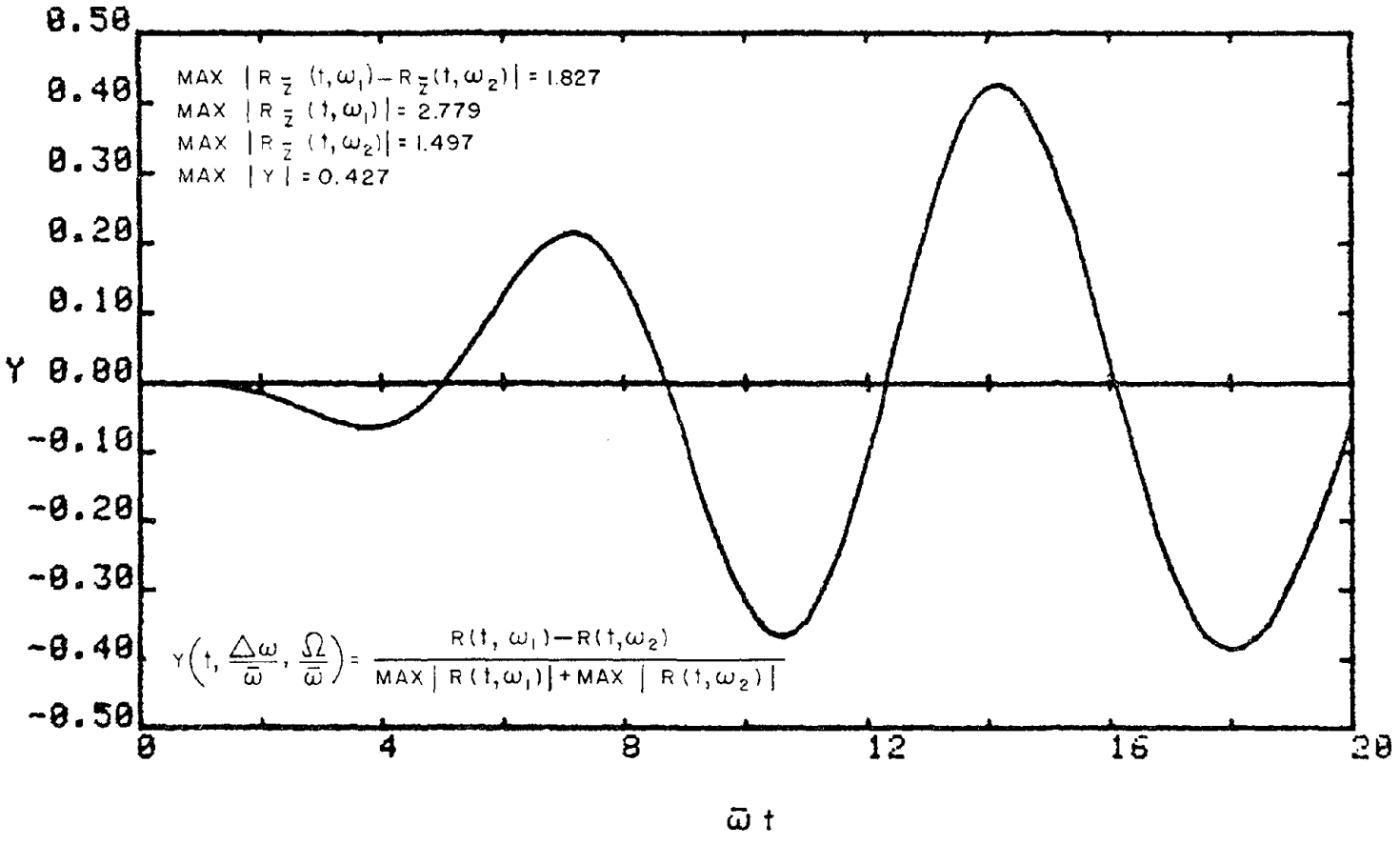

FIG.A16 NORMALIZED DIFFERENCE IN UNDAMPED RESPONSE WHEN $\bar{Z} = (1-\cos \Omega t)/2$, $\Delta\omega/\bar{\omega} = 0.3$ AND $\Omega/\bar{\omega} = 0.7$

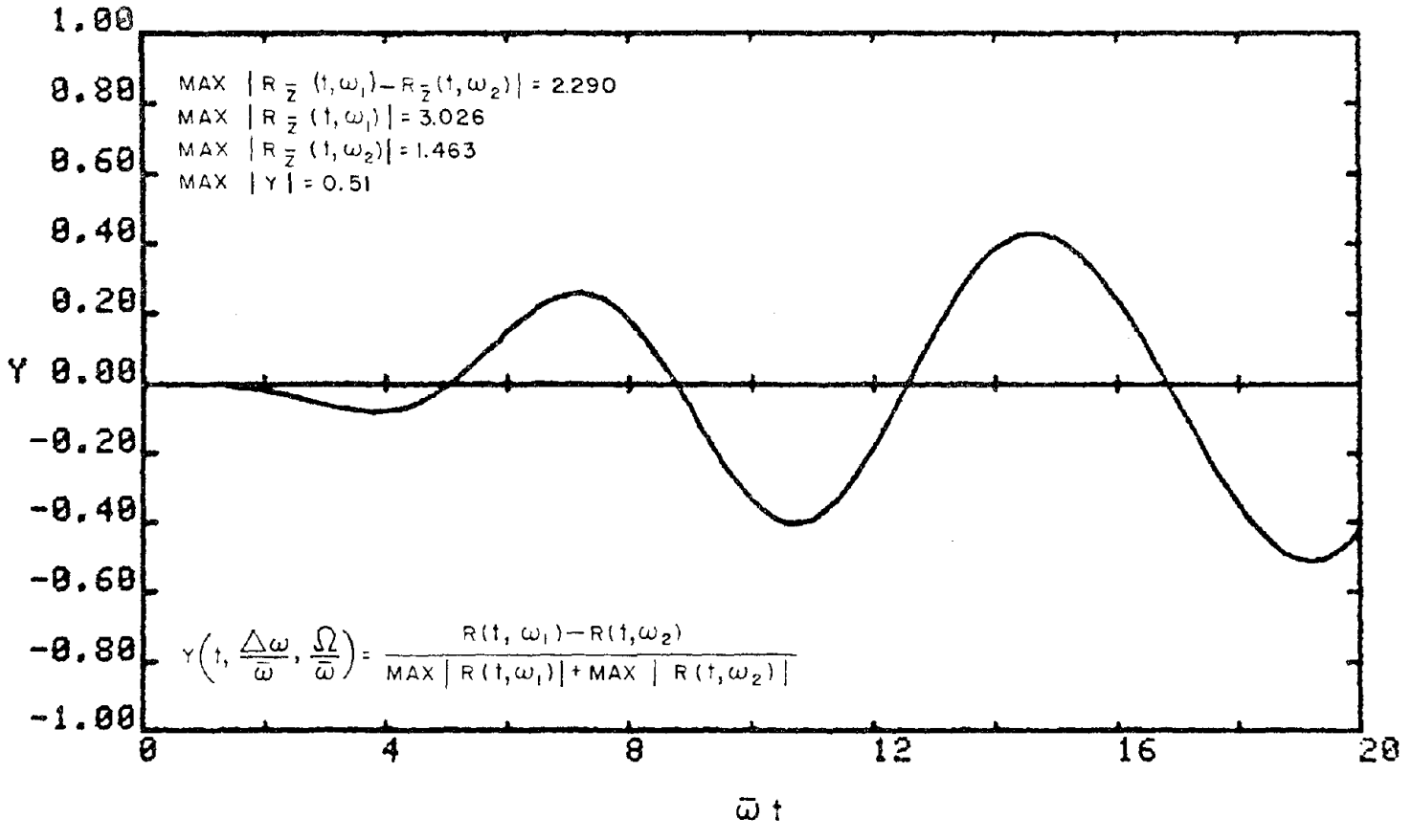

FIG.A17 NORMALIZED DIFFERENCE IN UNDAMPED RESPONSE WHEN $\bar{Z} = (1-\cos \Omega t)/2$, $\Delta\omega/\bar{\omega} = 0.4$ AND $\Omega/\bar{\omega} = 0.7$

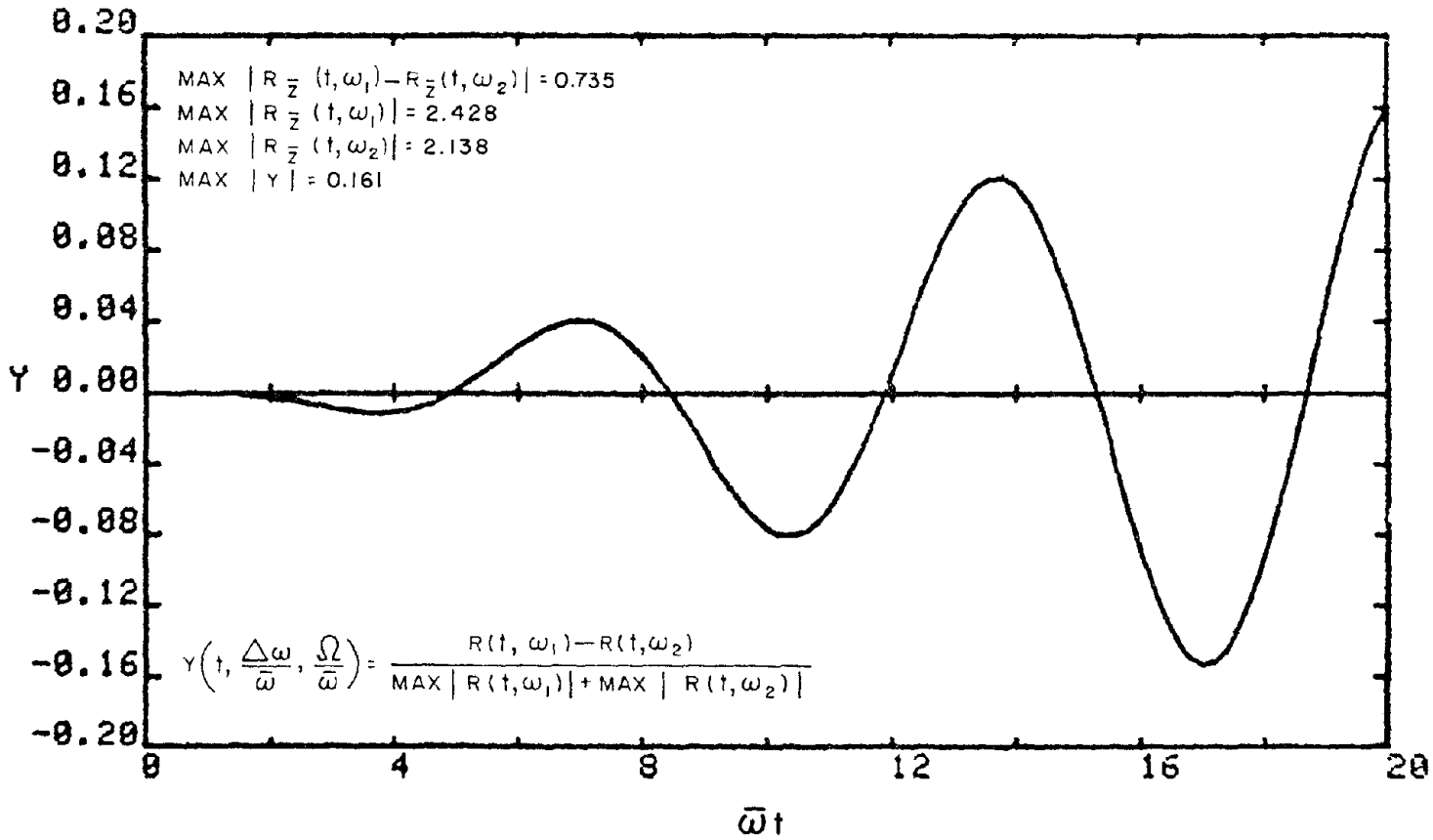

FIG.A18 NORMALIZED DIFFERENCE IN UNDAMPED RESPONSE WHEN $\bar{Z} = (1-\cos \Omega t)/2$, $\Delta\omega/\bar{\omega} = 0.05$ AND $\Omega/\bar{\omega} = 0.75$

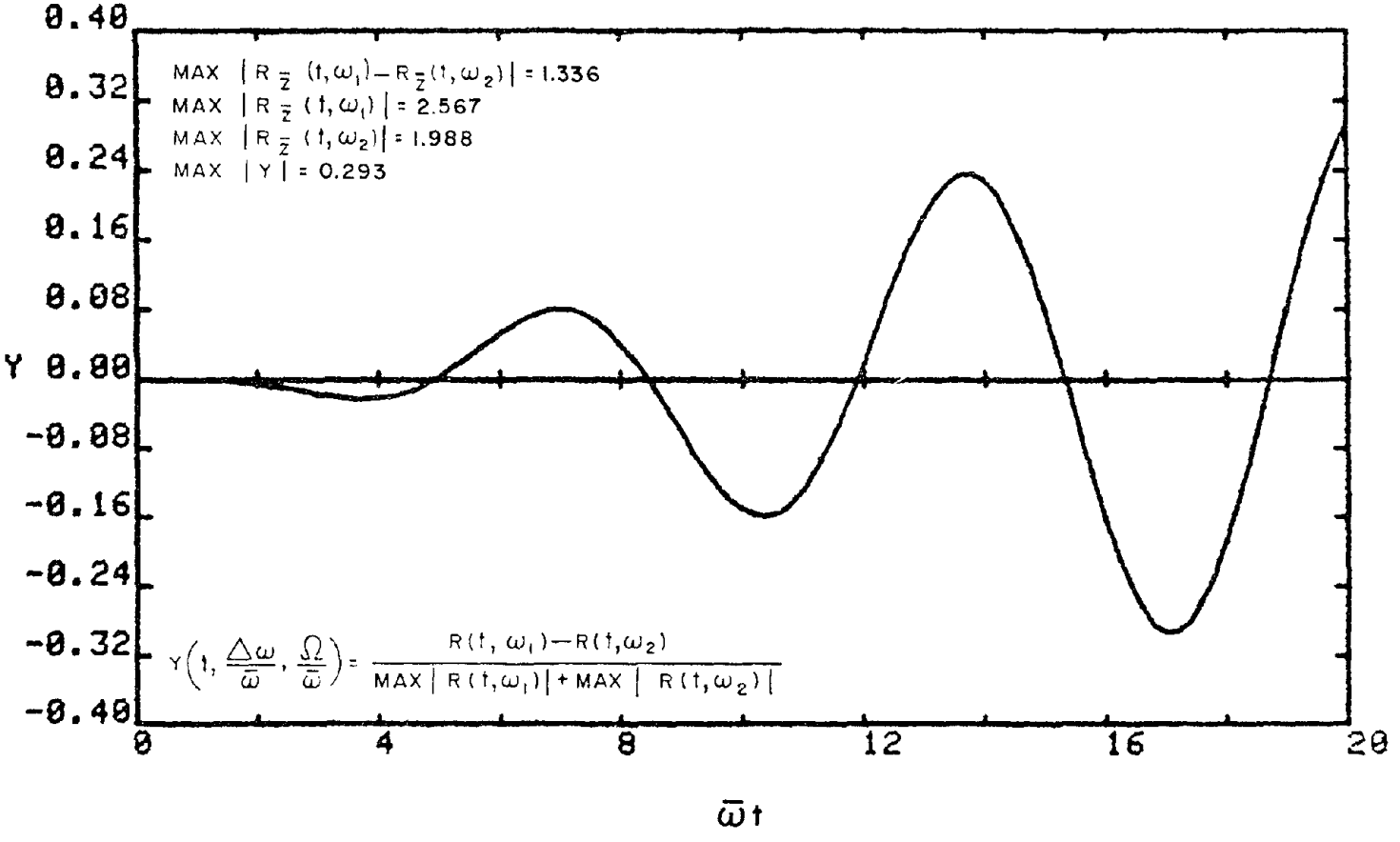

FIG.A19 NORMALIZED DIFFERENCE IN UNDAMPED RESPONSE WHEN $\bar{Z} = (1 - \cos \Omega t)/2$, $\Delta\omega/\bar{\omega} = 0.1$ AND $\Omega/\bar{\omega} = 0.75$

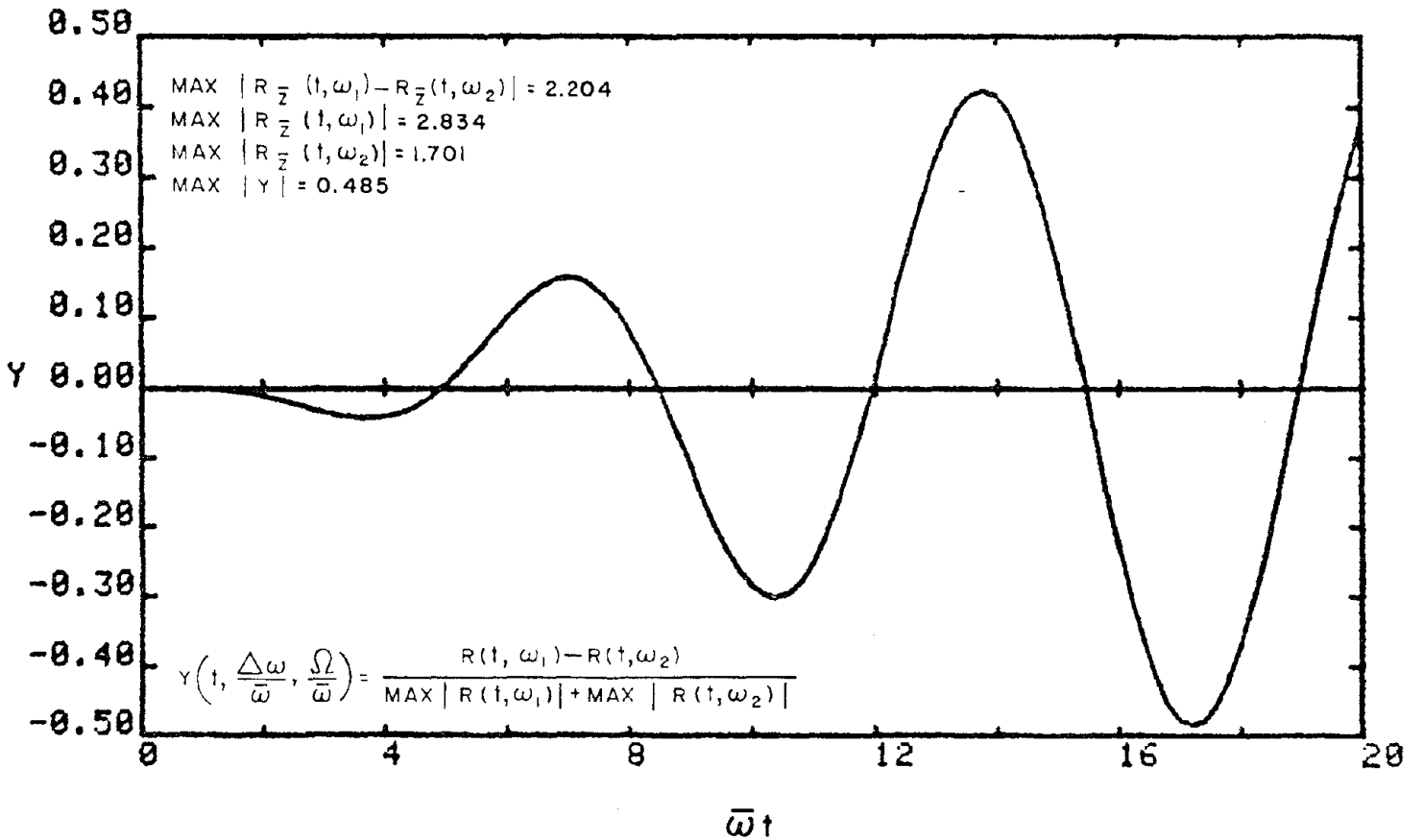

FIG. A20 NORMALIZED DIFFERENCE IN UNDAMPED RESPONSE WHEN $\bar{Z} = (1-\cos \Omega t)/2$, $\Delta\omega/\bar{\omega} = 0.2$ AND $\Omega/\bar{\omega} = 0.75$

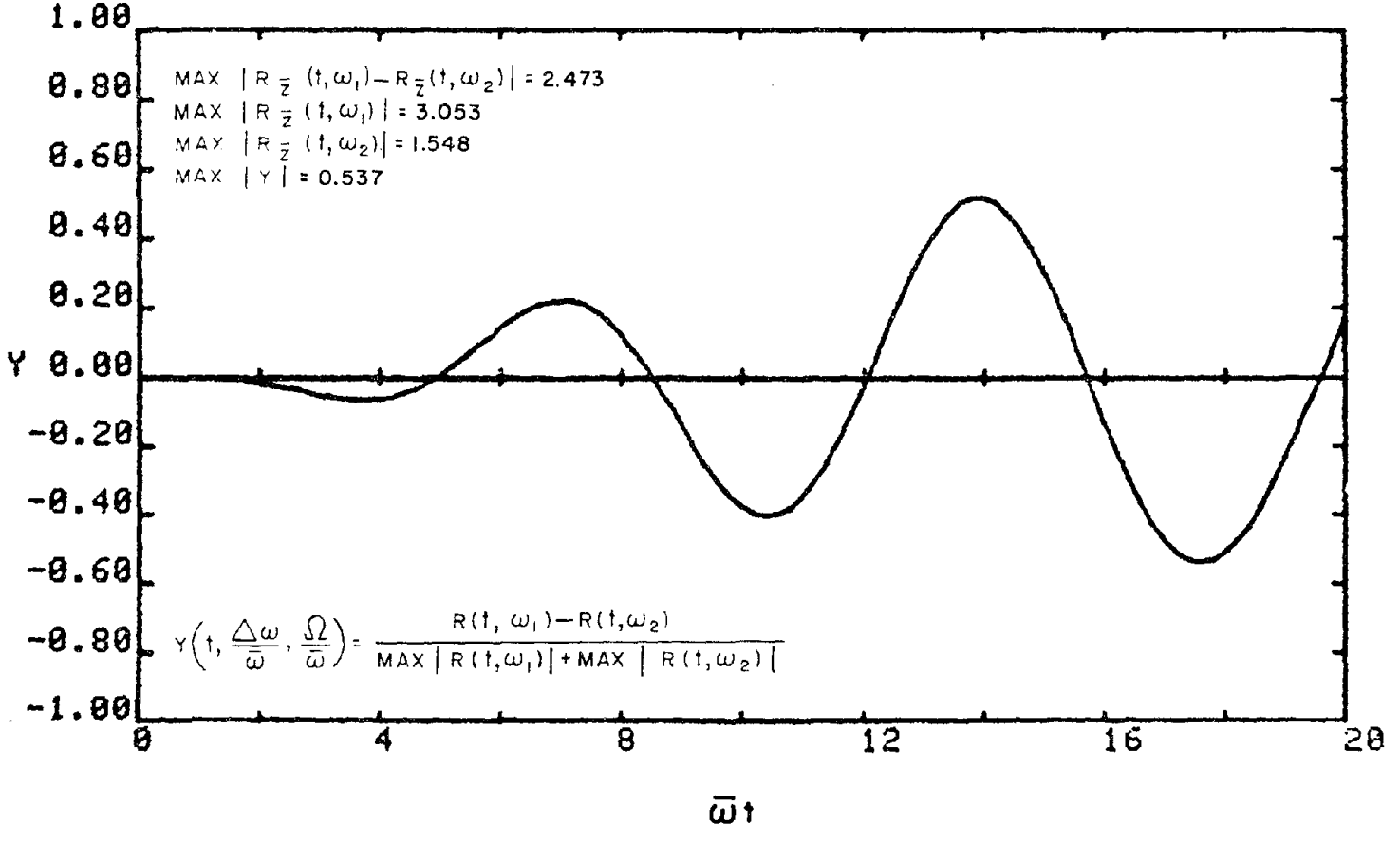

FIG.A21 NORMALIZED DIFFERENCE IN UNDAMPED RESPONSE WHEN $\bar{Z} = (1-\cos \Omega t)/2$, $\Delta\omega/\bar{\omega} = 0.3$ AND $\Omega/\bar{\omega} = 0.75$

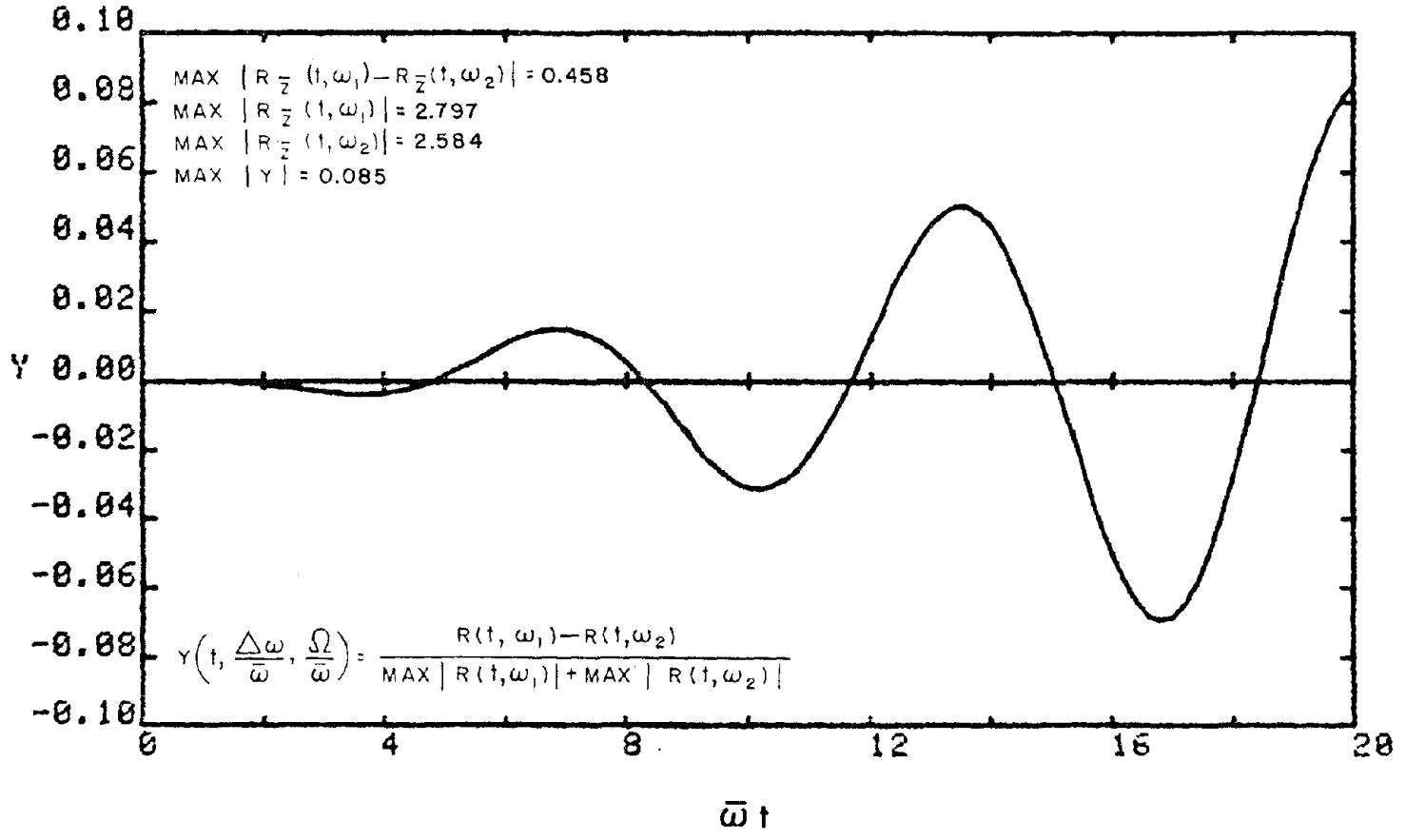

FIG. A22 NORMALIZED DIFFERENCE IN UNDAMPED RESPONSE WHEN $\bar{Z} = (1-\cos \Omega t)/2$, $\Delta\omega/\bar{\omega} = 0.02$ AND $\Omega/\bar{\omega} = 0.8$

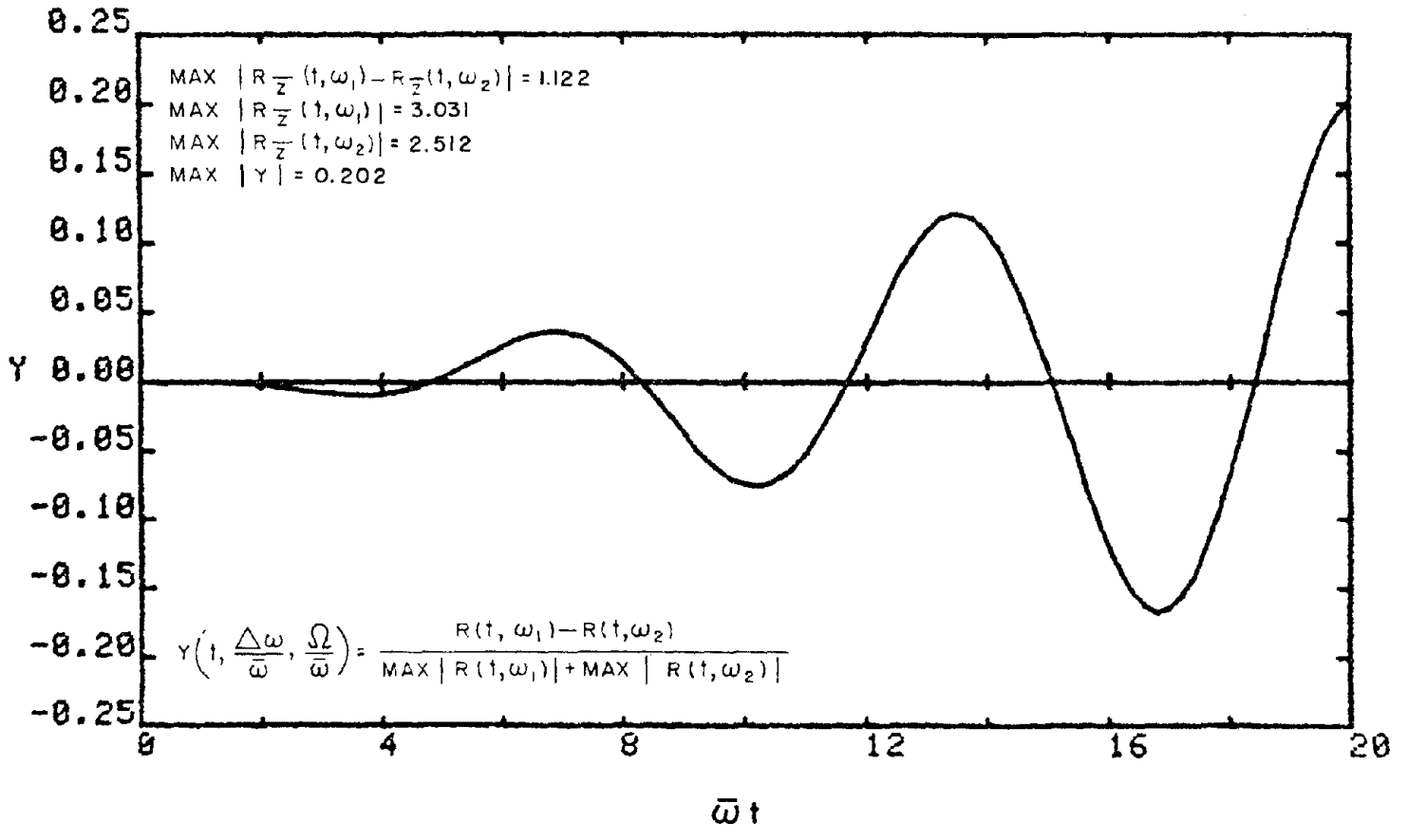

FIG. A23 NORMALIZED DIFFERENCE IN UNDAMPED RESPONSE WHEN $\bar{Z} = (1-\cos \Omega t)/2$, $\Delta\omega/\bar{\omega} = 0.05$ AND $\Omega/\bar{\omega} = 0.8$

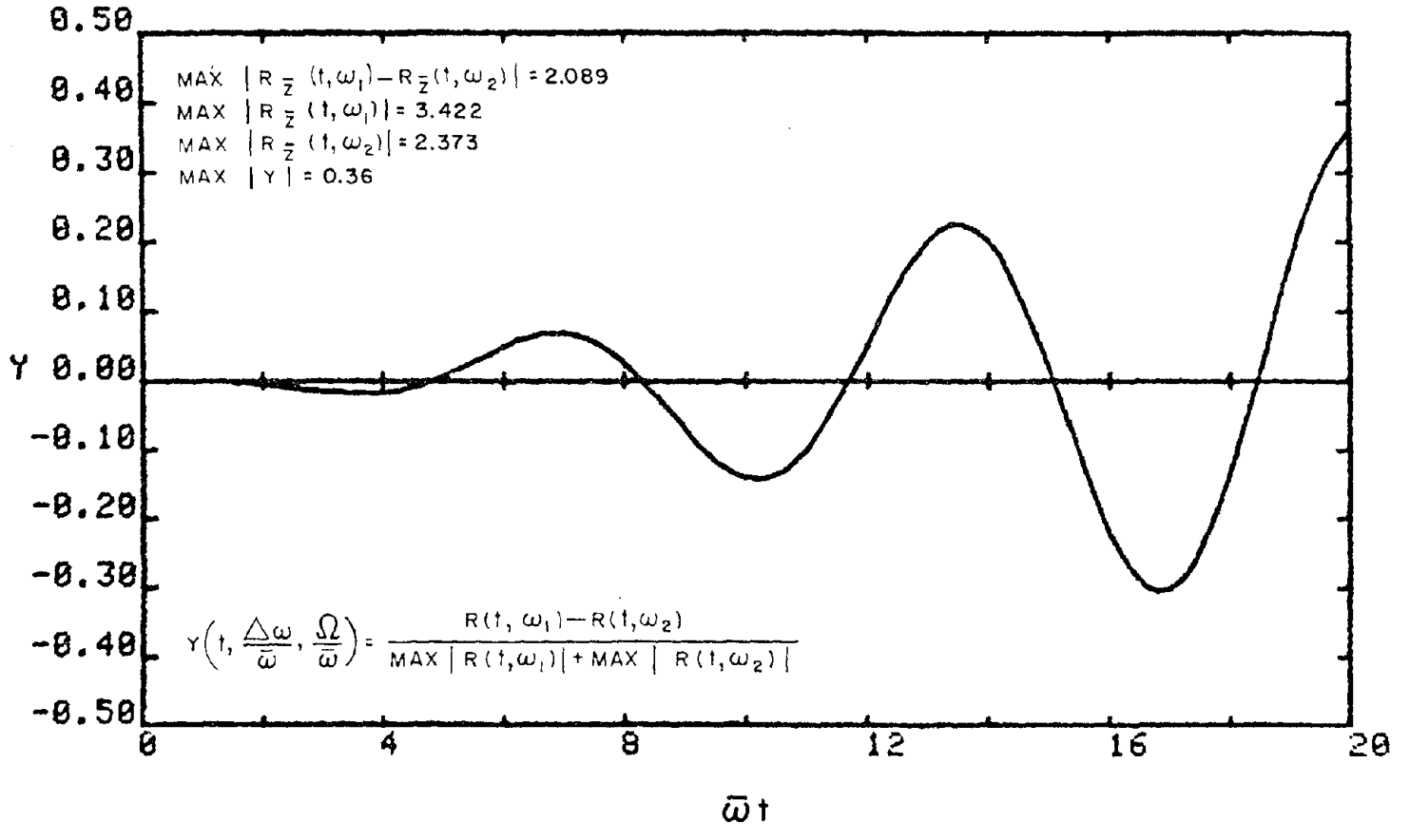

FIG. A24 NORMALIZED DIFFERENCE IN UNDAMPED RESPONSE WHEN $\bar{Z} = (1-\cos \Omega t)/2$, $\Delta\omega/\bar{\omega} = 0.1$ AND $\Omega/\bar{\omega} = 0.8$

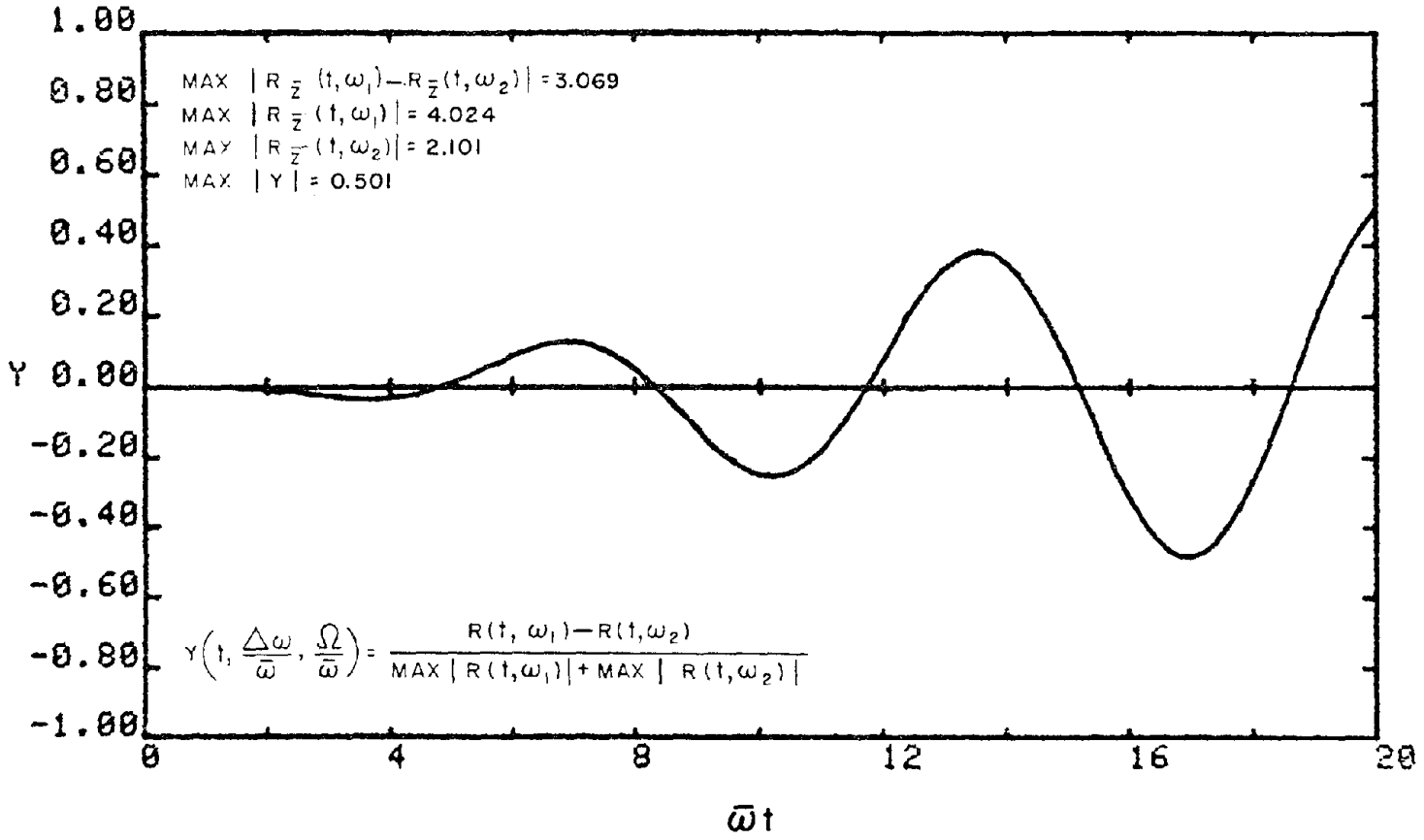

FIG. A25 NORMALIZED DIFFERENCE IN UNDAMPED RESPONSE WHEN $\bar{Z} = (1 - \cos \Omega t)/2$, $\Delta\omega/\bar{\omega} = 0.2$ AND $\Omega/\bar{\omega} = 0.8$

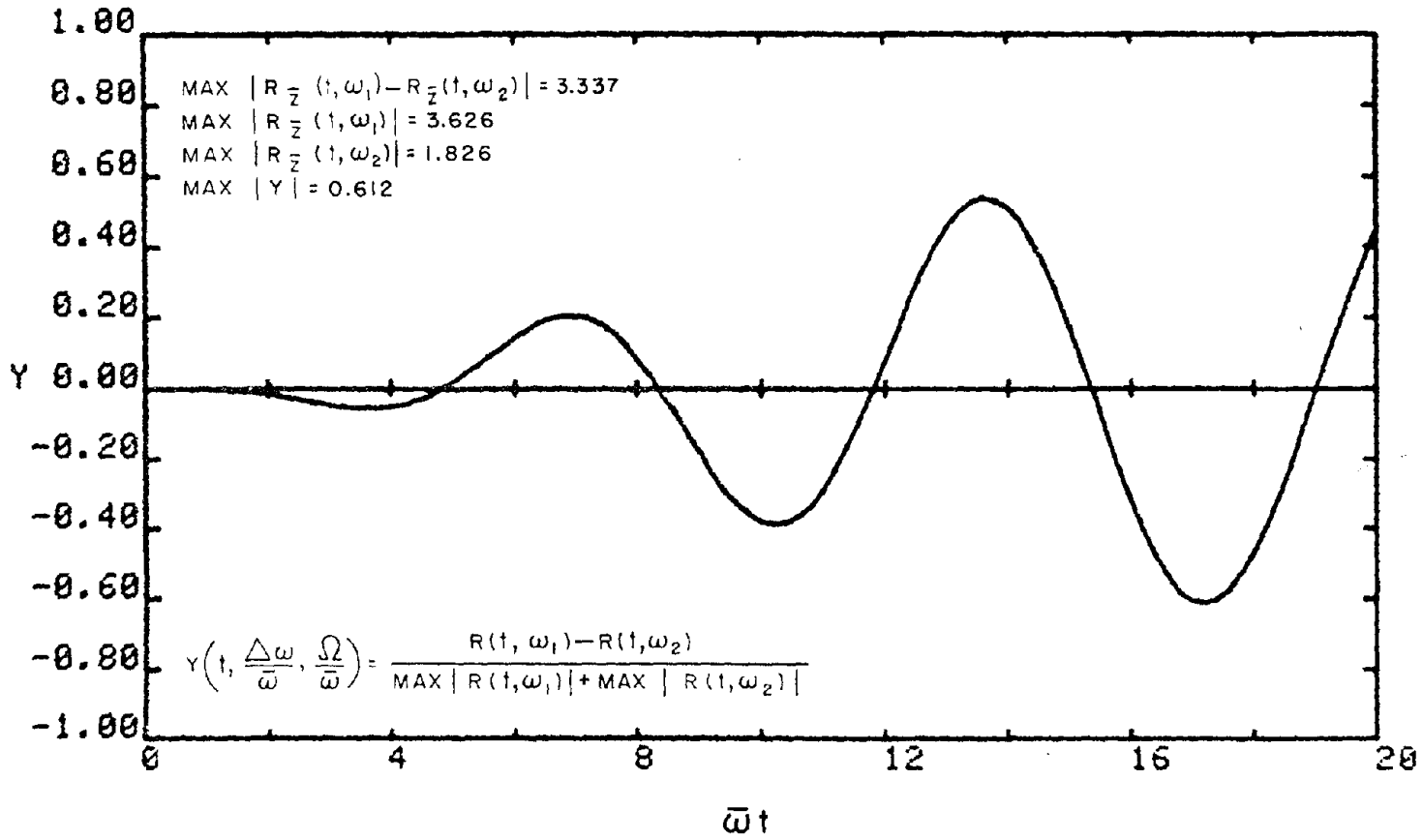

FIG. A26 NORMALIZED DIFFERENCE IN UNDAMPED RESPONSE WHEN $\bar{Z} = (1-\cos \Omega t)/2$, $\Delta\omega/\bar{\omega} = 0.3$ AND $\Omega/\bar{\omega} = 0.8$

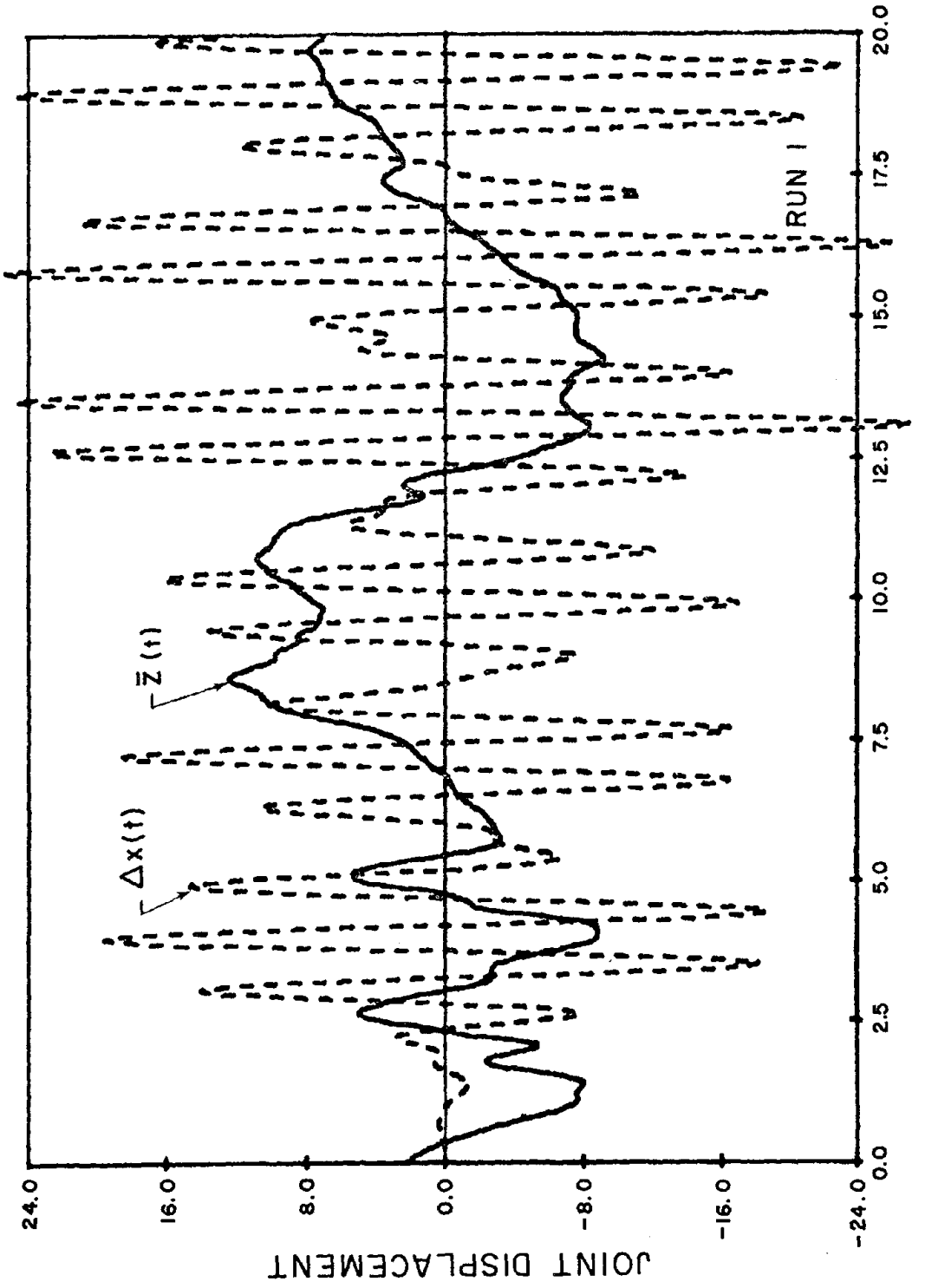

FIG. A27 TOTAL JOINT DISPLACEMENT $\Delta x(t)$ DUE TO COHERENT EL CENTRO N-S INPUT FOR $K_{G1} / K_{G2} / K_p = 2.93/5.07/1$ AND FOR 0% DAMPING

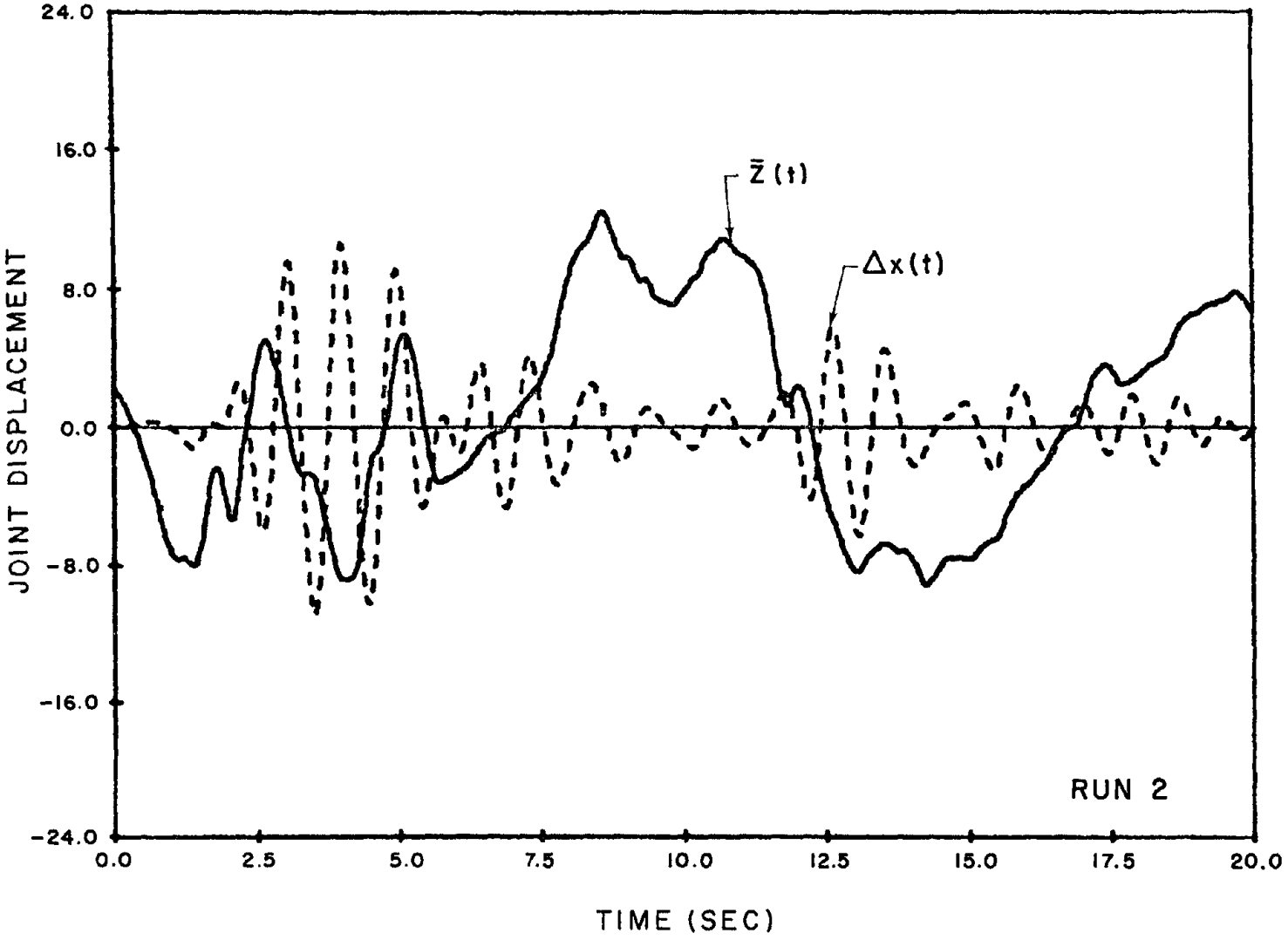

FIG. A28 TOTAL JOINT DISPLACEMENT $\Delta x(t)$ DUE TO COHERENT EL CENTRO N-S INPUT FOR $K_{G1}/K_{G2}/K_p = 2.93/5.07/1$ AND FOR 5% DAMPING

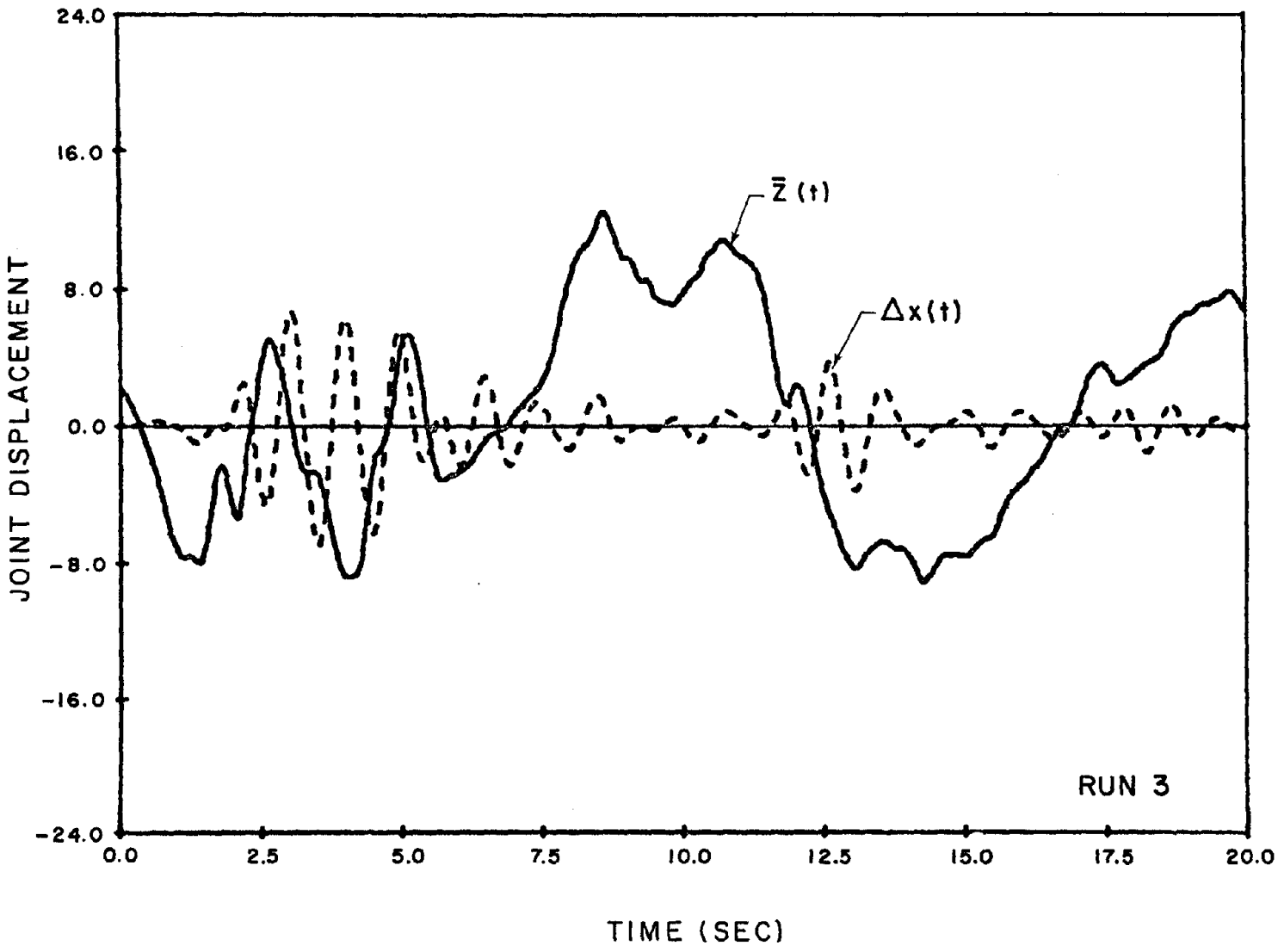

FIG. A29 TOTAL JOINT DISPLACEMENT $\Delta x(t)$ DUE TO COHERENT EL CENTRO N-S INPUT FOR $K_{G1}/K_{G2}/K_p = 2.93/5.07/1$ AND FOR 10% DAMPING

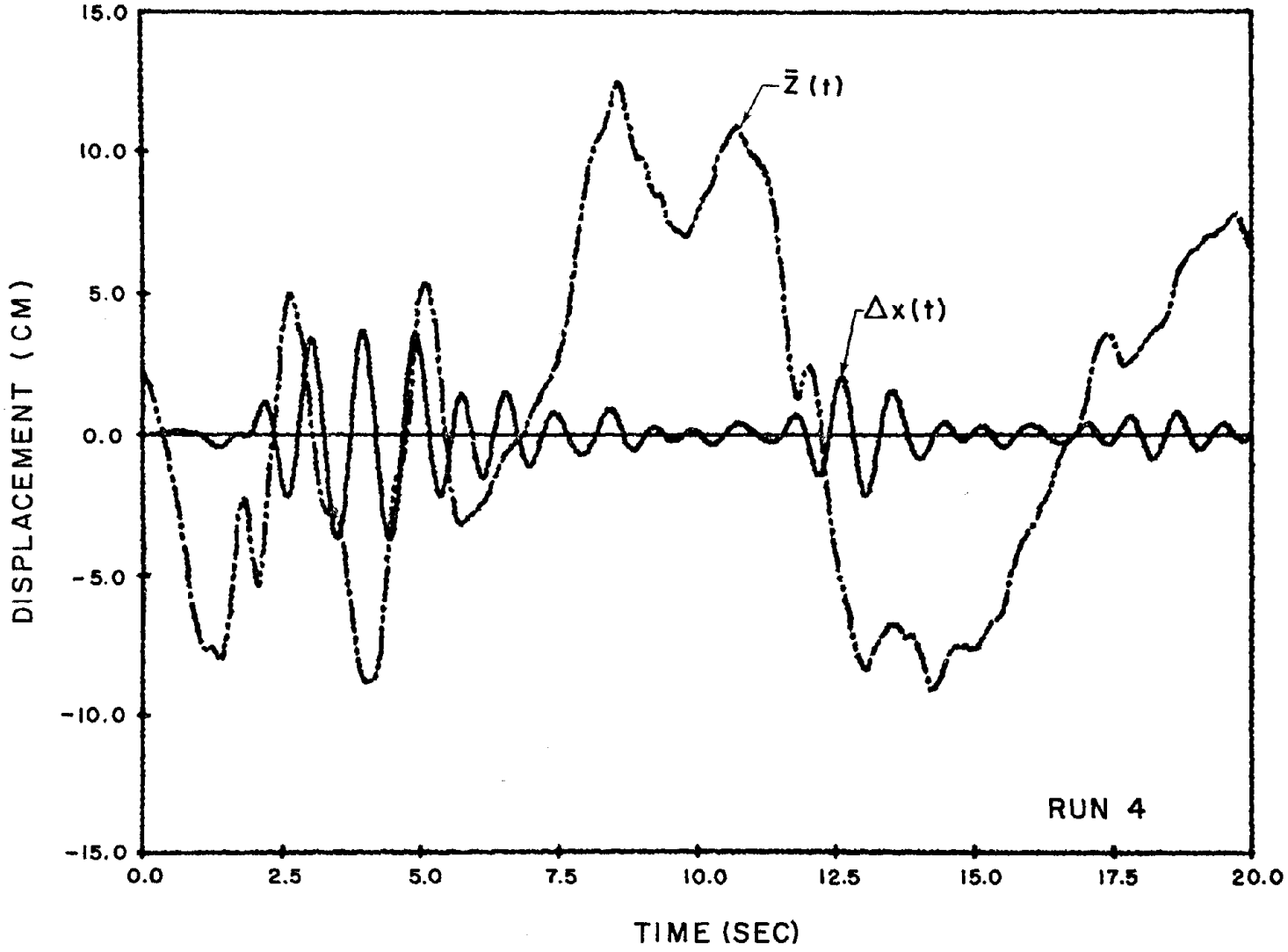

FIG. A30 TOTAL JOINT DISPLACEMENT $\Delta x(t)$ DUE TO COHERENT EL CENTRO N-S INPUT FOR $K_{G1}/K_{G2}/K_p = 3.5/4.5/1$ AND FOR 10% DAMPING

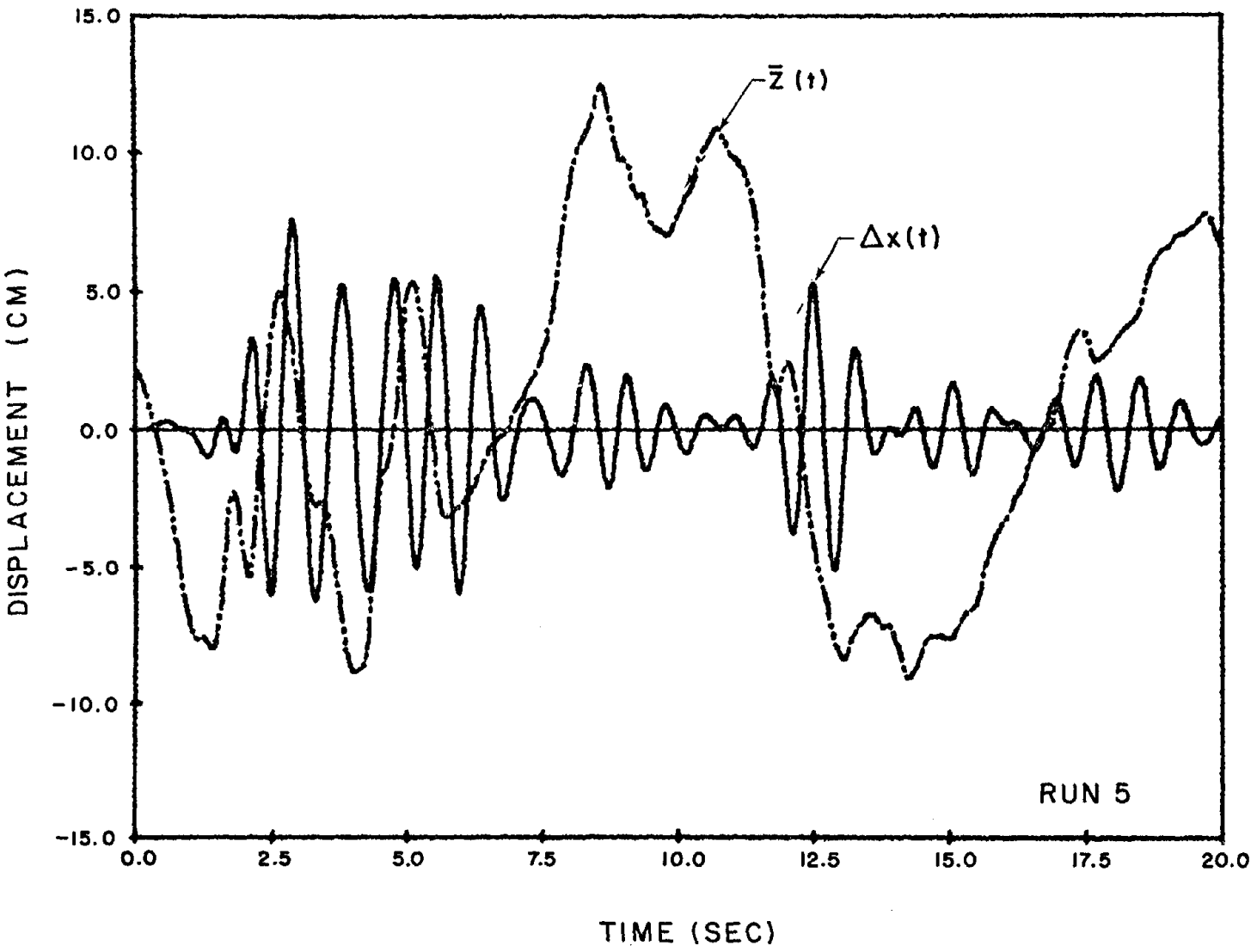

FIG. A31 TOTAL JOINT DISPLACEMENT Δx(t) DUE TO COHERENT EL CENTRO N-S INPUT FOR $K_{G1}/K_{G2}/K_p$ = 4.0/8.0/1 AND FOR 10% DAMPING

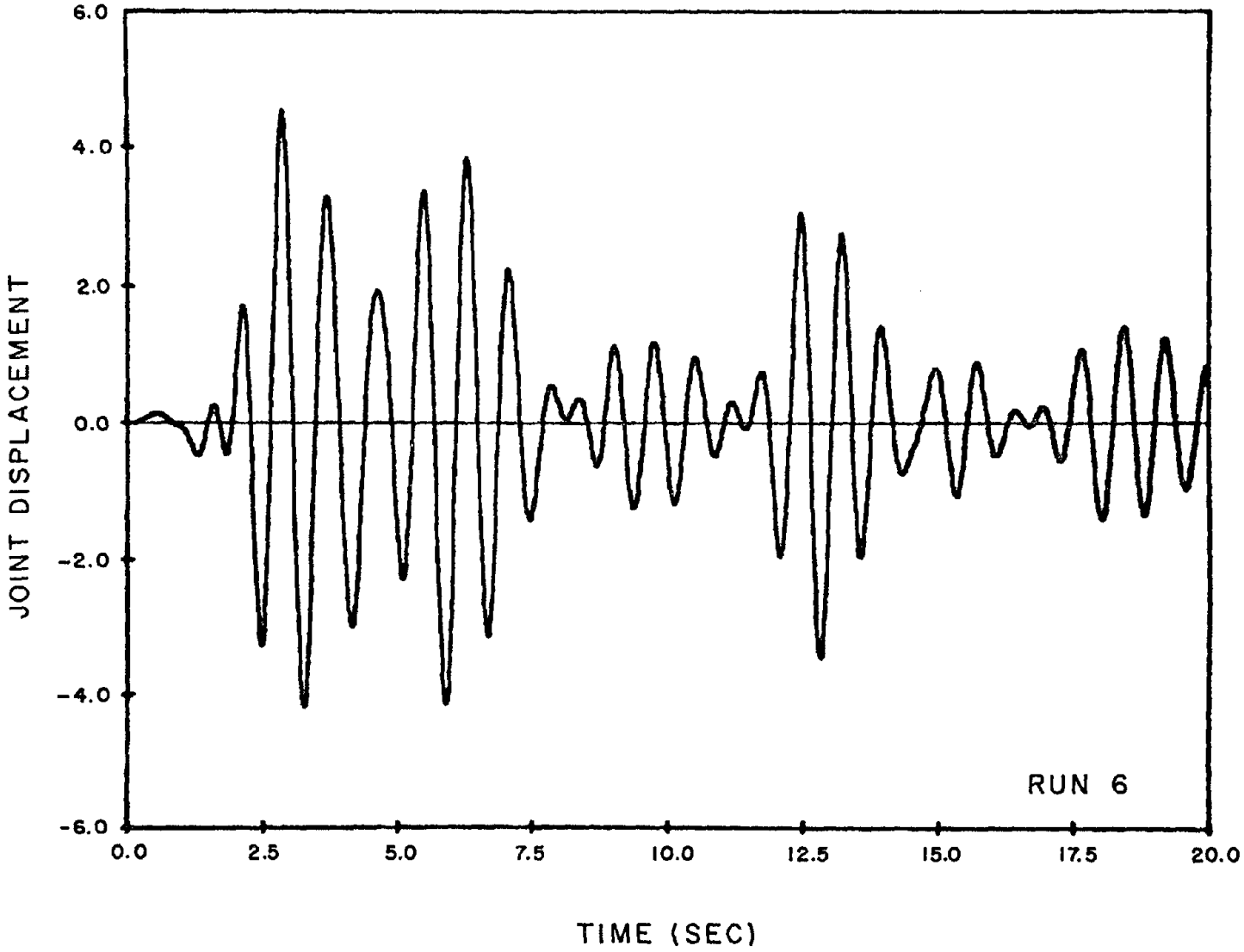

FIG. A32 TOTAL JOINT DISPLACEMENT $\Delta x(t)$ DUE TO COHERENT EL CENTRO N-S INPUT FOR $K_{G1}/K_{G2}/K_p = 5.0/7.0/1$ AND FOR 10% DAMPING

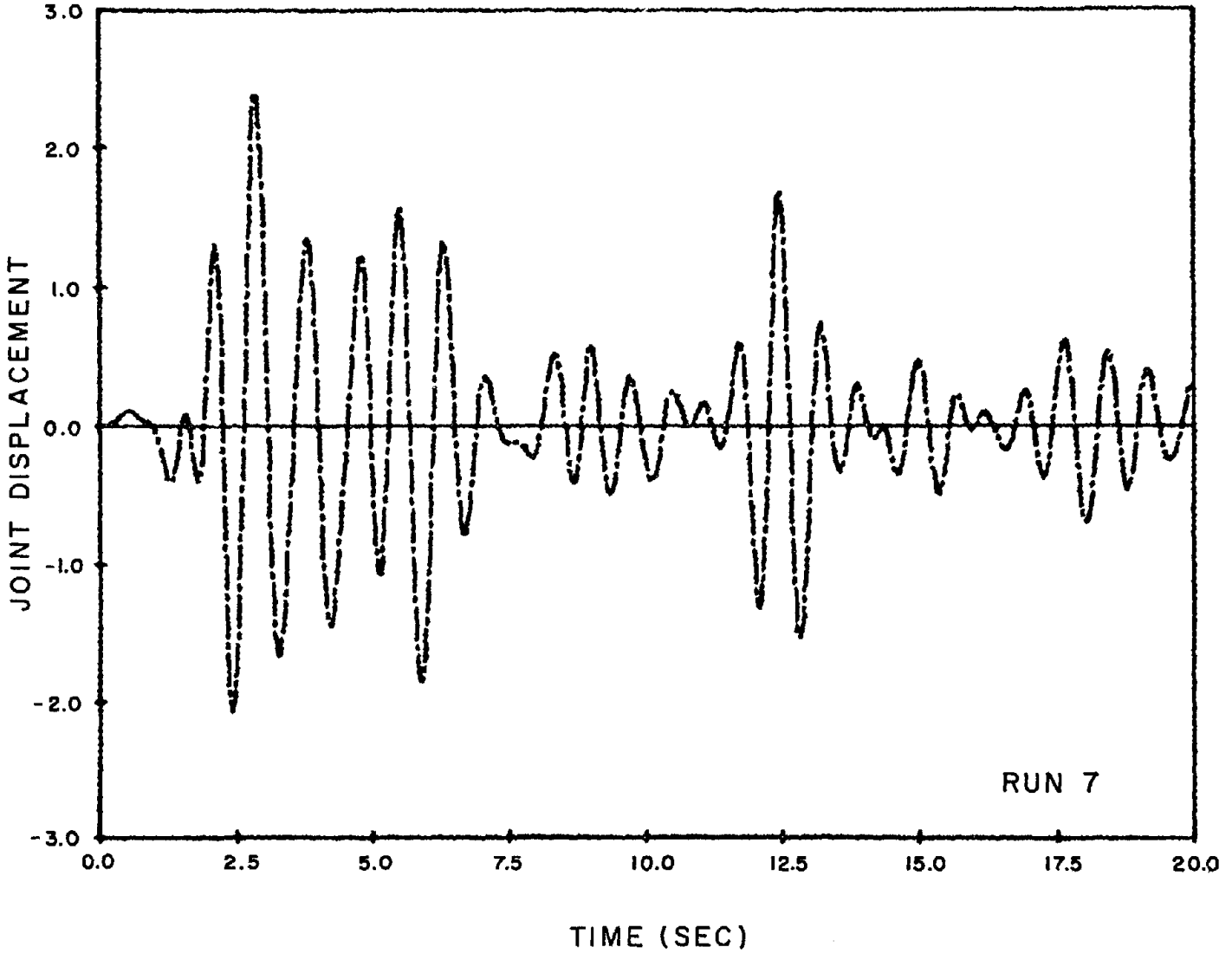

FIG. A33 TOTAL JOINT DISPLACEMENT $\Delta x(t)$ DUE TO COHERENT EL CENTRO N-S INPUT FOR $K_{G1}/K_{G2}/K_p = 5.0/7.0/1$ AND FOR 20% DAMPING

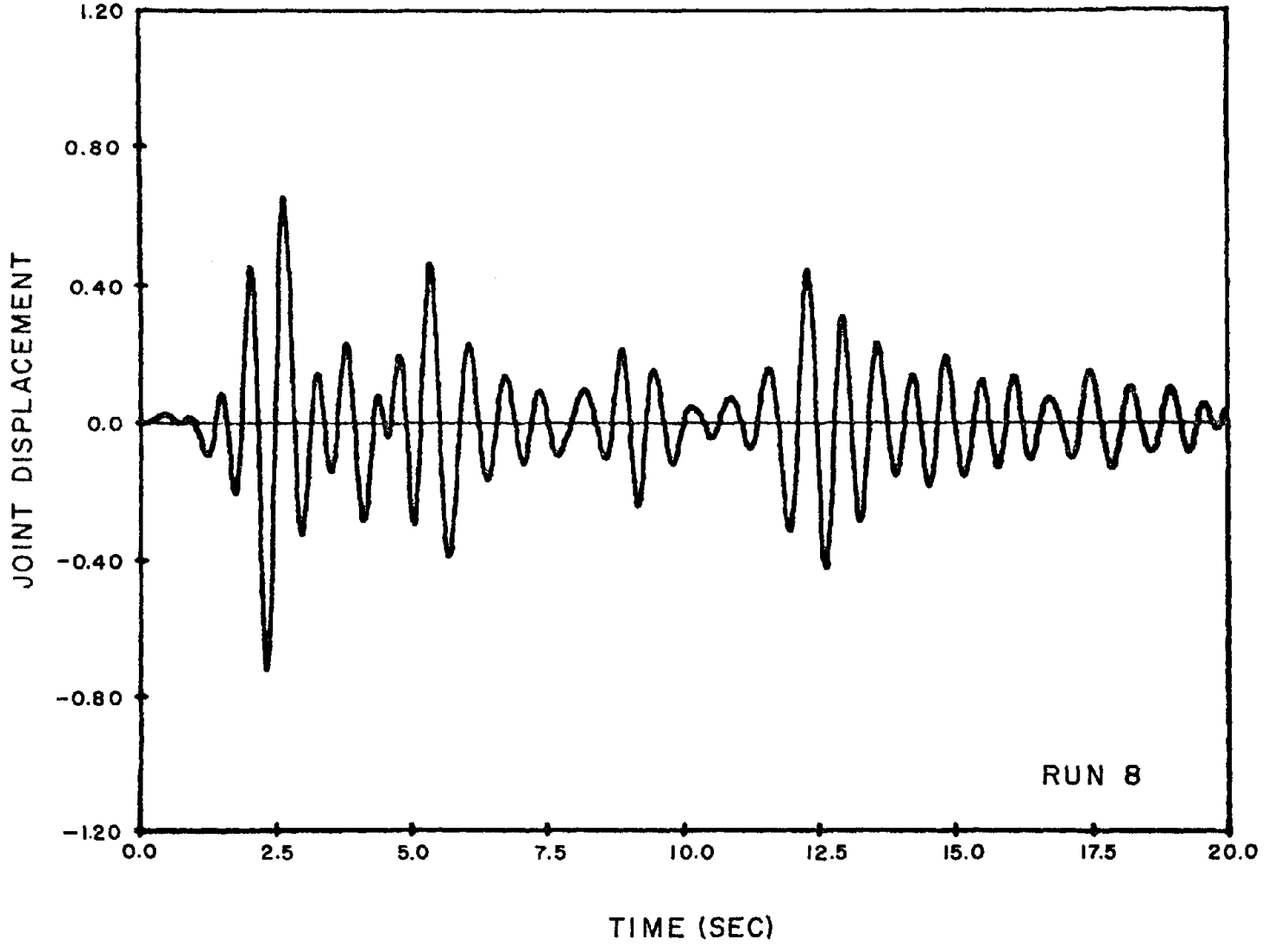

FIG. A34 TOTAL JOINT DISPLACEMENT $\Delta x(t)$ DUE TO COHERENT EL CENTRO N-S INPUT FOR $K_{G1}/K_{G2}/K_p = 9.5/10.5/1$ AND FOR 20% DAMPING

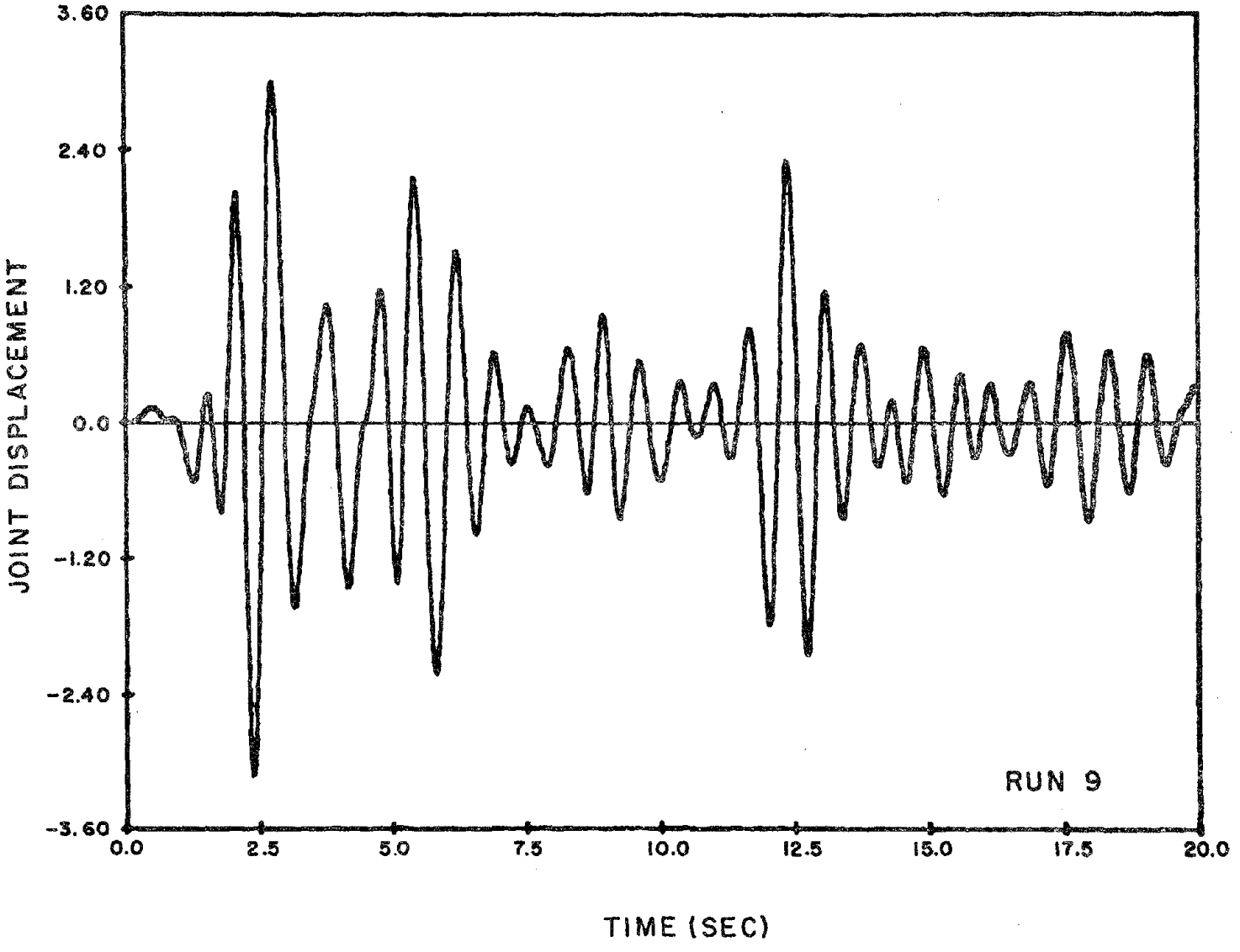

FIG. A35 TOTAL JOINT DISPLACEMENT $\Delta x(t)$ DUE TO COHERENT EL CENTRO N-S INPUT FOR $K_{G1}/K_{G2}/K_p = 6.0/10.0/1$ AND FOR 20% DAMPING

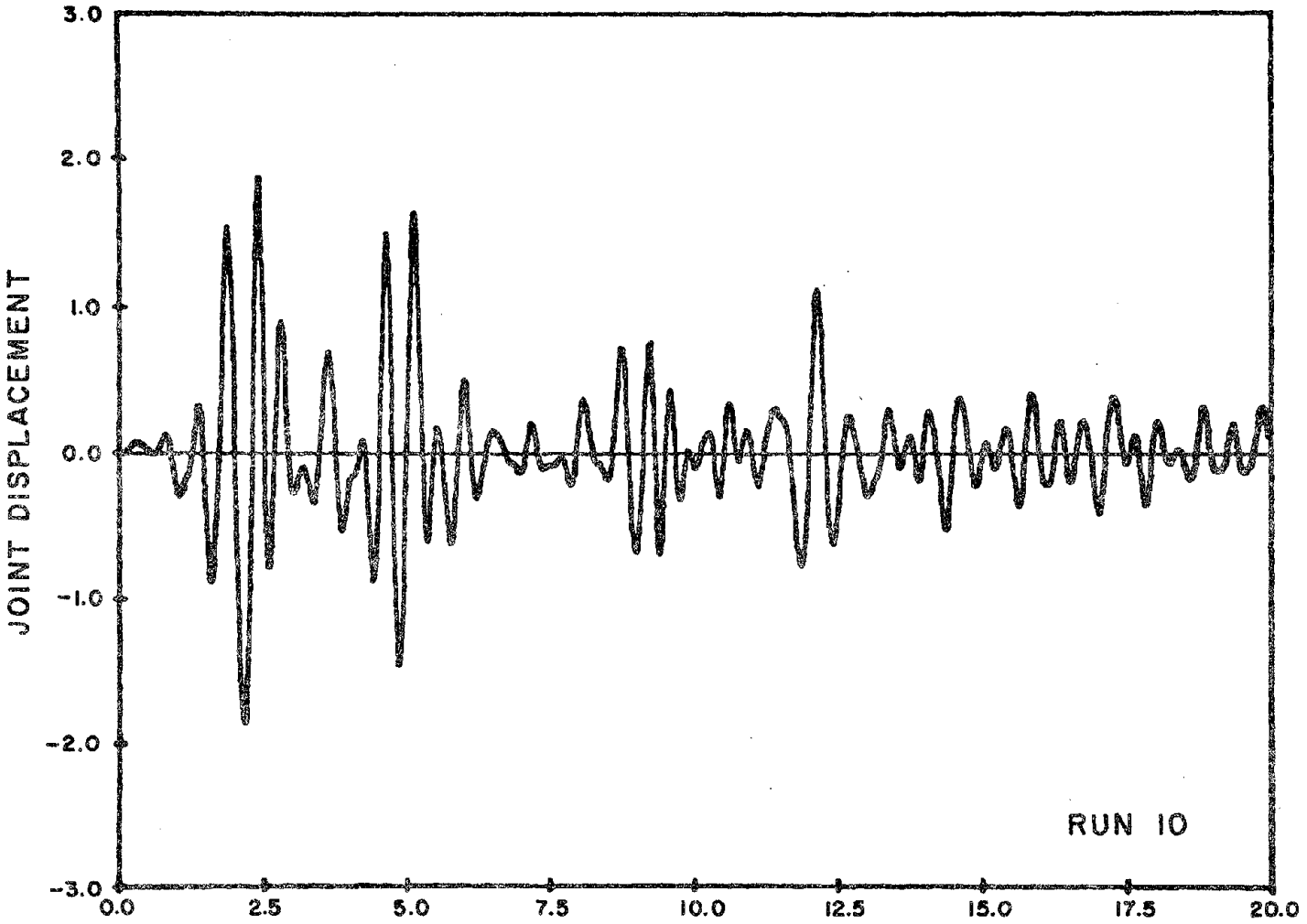

FIG. A36 TOTAL JOINT DISPLACEMENT $\Delta x(t)$ DUE TO COHERENT EL CENTRO N-S INPUT FOR $K_{G1}/K_{G2}/K_p = 16.0/36.0/2$ AND FOR 20% DAMPING